Self-association of Oligoquinoline Foldamers Probed by Time-Resolved Fluorescence Anisotropy

by

Kristijan Lulic

A thesis

presented to the University of Waterloo

in fulfillment of the

thesis requirement for the degree of

Master of Science

in

Chemistry

Waterloo, Ontario, Canada, 2022

Author's Declaration

I hereby declare that I am the sole author of this thesis. This is a true copy of the thesis, including any required final revisions, as accepted by my examiners.

I understand that my thesis may be made electronically available to the public.

Abstract

The self-associations of oligoquinoline-based foldamers (OPV-Q_nA with n = 4, 8, 17, and 33) terminated at one end with a carboxylic acid (A) and at the other end with the fluorescent dye oligo(phenylene vinylene) (OPV) with themselves, the octadecaquinoline $Q_{16}A$ terminated with one carboxylic acid, and the AQ_2PQ_2A monomer made of a central pyridine flanked on each side by a quinoline dyad terminated with a carboxylic acid have been characterized in solution by time-resolved fluorescence anisotropy (TRFA). Complexation of the acid-terminated constructs was induced by the addition of 0.1 g of 16 M sodium hydroxide aqueous solution to the foldamer solutions in chloroform. Dimerization of the OPV-Q_nA foldamers and the complexation of OPV-Q_8A with $Q_{16}A$ followed a close association mechanism. Complexation of OPV-Q_8A with AQ_2PQ_2A occurred through an open association mechanism. Measurements were conducted on the solutions before and after addition of NaOH. Each sample was analyzed by UV-Visible absorption to determine the concentration of the species in solution and by TRFA to determine the average rotational time $<\phi>$ of the unassociated and associated OPV-Q_nA foldamers across concentrations spanning 5 orders of magnitudes in some cases.

Plots of $<\phi>$ as a function of acid group concentration for the dimerization of the OPV-Q_nA samples and complexation of OPV-Q_8A with $Q_{16}A$ indicated that $<\phi>$ increased with increasing foldamer concentration, exclusively after addition of 16 M $NaOH_{(aq)}$. $<\phi>$ reached a plateau at high foldamer concentrations, indicative of a closed association mechanism. The increase in $<\phi>$ with increasing foldamer concentration reflected the association of the foldamers into larger objects. A plot of the $<\phi>$ values obtained in the high concentration plateaus, which were expected to represent foldamer dimerization, as a function of the number of quinoline units

(*NU*) for the corresponding foldamer dimer, yielded a straight line, whose slope was the same as the slope of the straight line obtained by plotting $<\phi>$ of the unassociated foldamers as a function of their *NU*. This result was taken as evidence that complexation of the OPV-Q_nA foldamers resulted in their dimerization. The $<\phi>$-*vs*-[foldamer] profiles could be analyzed to determine the equilibrium constants *K* for these complexations. Large *K* values of 1.0 $(\pm 0.2)\times 10^6$ M^{-1} were obtained which were similar in magnitude to those reported for other self-assembling systems, although the shortest foldamer made of four quinoline units had an equilibrium constant of 1.1 $(\pm 0.1)\times 10^5$ M^{-1}, that was one order of magnitude lower than its longer counterparts.

The same methodology was then applied to investigate the complexation between AQ_2PQ_2A and OPV-Q_8A acting as a fluorescent stopper. Mixtures of AQ_2PQ_2A and OPV-Q_8A were analyzed by UV-Visible absorption to determine the concentration of both species in solution. These experiments led to the conclusion, that complexation of AQ_2PQ_2A under basic conditions resulted in hypochromicity due to aromatic stacking of the end-quinoline units of AQ_2PQ_2A. This observation suggested that upon complexation, AQ_2PQ_2A would form linear chains rather than random aggregates. TRFA was applied to determine the average rotational time $<\phi>$ of the products obtained from mixtures of either 1 μM or 10 μM OPV-Q_8A with varying concentrations of AQ_2PQ_2A. The trends obtained for $<\phi>$ as a function of the [AQ_2PQ_2A]/[OPV-Q_8A] ratio displayed an exponential increase at high foldamer concentration, indicative of an open association mechanism. Further analysis of these trends yielded the equilibrium constant, which was half that obtained for the dimerization of the longer OPV-Q_nA with n = 8, 17, and 33, but four times larger than that of OPV-Q_4A. The complexation between AQ_2PQ_2A and OPV-Q_8A is reminiscent of a condensation polymerization, leading to the formation of many products with a

broad size distribution, taking an average size similar to that of the longest oligoquinoline foldamer synthesized to date by conventional techniques. Consequently, the experiments described in this thesis demonstrate that large foldamers can be generated through the self-association of smaller specially designed molecules in solution.

Acknowledgements

I would like to thank my supervisor, Professor Jean Duhamel for his guidance throughout this project and his unparalleled enthusiasm that made working in his lab a rewarding and enjoyable experience. In addition, I would like to thank my committee members Professors Thorsten Dieckmann and Xiaosong Wang for their advice on the project. I would like to thank the Huc Group at the University of Bordeaux, especially Dr. Victor Maurizot, as well as Jingqi Wang for providing the foldamer samples, that I have used to conduct my research. I would also like to thank the members of the Duhamel Lab group for always making the lab a pleasant learning environment. Finally, I would like to thank my family and friends for the encouragement throughout my academic career and all the memories made.

Table of Contents

Author's Declaration…… ii

Abstract…….... v

Acknowledgements……vi

List of Figures…… x

List of Tables…… xiv

List of Abbreviations…… xvii

Chapter 1 1

1.1.0 Foreword 2

1.1.1 Foldamers 3

1.1.2 Self-Assembly 3

1.1.3 Synthesis 4

1.2.1 Characterization 8

1.2.2 Fluorescence of Oligo(phenylene vinylene) (OPV) 9

1.2.3 Time-Resolved Fluorescence Anisotropy 12

1.2.4 Applications..... 15

1.2.5 Conclusions 16

1.2.6 Thesis Outline and Objectives 17

Chapter 2 19

2.1.0 ABSTRACT 20

2.1.1 INTRODUCTION 21

2.2 EXPERIMENTAL 24

2.3 RESULTS 30

2.3.1 Characterization of the OPV-Q_nA Foldamers by TRFA 30

2.3.2 Dimerization and Complexation of Foldamers Characterized by TRFA 31

2.3.3 Model and Results for the Dimerization of the OPV-Q_nA Foldamers 34

2.3.4 Results for the Complexation of OPV-Q_8A and Q_{16}A and their Analysis 40

2.3.5 Analysis of the Intrinsic Anisotropy of the Foldamer Complexes 44

2.4. DISCUSSION 47

2.5 CONCLUSIONS 51

Chapter 3 53

3.1.0 ABSTRACT 54

3.1.1 INTRODUCTION 55

3.2 EXPERIMENTAL 59

3.3 RESULTS 65

3.3.1 Oligomerization of AQ_2PQ_2A with OPV Q_8A Foldamers Characterized by TRFA 65

3.3.2 Model and Results for Oligomerization between AQ_2PQ_2A and OPV-Q_8A..... 69

3.3.3 Analysis of the Intrinsic Anisotropy of the AQ_2PQ_2A Oligomers..... 73

3.3.4 DISCUSSION..... 75

3.4 CONCLUSIONS..... 79

Chapter 4 81

4.1 Summary of Thesis..... 82

4.2 Future Work 90

References..... 93

Appendices..... 115

Appendix A – Supporting Information for Chapter 2..... 115

Appendix B – Supporting Information for Chapter 3..... 124

List of Figures

Figure 1.1. A) Basic quinoline unit (Q1), B) an oligoquinoline (Q_n) segment, and C) its corresponding three-dimensional structure. 5

Figure 1.2. Reaction schemes for the synthesis of oligoquinoline foldamers by (left panel) the chromatography-free large-scale synthesis and (right panel) the segment doubling strategy. 6

Figure 1.3. Jablonski Diagram[44] 10

Figure 1.4. Molar extinction coefficient of A) Q_8 and B) OPV. C) Fluorescence spectrum of OPV 11

Figure 1.5. Schematic representation of the experimental set up required to conduct a TRFA experiment. The excitation is provided by a nano-LED with a narrow emission bandwidth. 12

Figure 2.1. Plot of ϕ as a function of NU in chloroform for the (○) OPV-Q_nA and (×) OPV-Q_nE foldamers. 30

Figure 2.2. Plots of $< \phi >$ of (blue) OPV-Q_4A, (green) OPV-Q_8A, (red) OPV-Q_{17}A, and (purple) OPV-Q_{33}A with (triangles) and without (circles) NaOH. 32

Figure 2.3. Plots of ϕ as a function of the number of quinoline units (*NU*) for (○) unassociated foldamers obtained without NaOH, (△) $\phi(\infty)$ for the OPV-Q_nNaC foldamers with NaOH as a function of *NU*, and (◇) $\phi(\infty)$ for the OPV-Q_nNaC foldamers with NaOH as a function of 2×*NU*. Solvent: chloroform. 34

Figure 2.4. Results for the dimerization of OPV-Q_8A: A) Plot of χ^2 as a function of $log_{10}(K)$ fitted with a second order polynomial yielding a *K* value of 1.1 (±0.2)×10^6 M^{-1} at the minimum. Plot of B) the molar fractions of (○) unimer and (●) dimer and C) the average rotational time

for solutions (●) with and (○) without 0.1 g of 16 M NaOH aqueous solution as a function of OPV-Q_8A concentration. 37

Figure 2.5. Results for the dimerization of OPV-Q_8A: A) Plot of the molar fractions of (○) unimer and (●) dimer and B) the average rotational time for solutions (●) with and (○) without 0.1 g of 16 M NaOH aqueous solution as a function of OPV-Q_8A concentration. 39

Figure 2.6. Results for the complexation of OPV-Q_8A and Q_{16}A. Plot of A) the (●) experimental and (×) calculated average rotational time as a function of total acid concentration for solutions with and (○) without 0.1 g of 16 M NaOH aqueous solution and B) the molar fractions of (○) free acids, (△) OPV-Q_8A dimers, and (●) complexes as a function of total acid concentration for the K_c value of 7.50×10^5 M^{-1}. C) Plot of χ^2 as a function of $log_{10}(K_c)$ fitted with a fourth order polynomial yielding a K_c-value of 7.50×10^5 M^{-1} at the minimum. 41

Figure 2.7. Plot of the intrinsic anisotropy (r_o) as a function of acid concentration before (○) and after (△) the addition of 0.1 g of 16 M $NaOH_{(aq)}$ for A) OPV-Q_4A, B) OPV-Q_8A, C) OPV-Q_{17}A, D) OPV-Q_8A + Q_{16}A, and E) OPV-Q_{33}A with r_∞ (×) as a function of acid concentration. 46

Figure 2.8. Plot of the equilibrium constants for (black) the dimerization of OPV-Q_4A, OPV-Q_8A, OPV-Q_{17}A, OPV-Q_{33}A and (red) the complexation of OPV-Q_8A with Q_{16}A. 50

Figure 3.1. A) Plot of the molar extinction coefficient (ε) at 326 nm of AQ_2PQ_2A in chloroform (○) without NaOH and (△) with NaOH as a function of concentration. B) Plot of absorbance as

a function of AQ_2PQ_2A concentration in chloroform with NaOH showing the breakpoint at ~ 7 μM marking the onset of hypochromicity upon AQ_2PQ_2A oligomerization..... 62

Figure 3.2. A) Plot of $<\phi>$ as a function of the $[AQ_2PQ_2A]/[OPV\text{-}Q_8A]$ ratio for sample mixtures in chloroform (empty) before and (filled) after addition of 0.1 g of 16 M $NaOH_{(aq)}$ with (circle) 1 μM and (triangle) 10 μM of OPV-Q_8A. B) Plot of $<\phi>$ as a function of [OPV-Q_8A] in chloroform with (●) and without (O) the addition of 0.1 g of 16 M NaOH aqueous solution. 68

Figure 3.3. Plot of the intrinsic anisotropy (r_o) as a function of the $[AQ_2PQ_2A]/[OPV\text{-}Q_8A]$ ratio before (O) and after (△) the addition of 0.1 g of 16 M $NaOH_{(aq)}$ for the complexation of AQ_2PQ_2A with A) 1 μM and B) 10 μM of OPV-Q_8A. 74

Figure 3.4. Plot of the concentrations of (·····) M_i, (– – ·) EM_i, and (———) EM_iE species in the solution prepared with [OPV-Q_8A] = 9.5×10^{-6} M and $[AQ_2PQ_2A] = 7.2\times10^{-4}$ M. Vertical red and green lines represent the number and weight average *NU* equal to 88 and 158, respectively. 78

Figure A1. Fluorescence decays for OPV-labeled octamer in chloroform (with residuals and autocorrelation of the residuals) acquired with vertically polarized light at 479 nm and with the emission at 510 nm obtained with the emission polarizer placed A) at the magic angle ($I_{VM}(t)$), B) vertically ($I_{VV}(t)$), and C) horizontally ($I_{VH}(t)$)…….116

Figure A2. Fluorescence decays for OPV-labeled octamer in chloroform after the addition of 0.1 g of 16 M NaOH aqueous solution (with residuals and autocorrelation of the residuals) acquired with vertically polarized light at 479 nm and with the emission at 510 nm obtained with the emission polarizer placed A) at the magic angle ($I_{VM}(t)$), B) vertically ($I_{VV}(t)$), and C) horizontally ($I_{VH}(t)$)……..117

Figure A3. Plot of χ^2 as a function of $log_{10}(K)$ for A) OPV-Q_4A, B) OPV-Q_{17}A, and C) OPV-Q_{33}A fitted with third order polynomials yielding K values of 1.1 (±0.1)×10^5 M^{-1}, 7.8 (±0.4)×10^5 M^{-1} , and 1.10 (±0.03)×10^6 M^{-1} at their minimum, respectively……118

Figure B1. Fluorescence decays for a mixture of 261 µM AQ_2PQ_2A with 10 µM of OPV-labeled octamer in chloroform without 16 M $NaOH_{(aq)}$ (with residuals and autocorrelation of the residuals) acquired with vertically polarized light at 479 nm and with the emission at 510 nm obtained with the emission polarizer placed A) at the magic angle ($I_{VM}(t)$), B) vertically ($I_{VV}(t)$), and C) horizontally ($I_{VH}(t)$)……..125

Figure B2. Fluorescence decays for a mixture of 384 µM AQ_2PQ_2A with 10 µM of OPV-labeled octamer in chloroform after the addition of 0.1 g of 16 M NaOH aqueous solution (with residuals and autocorrelation of the residuals) acquired with vertically polarized light at 479 nm and with the emission at 510 nm obtained with the emission polarizer placed A) at the magic angle ($I_{VM}(t)$), B) vertically ($I_{VV}(t)$), and C) horizontally ($I_{VH}(t)$)…….126

Figure B3. Plot of χ^2 as a function of $log_{10}(K)$ for mixtures of AQ_2PQ_2A and OPV-Q_8A fitted with a fourth order polynomial yielding a K value of 4.25×10^5 M^{-1}…….127

Figure B4. Plot of the molar extinction coefficient of OPV-Q_8A (red) and AQ_2PQ_2A (black) in chloroform (solid) without and (dashed) with the addition of 0.1 g of 16 M NaOH aqueous solution…….128

List of Tables

Table 2.1. Rotational times ϕ_1 and ϕ_2 used in the analysis of the sigmoidal curves in Figure 2.2 to obtain the dimerization constant (K) for the OPV-Q_nA samples with n = 4, 8, 17, and 33……..36

Table A1. Parameters obtained from the global analysis of $I_{VV}(t)$ and $I_{VH}(t)$ for the OPV-Q_4A samples in chloroform……..118

Table A2. Parameters obtained from the global analysis of $I_{VV}(t)$ and $I_{VH}(t)$ for the OPV-Q_4A samples in chloroform after addition of 0.1 g of 16 M NaOH aqueous solution……....119

Table A3. Parameters obtained from the global analysis of $I_{VV}(t)$ and $I_{VH}(t)$ for the OPV-Q_8A samples in chloroform……..119

Table A4. Parameters obtained from the global analysis of $I_{VV}(t)$ and $I_{VH}(t)$ for the OPV-Q_8A samples in chloroform after addition of 0.1 g of 16 M NaOH aqueous solution……120

Table A5. Parameters obtained from the global analysis of $I_{VV}(t)$ and $I_{VH}(t)$ for the OPV-Q_{17}A samples in chloroform…….120

Table A6. Parameters obtained from the global analysis of $I_{VV}(t)$ and $I_{VH}(t)$ for the OPV-Q_{17}A samples in chloroform after addition of 0.1 g of 16 M NaOH aqueous solution……121

Table A7. Parameters obtained from the global analysis of $I_{VV}(t)$ and $I_{VH}(t)$ for the OPV-Q_{33}A samples in chloroform……..122

Table A8. Parameters obtained from the global analysis of $I_{VV}(t)$ and $I_{VH}(t)$ without r_∞ for the OPV-Q_{33}A samples in chloroform after addition of 0.1 g of 16 M NaOH aqueous solution…..122

Table A9. Parameters obtained from the global analysis of $I_{VV}(t)$ and $I_{VH}(t)$ with r_∞ for the OPV-Q_{33}A samples in chloroform after addition of 0.1 g of 16 M NaOH aqueous solution……...123

Table A10. Parameters obtained from $I_{VM}(t)$ with in1xpscbgk and the global analysis of $I_{VV}(t)$ and $I_{VH}(t)$ with inaniso01d7k for OPV-Q_8A and Q_{16}A sample mixtures in chloroform…….124

Table A11. Parameters obtained from the global analysis of $I_{VV}(t)$ and $I_{VH}(t)$ for the OPV-Q_8A and Q_{16}A samples in chloroform after addition of 0.1 g of 16 M NaOH aqueous solution..…..124

Table B1. Parameters obtained from the global analysis of $I_{VV}(t)$ and $I_{VH}(t)$ for mixtures of AQ_2PQ_2A and 1 μM OPV-Q_8A samples in chloroform without 16 M $NaOH_{(aq)}$……129

Table B2. Parameters obtained from the global analysis of $I_{VV}(t)$ and $I_{VH}(t)$ for mixtures of AQ_2PQ_2A and 10 μM OPV-Q_8A samples in chloroform without 16 M $NaOH_{(aq)}$……129

Table B3. Parameters obtained from the global analysis of $I_{VV}(t)$ and $I_{VH}(t)$ using one rotational time for the mixtures of AQ_2PQ_2A and 1 μM OPV-Q_8A samples in chloroform with 0.1 g of 16 M NaOH aqueous solution……...130

Table B4. Parameters obtained from the global analysis of $I_{VV}(t)$ and $I_{VH}(t)$ using two rotational time for the mixtures of AQ_2PQ_2A and 1 μM OPV-Q_8A samples in chloroform with 0.1 g of 16 M NaOH aqueous solution……...130

Table B5. Parameters obtained from the global analysis of $I_{VV}(t)$ and $I_{VH}(t)$ using one rotational time for the mixtures of AQ_2PQ_2A and 10 μM OPV-Q_8A samples in chloroform with 0.1 g of 16 M NaOH aqueous solution……...131

Table B6. Parameters obtained from the global analysis of $I_{VV}(t)$ and $I_{VH}(t)$ using two rotational time for the mixtures of AQ_2PQ_2A and 10 μM OPV-Q_8A samples in chloroform with 0.1 g of 16 M NaOH aqueous solution……...132

List of Abbreviations

A	Carboxylic acid functionality
A	Unimer or unassociated foldamer
$[A]_o$	Overall concentration of foldamer in the solution.
A_2	Foldamer dimer
Abs	Absorbance
AFM	Atomic force microscopy
a_i	Pre-exponential factor
AQ_2PQ_2A	Monomer made of a central pyridine flanked by two quinoline units and terminated at both ends with a carboxylic acid
CPS	*E.coli* carbamoyl-phosphate synthase
DIPEA	*N*,*N*-Diisopropylethylamine
DLS	Dynamic light scattering
DLVO	Derjaguin-Landau-Verwey-Overbeek theory
DNA	Deoxyribonucleic acid
E	Free OPV-$Q_{16}A$ end group
EM_i	AQ_2PQ_2A oligomers with one OPV-$Q_{16}A$ end group
EM_iE	AQ_2PQ_2A oligomers with two OPV-$Q_{16}A$ end groups
FA	Fluorescence anisotropy
$f_{complex}$	Molar fraction of complexed foldamers
f_{dimer}	Molar fraction of dimers
f_{free}	Molar fraction of unassociated foldamers
G	G-factor
I_o	Initial fluorescence intensity
$I_{VH}(t)$	Horizontally polarized fluorescence decay
$I_{VM}(t)$	Fluorescence decay acquired at the magic angle (54.7°)
$I_{VV}(t)$	Vertically polarized fluorescence decay
K	Equilibrium constant
K_c	Equilibrium constant for complexation
K_d	Dissociation constant
K_n	Equilibrium constant for dimerization of OQ_n
L	Pathlength
M_1	Concentration of unassociated unimers
M_i	Oligomer made of *i* AQ_2PQ_2A monomers
$NaCQ_2PQ_2NaC$	Di(sodium carboxylate) of AQ_2PQ_2A
NMR	Nuclear magnetic resonance
NU	Number of quinoline units
NU_n	Number-average number of quinoline units
NU_w	Weight-average number of quinoline units
OPV	Oligo(phenylene vinylene)
OPV-Q_nA	Oligoquinoline foldamer terminated at one end with a carboxylic acid and at the other end with an oligo(phenylene vinylene)

OPV-Q_nE	Oligoquinoline foldamer terminated at one end with a methyl ester and at the other end with an oligo(phenylene vinylene)
OPV-Q_nNaC	Oligoquinoline foldamer terminated at one end with a sodium carboxylate and at the other end with an oligo(phenylene vinylene)
OQ_n	OPV-Q_nA
$(OQ_n)_2$	OPV-Q_nA dimer
(OQ_nQ_p)	OPV-Q_nA complexed with Q_p
Q_1	Methyl 4-isobutoxy-8-nitroquinoline-2-carboxylate
Q_{16}A	Unlabeled 16-mer oligoquinoline terminated at one end with a carboxylic acid
Q_2	Methyl 4-isobutoxy-8-nitroquinoline-2-carboxylate dimer
Q_n or Q_p	Foldamer composed of *n* or *p* quinoline units
$(Q_p)_2$	Q_p dimer
R	Ideal gas constant
r_∞	Infinite intrinsic anisotropy
$r(t)$	Time-dependent anisotropy
r_o	Intrinsic anisotropy
S_0	Ground electronic state
S_1	First electronic state
S_2	Second electronic state
SCXRD	Single crystal X-ray Diffraction
SSF	Steady-state fluorescence
T	Absolute Temperature
t	Time
TRFA	Time-resolved fluorescence anisotropy
vdW	Van der Waal forces
V_h	Hydrodynamic volume
εAMP	1,N^6-ethenoadenosine 5'-monophosphate
$\phi(\infty)$	Rotational time at infinite foldamer concentration
ϕ_E	Rotational time associated with one OPV end group
ϕ_{E2}	Rotational time associated with two OPV end groups
Φ_F	Fluorescence quantum yield
χ^2	Chi-square
$\varepsilon_{AQ2PQ2A}$	Molar extinction coefficient of AQ_2PQ_2A
ε_{OPV}	Molar extinction coefficient of OPV
ε_Q	Molar extinction coefficient of a quinoline unit
ϕ	Rotational time
$<\phi>$	Average rotational time
$<\phi>_{cal}$	Calculated average rotational time
$<\phi>_{exp}$	Experimental average rotational time
ϕ_1	Unimer rotational time
ϕ_2	Dimer rotational time
η	Solvent viscosity
τ_o	Natural fluorophore lifetime

Chapter 1

Literature Review

1.1.0 Foreword

This thesis describes the application of fluorescence anisotropy to characterize the self-association of oligoquinoline (Q_n) foldamers in solution by using Q_n foldamers labeled with the fluorescent dye oligo(phenylene vinylene) (OPV). The Q_n foldamers were terminated with a carboxylic acid (A) at one end for the species OPV-Q_nA or Q_nA or both ends for AQ_2PQ_2A, a special oligoquinoline, where a central pyridine is flanked by two quinoline dimers. After deprotonation with a strong base, complexation of oligoquinolines terminated with a single sodium carboxylate yields dimers through a closed association mechanism, whereas AQ_2PQ_2A with two sodium carboxylates can polymerize into longer complexes through an open association mechanism. Since complexation of the sodium carboxylates in chloroform is the result of an equilibrium, the determination of the equilibrium constants, that dictate the complexation of these foldamers, is the focus of this thesis. This introductory chapter begins with a discussion on foldamers, which constitute a general class of synthetic compounds inspired by biological macromolecules, whose functions foldamers attempt to mimic. This introduction on foldamers is followed by a description of the self-assembly of macromolecules, a principle that controls many biological processes, but also whose influence extends into other fields such as material science and nano-engineering, by providing alternative methods to generate larger objects from smaller building blocks in a simpler manner compared to conventional synthetic strategies. The methodology used to synthesize these foldamers is then presented, as well as the numerous techniques applied to characterize them, including a short discussion about their limitations. This introduction continues with a review of fluorescence before describing fluorescence anisotropy, the technique of choice to monitor the

self-association of the OPV-Q_nA foldamers. The chapter concludes with an overview of the thesis objectives and a summary of the research conducted in the following chapters.

1.1.1 Foldamers

Foldamers are synthetic oligomers designed to fold into specific molecular conformations in solution via non-covalent and intramolecular interactions.[1-3] When proteins and oligoribonucleotides fold into well-defined structures, that exhibit catalytic activity, they are referred to as enzymes or ribozymes, respectively. This feature makes them indispensable in numerous biological processes such as for energy conversion and DNA repair, to name but a few.[4] The ability to build by self-assembly such complex architectures, that result in catalytic activity from an unrestricted set of building blocks is the prime motivation to develop chemical systems that are able, as a first step, to replicate well-defined secondary structures and perform tasks commonly observed in nature.[4] Indeed chemists are not hampered by the limited set of building blocks found in nature such as nucleotides, amino acids, or sugars, and foldamers have been prepared from quinolines, phenylene ethynylene, benzene triazole, and many other chemical building blocks.[5]

1.1.2 Self-Assembly

Self-assembly is another experimental process, that can be employed to generate complex architectures. It involves the spontaneous association of molecules or macromolecules under equilibrium conditions to form ordered structures.[6,7] Self-assembly rules numerous biological processes and its principles have been applied in chemistry and material science to create large objects from synthetic building blocks.[6,8] The formation of crystals, surfactant micelles, and phase-separated polymers are all examples of molecular self-assembly[9-11] and these processes play

important roles in chemistry in just the same manner as the docking of a ligand in an enzyme or the hybridization of two complementary oligonucleotides in biology.[12] The building blocks of a self-assembling system are usually molecules or macromolecules containing motifs capable of specific interactions with one another. These interactions are usually weak and non-covalent in nature and can involve aromatic stacking,[13,14] hydrophobic interactions,[15] or hydrogen-bonding.[16,17] Other examples of interactions include metal coordination, which can be used to generate metal-containing polymers.[18,19] The associations between these molecules or segments of larger macromolecules are reversible due to the nature of these bonds, and they allow for the generation of ordered structures.[6] This allows their examination by thermodynamic methods through the determination of their equilibrium constant.[6,20] Self-assembly can go beyond traditional molecular synthetic strategies to generate much larger nanometer-sized macromolecular objects, that may be used as biological, electrical, or optical components.[6] In this context, if foldamers could be made to self-assemble, they could potentially be used as building blocks to generate a new genre of macromolecular objects. They would take advantage of the wide variety of synthetic structural units that have already been shown to generate foldamers with different polymeric backbones.[21] Furthermore, foldamer self-assembly could be used in applications that would go beyond the mere mimicry of biological processes, by creating novel components for molecular electronics[22-24] and the nano-engineering field.[25-27]

1.1.3 Synthesis

The study of foldamers prepared with an oligoquinoline backbone and referred to as Q_n, where *n* represents the number of quinolines in the foldamer, has been the object of a concerted effort since they fold predictably into helices stabilized by intramolecular hydrogen bonding and aromatic

stacking.[28] This thesis will focus on the study of foldamers synthesized from methyl 4-isobutoxy-8-nitroquinoline-2-carboxylate, otherwise referred to as Q_1 (Figure 1.1A).[29] This class of foldamers (Figure 1.1B) is popular due to the stability of their secondary structure (Figure 1.1C), their ability to crystallize, and the relative ease of their synthesis.[29]

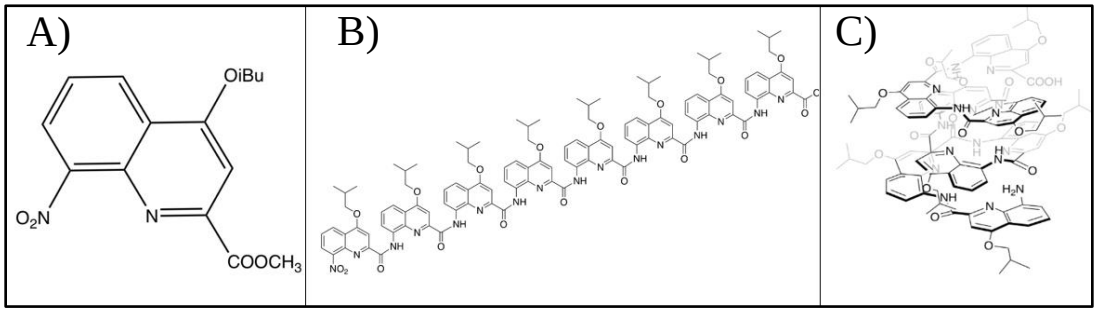

Figure 1.1. A) Basic quinoline unit (Q1), B) an oligoquinoline (Q_n) segment, and C) its corresponding three-dimensional structure.

As depicted in the left panel of Figure 1.2, the synthesis of Q_n foldamers begins with the reduction of the nitro group of Q_1 (O_2N-Q_1-COO-CH_3) using a palladium catalyst in the presence of hydrogen gas to yield the corresponding amine (H_2N-Q_1-COO-CH_3). The methyl ester portion of another batch of Q_1 is then deprotected using potassium hydroxide (KOH) to generate the acid functionality (NO_2-Q-COOH). Reaction of the carboxylic acid with oxalyl chloride yields the corresponding acyl chloride (NO_2-Q_1-COCl). Coupling of H_2N-Q_1-COO-CH_3 and NO_2-Q_1-COCl in the presence of *N*,*N*-diisopropylethylamine (DIPEA) results in the dimer, Q_2. Theoretically, a Q_n foldamer with *n* quinolines could be produced through successive amide coupling of Q_1 to Q_{n-1}. In practice, elongation of the quinoline foldamer is done sequentially in unit additions of the Q_2 dimer, as it is too short to form stable anhydrides in contrast to longer Q_n oligomers for which anhydride formation is a serious complication during the coupling step. This method is referred to

as the chromatography-free large-scale synthesis method. While it is efficient, the number of quinolines is increased by solely two units at a time, which makes it a tedious procedure, that requires a lengthy sequence of reaction steps to generate the longer foldamers, whose structure would more closely mimic biological structural motives found in nature. By contrast, longer foldamers can be obtained more rapidly with the segment doubling strategy[29] shown in the right panel of Figure 1.2.

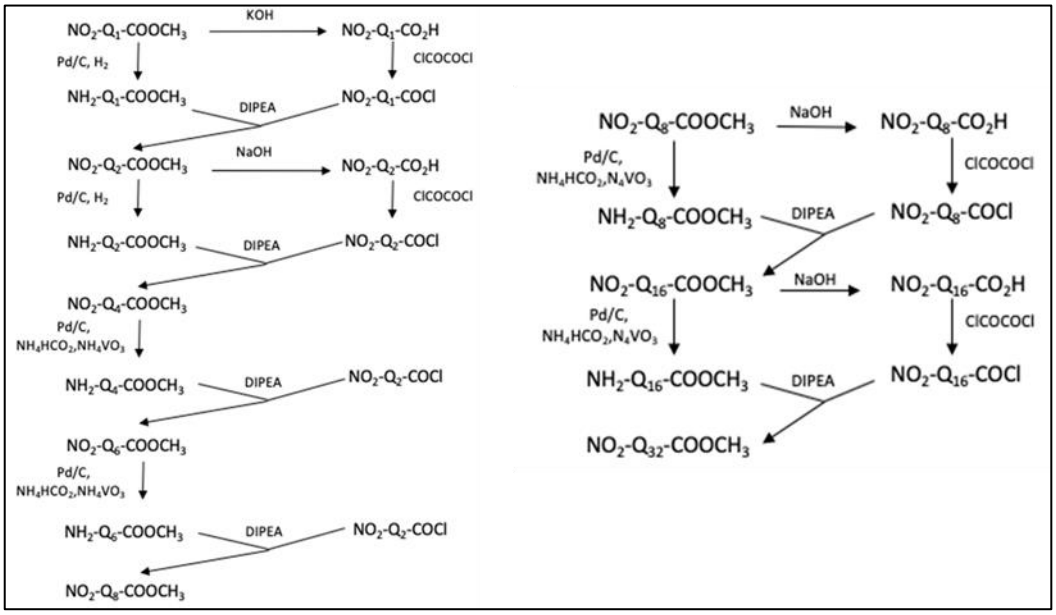

Figure 1.2. Reaction schemes for the synthesis of oligoquinoline foldamers by (left panel) the chromatography-free large-scale synthesis and (right panel) the segment doubling strategy.

With the segment doubling strategy, two foldamers with a same length are coupled together using the synthetic protocol described in Figure 1.2, to produce a foldamer with a length that is double the length of the original foldamer. For these longer constructs, the anhydride resulting

from the dehydration of the carboxylic acid terminals of two foldamers can be separated from the foldamer of interest by column chromatography, and it was found that the acid could be recovered by keeping the anhydride in a refluxing pyridine-water mixture.[29] Using the protocols described in Figure 1.2, foldamers of up to 64 units were prepared.[29,30] However elongation of foldamers with 30 or more units becomes challenging due to their poor solubility.[25] Furthermore, the stepwise synthesis of foldamers, whether it is done with either procedure described in Figure 1.2, is time-consuming as it follows a multistep protocol. To shorten the synthetic pathway, the coordination of a carboxylic acid at the end of Q_nA foldamers with a metal cation has been proposed as a means to elongate oligoquinolines via self-assembly. Foldamer self-assembly might circumvent the solubility issues encountered with larger foldamers[25] and would be expected to generate the longer foldamers required for applications, where the length of the object being generated matters, such as for the preparation of molecular wires.

As it turns out, Q_n foldamers combine a helical conformation with an electron-rich backbone endowing them with the conductive properties and rigidity expected for molecular wires used in molecular electronic applications.[29] In particular, molecular systems designed to undergo photoinduced charge transfer are often composed of an electron donor and acceptor separated by macromolecular spacers long enough to prevent through-space electron transfer. With such long spacers, the observation of electron transfer from the donor to the acceptor requires that the electron travels through the macromolecular construct. These elongated constructs are referred to as organometallic wires. In the case of Q_n foldamers, electron hopping along the foldamer backbone has been observed, as long as the foldamers were more than 9 structural units long.[22]

Shorter Q_n foldamers would allow through-space electron transfer without involving the quinoline backbone. This example illustrates the importance of being able to prepare long foldamers.

1.2.1 Characterization

As a result of their intriguing properties, many analytical techniques have been applied to characterize foldamers in general and Q_n foldamers in particular.[25] These methods include single crystal X-ray diffraction (SCXRD),[31] nuclear magnetic resonance spectroscopy (NMR),[32] UV-Vis absorption spectroscopy,[33] and more recently, time-resolved fluorescence anisotropy.[25] SCXRD is the method of choice for determining the structure, and thus the conformation, of macromolecules in the solid state,[34] but crystal packing forces can also induce macromolecular conformations, that are not always representative of a macromolecule dissolved in solution.[35,36] This is where spectroscopy-based techniques become valuable, because they can probe the conformation of macromolecules in solution.[37]

NMR accompanied with molecular modelling can predict the conformation of macromolecules in solution, by measuring the helical twist of a foldamer.[38] Increasing the length of foldamers having an aromatic backbone results in changes in UV-Vis absorption.[39,40] Unfortunately, all of these techniques only probe short distances between the residues of a foldamer. Applying these spectroscopy-based techniques to characterize the overall size and geometry of a macromolecule in solution is more challenging.[25] In contrast, dynamic light scattering (DLS) can determine the dimension and geometry of nanometer-sized objects in solution.[41] Earlier studies have revealed that Q_n foldamers form helices with a 2.0 nm diameter and a raise of 0.136 nm per quinoline residue.[29] Considering that the foldamers, that were studied

to obtain these parameters, had between 4 and 66 structural units, they would have lengths ranging from 0.54 to 9.0 nm, respectively.[25] Unfortunately, the characterization of macromolecular objects with a size falling in this range is challenging for standard DLS instruments, particularly for sizes smaller than 2.0 nm. Also, standard DLS instruments approximate macromolecules as spheres, which could become an issue for longer foldamers with a large aspect ratio. Longer helical foldamers would be better represented as rigid symmetric top macromolecules, whose motions in solution are described by two diffusion coefficients, one for rotation around the main axis of the helix and another for tumbling around the axis perpendicular to the main helical axis.[42] Fortunately, earlier studies have demonstrated that time-resolved fluorescence anisotropy (TRFA) is ideally suited to probe helical macromolecules with a main axis that can be at least as long as 11 nm.[43] Furthermore, the high sensitivity of fluorescence means that TRFA experiments can be done at concentrations that are orders of magnitude lower than the concentrations used with the vast majority of the more traditional techniques applied to study foldamers so far.[25]

1.2.2 Fluorescence of Oligo(phenylene vinylene) (OPV)

Fluorescence is a process whereby a molecule is excited through the absorption of a photon, which brings the molecule from the ground state to the excited state. After a rapid ($\sim 10^{-12}$ s) relaxation period called internal conversion, the molecule relaxes to the lowest vibrational level of the first electronic state from where it will emit a photon at a wavelength longer than that of the excitation photon.[44] Any molecule capable of undergoing such a process is known as a fluorophore.

The absorption and emission of light by a fluorophore are illustrated by an energy-level scheme known as the Jablonski diagram (Figure 1.3). A fluorophore in the ground-state is in the

lowest vibrational state of the lowest electronic state denoted by $S_{0,0}$. When the fluorophore absorbs a photon, it is excited to one of the vibrational levels of the upper electronic states such as S_1, S_2, or higher, depending on the energy of the exciting photon. Once excited, the molecule will undergo internal conversion, relaxing to the lowest level of the S_1 state ($S_{1,0}$) without emission of a photon. Fluorescence corresponds to the relaxation of the excited fluorophore from $S_{1,0}$ to one of the vibrational levels of the lowest electronic state S_0.

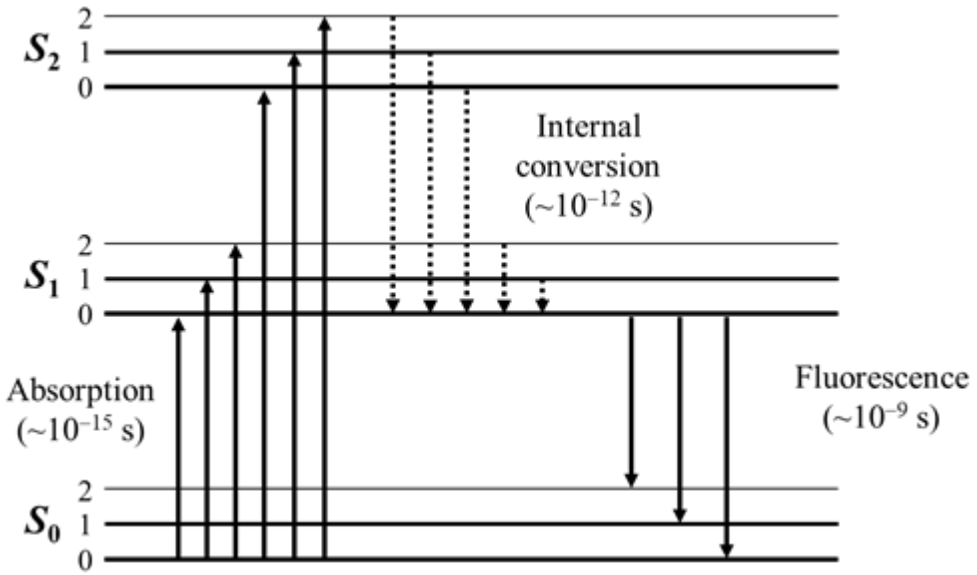

Figure 1.3. Jablonski Diagram.[44]

The absorption of a photon occurs within a few femtoseconds, while internal conversion occurs on a picosecond timescale.[44] Both of these timescales are inconsequential in terms of fluorescence lifetimes, which are usually orders of magnitude longer and expressed in nanoseconds. Molecules that fluoresce usually contain conjugated double bonds with electrons that can be delocalized fairly easily.[44] The fluorophore being used in this proposal is oligo(phenylene vinylene) or OPV. This dye was used due to its high fluorescence quantum yield

(Φ_F = 0.62 (±0.04))[45] and large molar extinction coefficient (ε = 32,400 (±750) $M^{-1}.cm^{-1}$ at 430 nm),[19] which allow its detection at concentrations as low as 1 nM, as will be illustrated in this thesis. Its natural lifetime in chloroform (τ_o = 1.61 (±0.05) ns)[45] should enable the study of oligoquinoline OPV-Q_nE foldamers terminated at one end with a methyl ester group and at the other end with an OPV label, with a rotational time ϕ, that could be as large as $5\times\tau_o$ = 8.0 ns for a 132-mer. Furthermore, earlier studies with OPV-Q_nE foldamers have shown that OPV does not photochemically interact with the oligoquinoline backbone.[29] The fluorescence and molar extinction coefficient spectra of the OPV label are shown in Figure 1.4 together with the molar extinction coefficient spectrum of the oligoquinoline backbone.

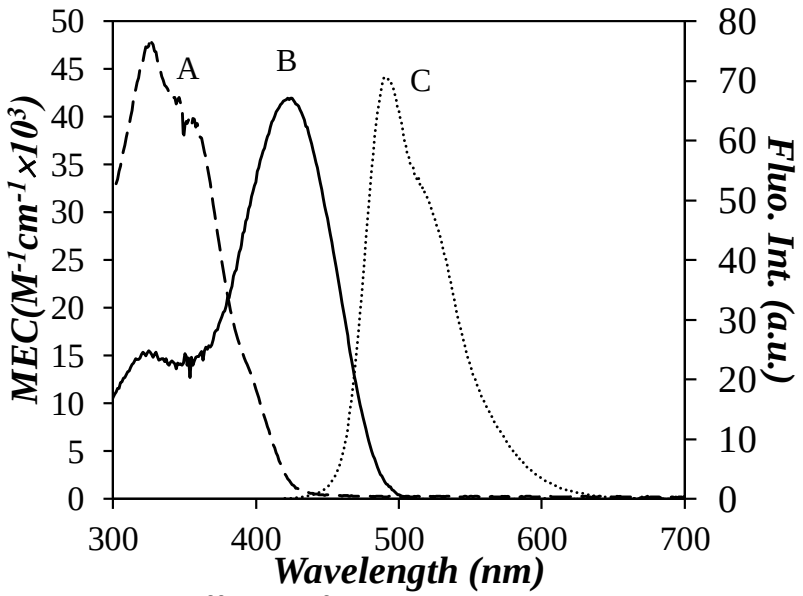

Figure 1.4. Molar extinction coefficient of A) Q_8 and B) OPV. C) Fluorescence spectrum of OPV.

The spectra shown in Figure 1.4 indicate that OPV has a maximum absorbance at 430 nm. However, the oligoquinoline backbone also exhibits residual absorption at this wavelength.

Therefore, an excitation of 479 nm was chosen instead. The fluorescence decays were collected at 510 nm.

1.2.3 Time-Resolved Fluorescence Anisotropy

TRFA experiments and the subsequent analysis of the fluorescence decays yielded the rotational time of the foldamers. The different elements that are needed with a fluorometer to conduct a TRFA experiment are depicted in Figure 1.5.

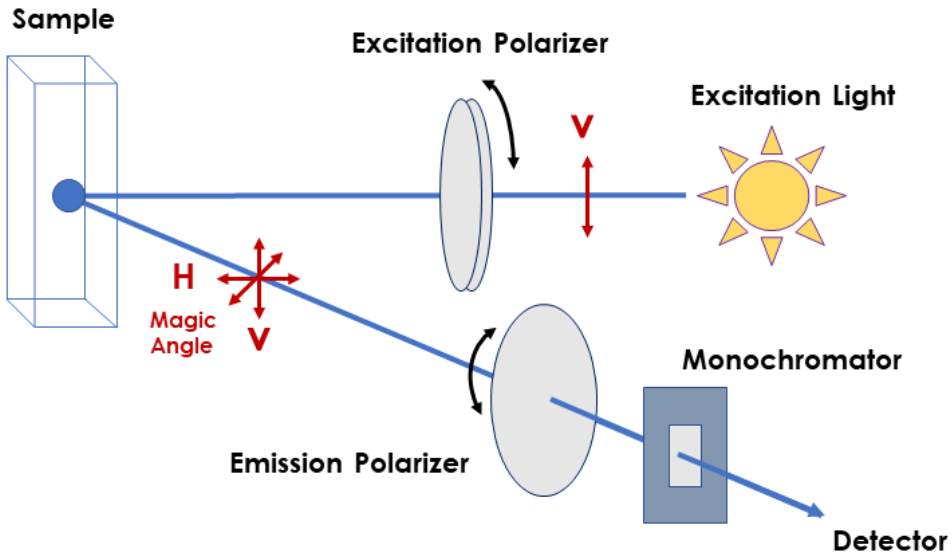

Figure 1.5. Schematic representation of the experimental set up required to conduct a TRFA experiment. The excitation is provided by a nano-LED with a narrow emission bandwidth.

The polarized fluorescence decays were obtained by using vertically polarized excitation light and collecting the emitted photons at a polarization angle that was parallel, perpendicular, and at the magic angle (54.7°, where polarization effects are eliminated) with respect to the

orientation of the excitation polarization.[44] Analysis of the decays involved first fitting the fluorescence decay acquired at the magic angle with a monoexponential function shown in Equation 1.1.

$$I_{VM}(t) = I_o e^{\left(\frac{-t}{\tau_o}\right)} \quad (1.1)$$

In Equation 1.1, I_o is the initial fluorescence intensity, t is the time in nanoseconds, and τ_o is the natural lifetime of the dye. The vertically and horizontally polarized decays were then fit globally according to Equations 1.2 and 1.3, respectively.

$$I_{VV}(t) = \frac{I_{VM(t)}}{3}(1 + 2r(t)) \quad (1.2)$$

$$I_{VH}(t) = \frac{I_{VM(t)}}{3G}(1 - r(t)) \quad (1.3)$$

In Equations 1.2 and 1.3, the G-factor is a scaling factor that is optimized during the analysis and $r(t)$ is the time-dependent anisotropy. The anisotropy $r(t)$ is well-represented by a sum of exponentials as shown in Equation 1.4.

$$r(t) = r_o \sum_{i=1}^{n} a_i e^{\left(\frac{-t}{\phi_i}\right)} \quad (1.4)$$

In Equation 1.4, r_o is the anisotropy at time t equal to zero. The pre-exponential factors a_i correspond to the i^{th} rotational time ϕ_i and they are normalized to unity ($\Sigma a_i = 1$). For the relatively

short foldamers investigated so far, $r(t)$ only needed one rotational time ($n = 1$ in Equation 1.4).[35] Global analysis of the polarized decays $I_{VV}(t)$ and $I_{VH}(t)$ yielded the rotational time ϕ of the macromolecule, which could be related to its hydrodynamic volume through Equation 1.5.

$$\phi = \frac{\eta V_h}{RT} \tag{1.5}$$

In Equation 1.5, η is the solvent viscosity, V_h is the hydrodynamic volume, the size of macromolecule and dye in solution, R is the ideal gas constant, and T is the absolute temperature in Kelvin. The rotational time determined from these studies provides insight into the internal dynamics, size, and geometry of a macromolecule.[25]

The characterization of a fluorescently labeled macromolecule by TRFA requires that the fluorophore be rigidly attached onto the macromolecule, so that the motions of the fluorophore probed by TRFA accurately represent those of the macromolecule. The solution of the fluorescently labeled macromolecule is then excited with vertically polarized light. The dyes, and the macromolecule to which they are attached, are randomly oriented in solution, but those dyes whose absorption dipole moment is parallel to that of the excitation light are most likely to become excited. This process is known as photoselection, where the selection of fluorophores through the absorption of polarized excitation light results in a polarized emission.[44] Once excited, the fluorophore continues to tumble randomly in solution and if rigidly attached to a macromolecule, its tumbling will closely reflect that of the macromolecule. The anisotropy is determined by measuring the intensity difference between vertically and horizontally polarized emissions. As time elapses and the population of vertically and horizontally polarized dyes equilibrates via diffusion, the difference between horizontally and vertically polarized emissions reaches zero and

so does the anisotropy. A measure of the time needed for the anisotropy to reach zero is given through the analysis of the TRFA decays, which yields the rotational time (ϕ). As was described in Equation 1.5, ϕ is a function of the solvent viscosity (η), absolute temperature (T) and most importantly, the hydrodynamic volume of the macromolecule (V_h). Consequently, TRFA enables one to assess the size of a macromolecular object in solution through the determination of ϕ.

1.2.4 Applications

Fluorescence anisotropy (FA) has been used to probe various phenomena encountered in biology such as protein-protein,[46] DNA-DNA,[47] and DNA-protein[48] interactions since the early 1950's as a result of the pioneering experiments conducted by Gregorio Weber.[49] FA was first used to study macromolecules, specifically proteins, as described in details by Weber in his study of bovine serum albumin and ovalbumin conjugated with 1-dimethylaminonaphthalene-5-sulfonyl chloride (dansyl chloride).[49] Since then, FA has been an indispensable tool for a variety of applications, including ligand binding and immunoassays.[50] An example of the application of FA to probe ligand binding is the study by Kasprzark and Villafranca, where they characterized the binding of fluorescent 1,N^6-ethenoadenosine 5'-monophosphate, otherwise referred to as εAMP, to *E.coli* carbamoyl-phosphate synthase (CPS) through FA titration experiments.[51] The binding of εAMP to CPS does not alter the fluorescence of the probe itself. By titrating small concentrations of the probe in the presence of excess enzyme, they were able to ascertain the intrinsic anisotropy of the fluorescent molecule as it approached a constant value of 0.176.[51] This, along with experiments using constant concentrations of the enzyme, allowed them to determine that εAMP binds to a single site on CPS with a dissociation constant K_d = 0.033 mM.[51]

More recently, fluorescence anisotropy has been used to probe the size and dynamics of foldamers with an oligoquinoline backbone.[25] Since ϕ increases linearly with increasing V_h, TRFA was applied to determine ϕ for a series of Q_n foldamers, that were terminated at one end with a methyl ester, and fluorescently labeled at the other end with an OPV dye rigidly attached to the foldamer via an amide bond. These constructs, referred to as OPV-Q_n, resulted in ϕ-values that increased linearly with increasing number (n) of quinoline units, thus implying that increasing the foldamer length by one quinoline unit increased the hydrodynamic volume of the OPV-Q_n foldamer by a fixed quantity equal to the volume of one quinoline unit.[25] This result strongly supported the notion that foldamers could be approximated as rigid cylinders, as expected from their helical conformation determined from X-ray crystallography,[29] and remained rigid in solution as symmetric top macromolecules as long as they were constituted of 33 quinoline units or less.[25] The linear relationship found between ϕ and the number of units (NU) constituting the OPV-Q_n foldamers could now be used as a calibration curve to assess, in terms of NU, the size of any OPV-Q_nE foldamers whose ϕ had been determined by TRFA.

1.2.5 Conclusions

The concepts of foldamers and the process of self-assembly were introduced in this chapter, exploring how they could be combined to prepare self-assembled foldamers. The synthesis and characterization methods relevant to the foldamers of interest to this thesis were discussed and their limitations were highlighted. The studies of some of the pioneering work of fluorescence anisotropy were presented to outline the importance and utility of this technique to chemical and clinical applications. This introduction also went over the fundamentals of time-resolved

fluorescence anisotropy and its usefulness in determining the size of macromolecules in solution. In the case of Q_n foldamers, the calibration curves constructed by TRFA in earlier work provide a simple, yet powerful, linear relationship between the size of a helical Q_n foldamer and its rotational time.[25] It has become a robust experimental technique, that allows the study of internal dynamics, geometry, and size of macromolecules in solution.

1.2.6 Thesis Outline and Objectives

The objective of this thesis was to characterize the self-assembly of helical Q_n foldamers terminated by carboxylic acids and fluorescently labeled with OPV using TRFA. A review of the different characterization techniques for oligoquinoline foldamers was provided in Chapter 1. Chapter 2 describes how these concepts were applied to characterize the closed association mechanism for the dimerization between two fluorescently labeled OPV-Q_nA foldamers as well as the asymmetric complexation of mixtures of OPV-Q_nA and unlabeled Q_mA foldamers of different sizes ($m \neq n$). Their absorption spectra provided a measure of the concentration of labeled and unlabeled species, while TRFA measurements allowed the determination of the rotational time, a measure of the macromolecular size in solution, after global analysis of the polarized fluorescence decays. Analysis of the association curves obtained by plotting the average rotational time of the different foldamer species in solution as a function of foldamer concentration yielded the equilibrium constants, that describe the formation of these self-assembled species. Chapter 3 discusses the open association mechanism with a mixture of AQ_2PQ_2A, a pentamer with two carboxylic acid groups on either end of the oligomer, and OPV-Q_8A, which in these experiments, acts as a fluorescent capping agent. The calculation of the concentration of the species in solution

was complicated by the change in the absorption spectrum of AQ_2PQ_2A upon complexation due to π-stacking. This effect needed to be taken into account to determine the exact concentration of that species in solution. Keeping the OPV-Q_8A concentration constant, the rotational time of the AQ_2PQ_2A pentamer and OPV-Q_8A mixture was monitored as a function of the molar ratio between the AQ_2PQ_2A pentamer and OPV-Q_8A. Two traces were obtained and treated with a similar mathematical procedure as was applied to the dimers and complex, in order to extract the constant describing this equilibrium. Finally, Chapter 4 summarizes the results obtained in this thesis and suggests possible experiments to be done in the future to increase the depth of this project.

Chapter 2

Closed Association Mechanism between Oligoquinoline Foldamers Probed by Time-Resolved Fluorescence Anisotropy

2.1.0 ABSTRACT

The dimerization of oligoquinoline foldamers terminated at one end with an oligo(phenylene vinylene) and at the other with a carboxylic acid (OPV-Q_nA, where n = 4, 8, 17, and 33) and the complexation of OPV-Q_8A and Q_{16}A were characterized in chloroform with the addition of a concentrated 16 M aqueous sodium hydroxide solution. UV-Vis absorption and time-resolved fluorescence anisotropy (TRFA) were applied to determine, respectively, the concentration and the average rotational time $<\phi>$ of the mixture of unassociated and associated foldamers across a range of foldamer concentrations spanning five orders of magnitude. Plots of $<\phi>$ as a function of acid group concentration revealed that $<\phi>$ increased with increasing foldamer concentration only when the foldamer solution in chloroform was vigorously mixed with the 16 M sodium hydroxide aqueous solution. Furthermore, all the plots showed that $<\phi>$ reached a plateau at high foldamer concentration. The increase in $<\phi>$ reflected the association of foldamers into larger objects by ion pairing of the carboxylate anions generated by deprotonation of the carboxylic acid of OPV-Q_nA with NaOH, while the plateau obtained at high foldamer concentration indicated that these interactions occurred via a closed association mechanism. Plotting $<\phi>$ in the high concentration plateau as a function of the number of quinoline units (*NU*) yielded a straight line, whose slope was double that of the unassociated OPV-Q_nA foldamers, thus demonstrating their dimerization. Analysis of the $<\phi>$ trends yielded the equilibrium constants (K) describing the foldamer dimerization, whose value equaled 1.0 ($\pm$0.2)$\times 10^6$ M^{-1} for the three longer OPV-Q_nA foldamers, but was about 10 times smaller for the shortest one (n = 4). The association of OPV-Q_8A and Q_{16}A yielded a complex with a $<\phi>$ matching that of OPV-Q_{24}A, and K for this complexation was similar

to that for dimerization. These experiments illustrate the robust nature of TRFA as an experimental method to probe the size of self-assembled foldamers in solution.

2.1.1 INTRODUCTION

The term foldamer describes a genre of artificial molecules, that fold into a conformationally ordered state in solution.[1-3] These states are stabilized by intramolecular, non-covalent interactions,[1,4] which are often involved in the process of intermacromolecular self-assembly.[5] Principally, self-assembly enables the production of complex architectures by spontaneous association under equilibrium conditions.[6] Many biological processes exist thanks to self-assembly and its underlying physical principles have been applied to various areas of chemistry,[7,8] materials science,[9,10] and nano-engineering.[11,12] The forces involved in a typical self-assembling system include hydrogen bonding,[13,14] hydrophobic interactions,[15] and π–π stacking between aromatic groups,[16,17] all of which are weak and reversible.[13] If these forces could be harnessed to drive the specific self-assembly of building blocks into large and ordered foldamers, it would provide a means to circumvent some of the challenges encountered with the conventional synthetic strategies applied in the preparation of long foldamers. In turn, these long and ordered foldamers could serve as molecular wires of adjustable length in molecular electronics.[18-20] From this perspective, investigation into whether oligoquinoline foldamers could be designed to self-assemble in solution would be an interesting avenue of research, since they adopt a rigid, helical conformation as a result of hydrogen bonding and aromatic stacking interactions.[21] Furthermore, their electron-rich backbone, combined with their helical structure, endows them with the ability to transfer electrons, making them suitable candidates for molecular wires.[18,22]

Beside their synthesis, the characterization of foldamers has been the focus of concerted research effort. To date, several analytical techniques have been applied to the characterization of foldamers, which include UV-Visible spectrophotometry,[23] nuclear magnetic resonance spectroscopy (NMR),[24] molecular modeling,[25,26] and single crystal X-ray Diffraction (SCXRD), [27] to name but a few.[28] While all these techniques demonstrate that the foldamers adopt a folded structure, they all have specific drawbacks particularly when it comes to characterizing their size in solution. Spectroscopy-based techniques can probe the structure of foldamers in solution, but usually not their size, whereas crystallography enables size determination of the foldamers in the solid state, but not in solution. Thus, an ideal characterization technique should be able to characterize the size of foldamers in solution. Recent developments have indicated that time-resolved fluorescence anisotropy (TRFA) meets these requirements, as it can be applied to characterize the size of helical oligoquinoline foldamers in solution.[28] Furthermore, earlier studies on helical oligonucleotide duplexes and hairpins cemented TRFA as a reliable analytical technique for the characterization of rigid, symmetric top macromolecules with a length of at least 11 nm.[29] It is also worth pointing out that the high sensitivity of fluorescence allows for the characterization of fluorescently labeled macromolecules at concentrations that are 2-to-3 orders of magnitude lower compared to the other techniques discussed earlier.[30]

In a typical TRFA experiment, a fluorophore is rigidly attached to a macromolecule and it is excited with vertically polarized light. Those fluorophores whose absorption dipole moment is parallel to the excitation light are the most likely to be irradiated, and their fluorescence is polarized along a defined orientation, a process known as photoselection.[31] As the fluorophore tumbles in solution, it reflects the tumbling of the macromolecule to which it is attached, and through

measurement of the vertically and horizontally polarized emissions, the anisotropy can be determined.[31] As time elapses, the intensities of the vertically and horizontally polarized emissions gradually approach the same value, and the anisotropy reaches zero. If the TRFA can be described by a single exponential, its decay time is referred to as the rotational time, ϕ, of the fluorophore and thus the macromolecule since the fluorophore is rigidly attached to it. The rotational time of the macromolecule found from the analysis of the TRFA decay can be used to calculate the hydrodynamic volume V_h of the macromolecule as shown in Equation 2.1,[31] where η, R, and T are the solvent viscosity, the ideal gas constant, and the absolute temperature in K, respectively.

$$\phi = \frac{\eta V_h}{RT} \tag{2.1}$$

Consequently, TRFA provides a measure of the size of a macromolecule in solution from its rotational time.

The linear relationship expressed by Equation 2.1 between the rotational time of a macromolecule and its volume led to the establishment of a calibration curve, where ϕ for oligoquinoline foldamers, terminated at one end with a methyl ester and at the other with an oligo(phenylene vinylene) (OPV), was plotted as a function of the number of quinoline units (*NU*) constituting the foldamer.[28] The linear relationship obtained between ϕ and *NU* suggested that TRFA could also be applied to predict the size of self-assembled oligoquinoline foldamers. The self-assembly of these foldamers would take place in an organic solvent like chloroform after replacing the ester functionality by a carboxylic acid, which once deprotonated with a strong base would induce the association of the negatively charged foldamers into larger entities through ion

pairing. Such ionic interactions are often evoked for anionic polymerization conducted in organic solvents to rationalize the lower polymerization rates resulting from the dimerization of the anionic propagating ends of growing chains.[32] The present study assesses the value of this proposal by considering the dimerization of four oligoquinoline foldamers terminated at one end with an OPV and at the other end with a carboxylic acid (OPV-Q_nA with n = 4, 8, 17, and 33), as well as the complexation of OPV-Q_8A with an unlabeled Q_{16}A foldamer. By monitoring the average rotational times ($<\phi>$) of mixtures of the different foldamers as a function of foldamer concentration under basic conditions, a sigmoidal curve was obtained where $<\phi>$ increased with increasing foldamer concentration from the ϕ value of the unassociated foldamer to that of their complex. This S-shaped curve described the equilibrium representing the complexation of the foldamers and could be analyzed to yield the equilibrium constant. In so doing, this study demonstrated the possible self-association of foldamers into larger foldamer-like entities and that TRFA could yield not only the size of a foldamer as had been done in earlier studies,[28,33] but also the size of self-assembled foldamers and the equilibrium constant for foldamer complexation. It further establishes TRFA as a major analytical technique for characterizing foldamer size in solution.

2.2 EXPERIMENTAL

Chemicals: Chloroform (HPLC grade, Sigma-Aldrich), sodium hydroxide (NaOH, ACS grade, Sigma Aldrich), and hydrochloric acid (HCl, 12.2 M Sigma-Aldrich) were used without further purification. The foldamer samples OPV-Q_4A, OPV-Q_8A, OPV-Q_{17}A, OPV-Q_{33}A, and Q_{16}A were supplied by the Institute of Chemistry and Biology of Membranes and Nano-objects (CBMN) at the University of Bordeaux, France.

Steady-State Fluorescence (SSF): A Horiba QM-400 spectrofluorometer equipped with a xenon arc lamp was used to acquire the fluorescence spectra. Solutions with an OPV concentration ranging from 1 nM to 1 mM were acquired with the right angle or front-face geometries for OPV concentrations, that were below or above 80 μM, respectively. The front face geometry was applied for the more concentrated solutions to minimize the inner filter effect.

UV-Visible Spectrophotometer: Absorption spectra were acquired with a Cary 100 UV-Visible spectrophotometer using quartz cells of path lengths equal to 0.1 mm, 1.0 mm, 1.0 cm, and 10.0 cm to ensure that an absorbance around unity would be obtained for improved accuracy.

Preparation of the foldamer solutions: The complexes of OPV-Q_nA with *n* equal to 4, 8, 17, and 33 were obtained by adding 0.1 g of 16 M $NaOH_{(aq)}$ solution into 7 mL of OPV-Q_nA solution in chloroform, while stirring the mixture vigorously for 2 min. Similarly, the complexes of OPV-Q_8A and Q_{16}A were generated by adding 0.1 g of 16 M $NaOH_{(aq)}$ solution to a 7 mL chloroform solution containing a 1:5 molar ratio of OPV-Q_8A:Q_{16}A and stirring the mixture vigorously for 2 min. The 5-fold excess of Q_{16}A used in these mixtures was meant to maximize the probability of having most fluorescently labeled OPV-Q_8A involved in a complex. After allowing for separation of the aqueous phase from the organic phase, the foldamer solution in chloroform was withdrawn and placed in a fluorescence cell to conduct fluorescence measurements.

Determination of the concentration of the foldamer species in solution: Since a residual fraction of the deprotonated foldamers might have partitioned themselves in the aqueous phase, using the absorbance of the chloroform solution ensured that the exact foldamer concentration in the solution could be determined. For the dimerization studies, the concentration was calculated by applying Beer-Lambert's Law based on the molar extinction coefficients ε_{OPV}(326 nm), ε_{OPV}(450 nm), and

ε_Q(326 nm), for OPV bound to a foldamer at 326 and 450 nm and a single quinoline unit at 326 nm, which had been determined to equal 13,284, 32,400, and 5,600 $M^{-1}\cdot cm^{-1}$, respectively.[28] For the complexation experiments between OPV-Q_8A and Q_{16}A, analysis of the concentration of the foldamers was complicated due to the mixture of absorbing species in solution. Taking advantage that both OPV and the quinoline units absorb at 326 nm and only OPV absorbs at 450 nm, the Beer-Lambert law could be applied to derive Equations 2.2 and 2.3, where *L* is the pathlength of the quartz cuvette used for the absorption measurements and [OPV] and [*Q*] are the concentrations of OPV and quinoline units in the solution.

$$Abs(326\ nm) = \varepsilon_{OPV}(326\ \text{nm})[OPV]\times L + \varepsilon_Q(326\ \text{nm})[\text{Q}]\times \text{L} \qquad (2.2)$$

$$Abs(450\ \text{nm}) = \varepsilon_{OPV}(450\ \text{nm})[\text{OPV}]\times \text{L} \qquad (2.3)$$

Rearrangement of Equation 2.3 into Equation 2.4 yielded the concentration of OPV and thus, the concentration of OPV-Q_8A foldamers.

$$[OPV] = \frac{Abs(450\ \text{nm})}{\varepsilon_{OPV}(450\ \text{nm})\times \text{L}} \qquad (2.4)$$

Since the concentration of OPV, ε_{OPV}(326 nm), and ε_{Q}(326 nm) were known, the concentration [*Q*] of quinolines could be obtained with Equation 2.5.

$$[Q] = \frac{Abs(326\text{ nm}) - [OPV] \times \varepsilon_{OPV}(326\text{ nm}) \times L}{\varepsilon_{Q}(326\text{ nm}) \times L} \quad (2.5)$$

The concentration of unlabeled foldamer, Q_{16}A in the mixture could therefore be determined from Equation 2.6.

$$[Q_{16}\text{ A}] = \frac{[Q] - 8 \times [OPV]}{16} \quad (2.6)$$

Time-Resolved Fluorescence Anisotropy (TRFA). The fluorescence decays were acquired with a HORIBA Ultima Ultrafast time-resolved fluorometer equipped with an excitation and emission polarizer using a 479 nm delta-diode laser as light source. The polarized fluorescence decays were acquired using a 480 nm bandpass filter on the excitation side and a 495 nm cut-off filter on the emission side to minimize residual stray light from reaching the detector. All the fluorescence decays were acquired up to a peak maximum of 20,000 counts. The same sample geometry employed for the SSF spectra was applied to acquire the TRFA decays according to their OPV concentration. The instrument response function was collected by reflecting the nano-LED light with a triangular aluminum monolith without the 495 nm cut-off filter. All the fluorescence decays were measured with a time-per-channel (TPC) of 1.28×10^{-2} ns/channel across 4,096 channels. The fluorescence decays were acquired using an excitation light that was vertically polarized, and with the polarization of the emission set at the magic angle (54.7 ^{o} for $I_{VM}(t)$) or the vertical (I_{VV}(t)) and horizontal (I_{VH}(t)) direction with respect to the vertical excitation light.

TRFA decay analysis: The analysis programs aniso01d-4k and aniso01d-7k were used to fit the I_{VV}(t) and I_{VH}(t) fluorescence decays globally with a single rotational time. The only difference

between the two programs was that the former optimized the OPV lifetime (τ_o) obtained at the magic angle and the latter used a fixed τ_o value. The parameters obtained with the program that gave a better χ^2 were reported in Tables A1-A11. The analysis of the fluorescence decays acquired to determine the TRFA of the OPV-Q_nA foldamers began by fitting the fluorescence decays acquired at the magic angle with a monoexponential function, shown in Equation 2.7, to determine the lifetime τ_o of the OPV label covalently attached to the foldamer.

$$I_{VM}(t) = I_o \exp(-t / \tau_o) \tag{2.7}$$

In Equation 2.7, I_o is the initial fluorescence intensity and t is the time in nanoseconds. The decays polarized vertically and horizontally were then fitted globally according to Equations 2.8 and 2.9, respectively.

$$I_{VV}(t) = \frac{I_o}{3} \exp(-t / \tau_o) \times [1 + 2r(t)] \tag{2.8}$$

$$I_{VH}(t) = \frac{I_o}{3G} \exp(-t / \tau_o) \times [1 - r(t)] \tag{2.9}$$

In these equations, the G-factor is a scaling constant, which was optimized during the analysis. Determination of the parameters describing the TRFA ($r(t)$) through the optimization of the G-factor has been found to be much more straightforward, accurate, rapid, and reliable than the traditional methodology involving the experimental determination of the G-factor.[28,33] $r(t)$ can be

approximated by a sum of 3 exponentials for a symmetric top macromolecule, as shown in Equation 2.10.[34]

$$r(t) = r_o \sum_{i=1}^{n} a_i \exp(-t/\phi_i) + r_\infty \qquad (2.10)$$

In Equation 2.10, r_o is the intrinsic anisotropy or anisotropy at time t equal to zero, and r_∞ describes those foldamers whose rotational time is much longer than τ_o and are most likely involved in large foldamer aggregates. Global analysis of the polarized fluorescence decays $I_{VV}(t)$ and $I_{VH}(t)$ provided the rotational times of the OPV-Q_nA foldamers. The parameters of the fit were optimized according to the Marquardt-Levenberg algorithm and are listed in Tables A1-A10 as Supporting Information (SI). The pre-exponential factors a_i are normalized to unity and correspond to the i^{th} rotational time ϕ_i. For all foldamer mixtures but those prepared with OPV-Q_{33}A, $r(t)$ required only one rotational time (n = 1 in Equation 2.10) and r_∞ equaled zero. Analysis of the fluorescence decays of OPV-Q_{33}A solutions required two rotational times (n = 2 in Equation 2.10) at intermediate to high concentrations (> 2 μM) and yielded a non-zero r_∞ at high foldamer concentration (> 60 μM), probably due to residual aggregation after mixing the foldamer solution with the 16 M $NaOH_{(aq)}$ solution. In the high concentration regime, the $I_{VM}(t)$ decays of OPV-Q_{33}A needed to be fitted with two exponentials, probably due to residual aggregation, that led to OPV excimer formation. The two pre-exponential factors and decay times representing $I_{VM}(t)$ were then fixed in the global analysis of $I_{VH}(t)$ and $I_{VV}(t)$ with the program aniso02d-4k to determine the TRFA at these concentrations.

2.3 RESULTS

TRFA was applied to characterize the size of oligoquinoline foldamers terminated with a carboxylic acid at one end in chloroform, with or without addition of 0.1 g of 16 M sodium hydroxide solution to induce their self-assembly into larger objects via ion pairing. The rotational time of the foldamers was monitored across a concentration range, that spanned five orders of magnitude, as determined from absorption measurements.

2.3.1 Characterization of the OPV-Q_nA Foldamers by TRFA

Before starting with the equilibrium experiments, the rotational time of the OPV-Q_nA foldamers were compared to those of their methyl ester equivalent (OPV-Q_nE), which had been studied earlier.[28,33] The ϕ values obtained for the OPV-Q_nA and OPV-Q_nE samples were plotted as a function of *NU* in Figure 2.1.

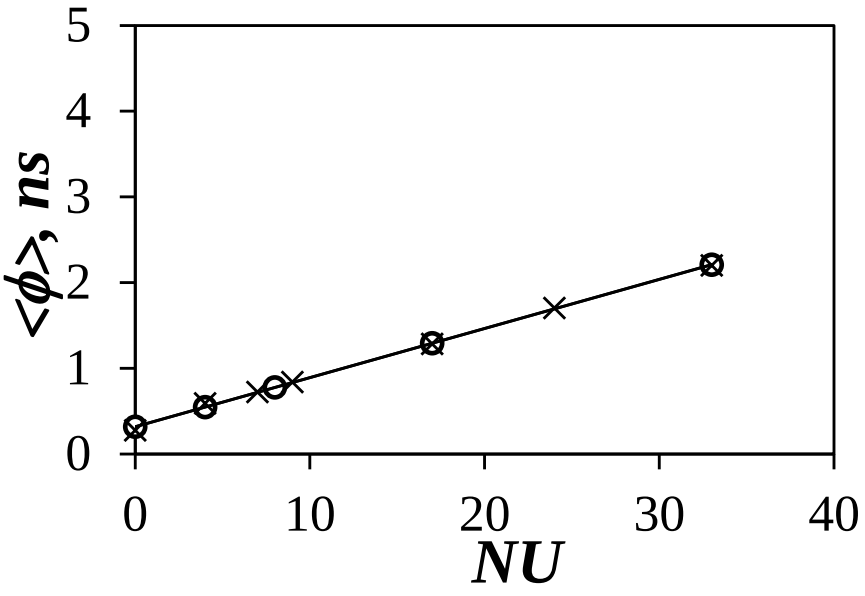

Figure 2.1. Plot of ϕ as a function of NU in chloroform for the (○) OPV-Q_nA and (×) OPV-Q_nE foldamers.

The ϕ values clustered along a common straight line indicating that in chloroform, the OPV-Q_nA foldamers exhibited the same hydrodynamic behavior as the OPV-Q_nE foldamers. Since the linear relationship shown in Figure 2.1 had been used as confirmation that the OPV-Q_nE foldamers adopted a helical conformation in chloroform,[28,33] the fact that the OPV-Q_nA constructs showed a same behavior indicated that they too adopted a helical conformation in solution. The common trend shown for OPV-Q_nA and OPV-Q_nE in Figure 2.1 demonstrated that the end functionality of these macromolecules, be it an acid or an ester, did not affect their conformation in chloroform.

2.3.2 Dimerization and Complexation of Foldamers Characterized by TRFA

Following the confirmation in Figure 2.1 that the protonated OPV-Q_nA and OPV-Q_nE samples behaved in a similar manner based on the TRFA measurements, the dimerization of OPV-Q_4A, OPV-Q_8A, OPV-Q_{17}A, and OPV-Q_{33}A and the complexation of OPV-Q_8A with a five-fold molar excess of Q_{16}A were studied by TRFA. These measurements were performed in chloroform, before and after addition of 0.1 g of 16 M sodium hydroxide solution. Since these experiments were expected to generate a mixture of unimers and complexes with different rotational times, the single rotational time retrieved from the global analysis of the polarized fluorescence decays was referred to as an average rotational time $<\phi>$ more representative of the mixture of species present in solution. Plots of the average rotational time $<\phi>$ determined by TRFA as a function of acid group concentration are presented in Figure 2.2. For the protonated samples in chloroform, $<\phi>$ remained constant with foldamer concentration and took the value expected for the unassociated foldamer over the entire foldamer concentration range covered. This result confirmed that the protonated

OPV-Q_nA remained as unimers in chloroform even at very high foldamer concentration (~ 1 mM). Upon addition of $NaOH_{(aq)}$, $<\phi>$ increased with increasing OPV-Q_nA concentration from the rotational time of the unassociated foldamer until a plateau was reached for foldamer concentrations larger than 80 μM.

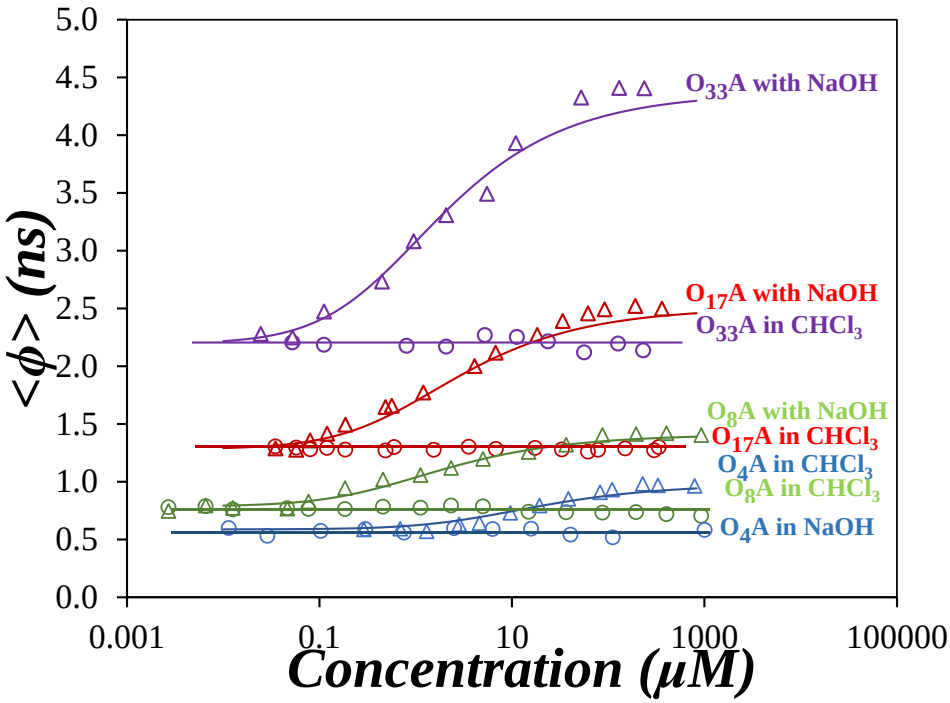

Figure 2.2. Plots of $<\phi>$ of (blue) OPV-Q_4A, (green) OPV-Q_8A, (red) OPV-Q_{17}A, and (purple) OPV-Q_{33}A with (triangles) and without (circles) NaOH.

The increase in $<\phi>$ shown in Figure 2.2 reflects the association of the OPV-Q_nA species into larger objects in solution after the addition of NaOH. The plateau observed for $<\phi>$ at high foldamer concentrations indicates that the generation of larger products must follow a closed association mechanism leading to the formation of a thermodynamically stable species, which must be the result of the deprotonation of the carboxylic acid terminals of the OPV-Q_nA foldamers. Deprotonation of the carboxylic acids by NaOH yields sodium carboxylate (NaC) ion pairs, whose

exposure to apolar chloroform is minimized through their association in solution, leading to the formation of OPV-Q_nNaC aggregates held together by the associated ion pairs and stabilized in chloroform by the oligoquinoline moieties. If this association mechanism were to involve two sodium carboxylate ion pairs, it would lead to the dimerization of the OPV-Q_nA foldamers.

To determine whether dimerization of the deprotonated OPV-Q_nNaC foldamers took place, the $<\phi>$ value referred to as $\phi(\infty)$ obtained from the plateau regions for the solutions prepared with 16 M NaOH in the $<\phi>$-*vs*-[OPV-Q_nA] profiles shown in Figure 2.2 were plotted as a function of *NU* and $2\times NU$ in Figure 2.3. $\phi(\infty)$ was found to increase linearly with increasing *NU*, indicating that the size of the OPV-Q_nNaC complexes formed in chloroform exposed to the 16 M NaOH aqueous solution was strongly correlated to the size of the OPV-Q_nA unimers. Furthermore, plotting $\phi(\infty)$ as a function of $2\times NU$ in Figure 2.3 yielded a straight line, whose slope was the same as for the straight line obtained by plotting $<\phi>$ as a function of *NU* for unassociated OPV-Q_nE foldamers in chloroform (see Figure 2.1). This result indicated that the size of the OPV-Q_nNaC complexes increased with increasing *NU* in the same manner as the size of OPV-Q_nA unimers. That this relationship was obtained by doubling the *NU* served as strong evidence, that the OPV-Q_nNaC complexes were in fact dimers.

A noticeable offset was also observed between the $\phi(\infty)$-*vs*-$2\times NU$ profile of the dimerized foldamers in chloroform with $NaOH_{(aq)}$ and the $<\phi>$-*vs*-*NU* profile of the unassociated foldamers in chloroform without $NaOH_{(aq)}$. This constant offset was attributed to the second OPV moiety in the foldamer dimers, which therefore added a constant value to the V_h probed by TRFA (see Equation 2.1). In contrast, this should not be observed for the complexation of OPV-Q_8A and unlabeled Q_{16}A, which would yield a complex with only one OPV unit. This asymmetric

complexation would result in a smaller V_h compared to the OPV-Q_nNaC dimers, which would be more comparable to the unassociated OPV-Q_nA foldamers.

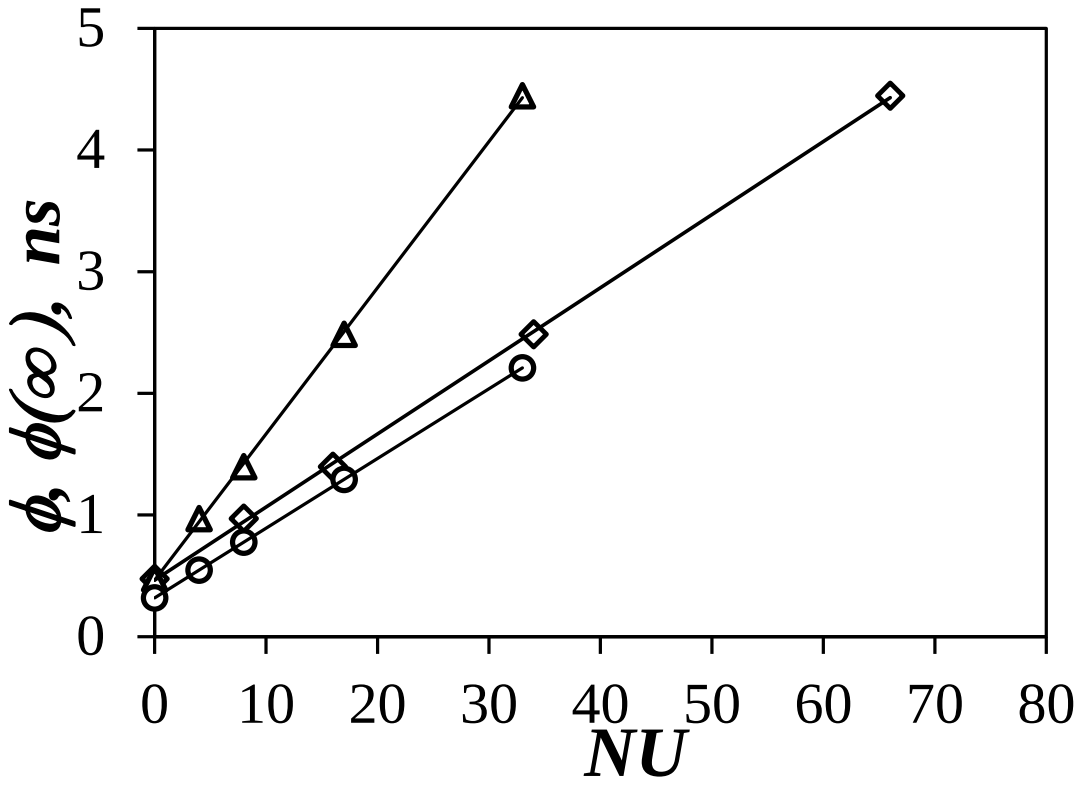

Figure 2.3. Plots of ϕ as a function of the number of quinoline units (*NU*) for (○) unassociated foldamers obtained without NaOH, (△) ϕ (∞) for the OPV-Q_nNaC foldamers with NaOH as a function of *NU*, and (◇) ϕ (∞) for the OPV-Q_nNaC foldamers with NaOH as a function of 2×*NU*. Solvent: chloroform.

2.3.3 Model and Results for the Dimerization of the OPV-Q_nA Foldamers

The model used to describe the dimerization of the OPV-Q_nA foldamers is based on three main equations described hereafter. The first equation comes from the assumption that the complexation of the foldamers can be viewed as a simple dimerization equilibrium shown in Equation 2.11,

which results in Equation 2.12, where the species A and A_2 represent the OPV-Q_nNaC unimers and dimers, respectively.

$$A + A \underset{}{\overset{K}{\rightleftharpoons}} A_2 \tag{2.11}$$

$$K = \frac{[A_2]}{[A]^2} \tag{2.12}$$

Application of the law of mass conservation yields Equation 2.13, where $[A]_o$ is the overall molar concentration of foldamer in the solution.

$$[A]_o = [A] + 2 \times [A_2] \tag{2.13}$$

Finally, the average rotational time $<\phi>$ is the experimental observable obtained from the fluorescence anisotropy measurements, which is related to the relative concentration of the OPV-Q_nNaC unimers and dimers as shown in Equation 2.14, where ϕ_1 and ϕ_2 are the rotational times of the unimer and dimer, respectively. ϕ_1 is obtained from the OPV-Q_nA unimers in chloroform without NaOH, whereas ϕ_2 equals $\phi(\infty)$ for the OPV-Q_nNaC dimers. The ϕ_1 and ϕ_2 values used in these analyses are listed in Table 2.1.

$$< \phi >_{cal} = \frac{[A] \times \phi_1 + 2 \times [A_2] \times \phi_2}{[A]_o} \tag{2.14}$$

Equations 2.12 and 2.13 can be re-arranged to yield the [A] and [A_2] concentrations as shown in Equations 2.15a and 2.15b, respectively.

$$[A] = \frac{-1 + \sqrt{1 + 4K[A]_o}}{2K} \tag{2.15a}$$

$$[A_2] = \frac{[A]_o - [A]}{2} \tag{2.15b}$$

Table 2.1. Rotational times ϕ_1 and ϕ_2 used in the analysis of the sigmoidal curves in Figure 2.2 to obtain the dimerization constant (K) for the OPV-Q_nA samples with n = 4. 8. 17. And 33.

Number of Units	ϕ_1 (ns)	ϕ_2 (ns)	K (M^{-1})
4	0.58 (±0.01)	0.98 (±0.01)	1.1 (±0.1)×10^5
8	0.8 (±0.0)	1.4 (±0.0)	1.1 (±0.2)×10^6
17	1.3 (±0.0)	2.5 (±0.0)	7.8 (±0.4)×10^5
33	2.2 (±0.1)	4.4 (±0.0)	1.10 (±0.03)×10^6

The procedure applied to extract K consists in calculating the [A] and [A_2] concentrations with Equations 2.15a and 2.15b, respectively, at the different OPV-Q_nNaC concentrations ($[A]_o$) used in the dimerization experiments for different assumed K values, determine $\langle\phi\rangle_{cal}$ with Equation 2.14, and obtain the χ^2 for this data set according to Equation 2.16, where N represents the number of experiments having been conducted.

$$\chi^2 = \frac{1}{N}\sum_{i=1}^{N} (<\phi>_{\exp} - <\phi>_{cal})^2 \qquad (2.16)$$

Plotting χ^2 as a function of K typically yields a well-behaved polynomial as shown in Figure 2.4A for the data obtained for the dimerization of OPV-Q_8A, whose minimum yields the optimal K value.

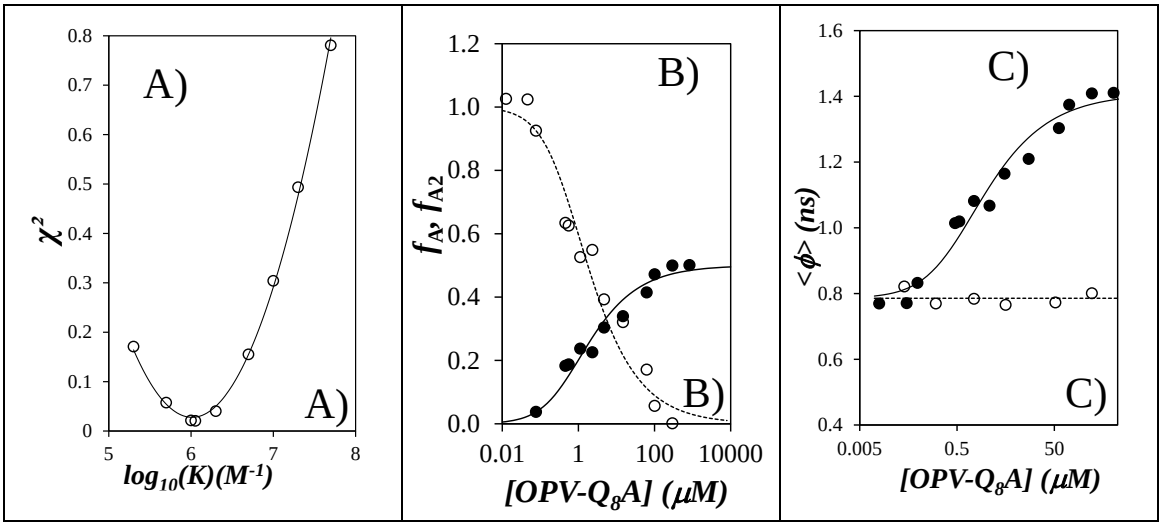

Figure 2.4. Results for the dimerization of OPV-Q_8A: A) Plot of χ^2 as a function of $log_{10}(K)$ fitted with a second order polynomial yielding a K value of 1.1 (±0.2)×10^6 M^{-1} at the minimum. Plot of B) the molar fractions of (O) unimer and (●) dimer and C) the average rotational time for solutions (●) with and (O) without 0.1 g of 16 M NaOH aqueous solution as a function of OPV-Q_8A concentration.

Finally, the [A] and [A_2] concentrations can be determined experimentally from Equations 2.13 and 2.14 as shown with Equations 2.17a and 2.17b, respectively.

$$[A] = [A]_o \times \frac{<\phi> - \phi_2}{\phi_2 - \phi_1} \tag{2.17a}$$

$$[A_2] = \frac{[A]_o}{2} \times \frac{<\phi> - \phi_1}{\phi_2 - \phi_1} \tag{2.17b}$$

Dividing [A] and [A_2] in Equations 2.17a and 2.17b by $[A]_o$ yields the molar fractions of unimer and dimer in the solution, respectively, which can be compared to the molar fractions predicted with Equations 2.15a and 2.15b by using the optimal K value. After optimization of the K value, a good agreement was obtained between the predicted and experimental molar fractions for the OPV-Q_nNaC unimers and dimers as shown in Figure 2.4B. Finally, the predicted $<\phi>_{cal}$ based on Equation 2.14 was compared in Figure 2.4C with $<\phi>_{exp}$. The good agreement obtained in Figures 2.4B and C between the predicted and experimental values supports the validity of the method.

This mathematical procedure was applied to determine the K value for the dimerization of OPV-Q_4A, OPV-Q_8A (shown in Figure 2.4), OPV-Q_{17}A, and OPV-Q_{33}A. The results obtained for the molar fractions and average rotational times after optimization are shown in Figure 2.5 for OPV-Q_4A, OPV-Q_{17}A, and OPV-Q_{33}A, yielding K values of 1.1 (±0.1)×10^5 M^{-1}, 7.8 (±0.4)×10^5 M^{-1}, and 1.10 (±0.03)×10^6 M^{-1}, respectively (see χ^2 plots in Figure A3 in SI). K for the larger foldamers took an average value of 1.0 (±0.2)×10^6 M^{-1}, which was one order of magnitude larger than for OPV-Q_4A, indicating that the equilibrium constant did not depend much on the oligomer size as long as the oligomer was 8 or more quinoline units long.

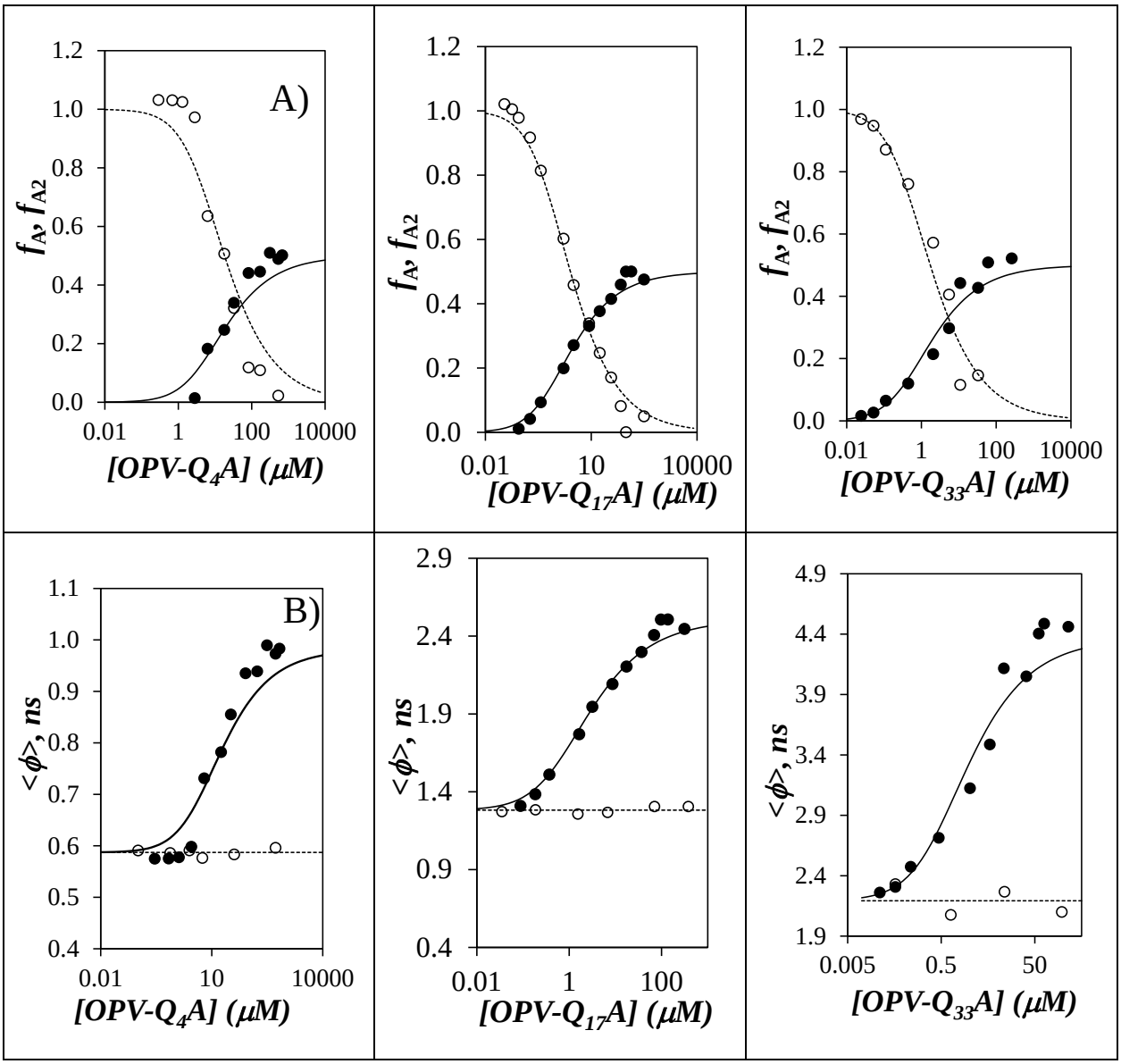

Figure 2.5. Results for the dimerization of OPV-Q_nA with n = 4, 17, and 33: A) Plot of the molar fractions of (O) unimer and (●) dimer and B) the average rotational time for solutions (●) with and (O) without 0.1 g of 16 M NaOH aqueous solution as a function of OPV-Q_nA concentration.

2.3.4 Results for the Complexation of OPV-Q_8A and Q_{16}A and their Analysis

Analysis of the polarized decays acquired with mixtures of OPV-Q_8A and Q_{16}A with and without addition of 16 M $NaOH_{(aq)}$ are shown in Figure 2.6A. As for the dimerization experiments, an increase in foldamer concentration resulted in a constant ϕ value for the protonated mixtures in chloroform indicating that OPV-Q_8A remained unassociated. Upon addition of 16 M $NaOH_{(aq)}$, $<\phi>$ increased with increasing foldamer concentration showing the same sigmoidal shape as that found for the dimerization experiments in Figure 2.2. This trend confirmed the association of OPV-Q_8A with itself and with Q_{16}A induced by the deprotonation of the carboxylic acids and their ionic interactions.

The mathematical description of the association mechanism reflected by the data shown in Figure 2.6A considered the three equilibria shown in Equations 2.18a, b, and c for the complexation of OPV-Q_8A and Q_{16}A, namely the equilibrium between first, two OPV-labeled oligoquinoline foldamers (OQ_n), second, two non-labeled oligoquinoline foldamers (Q_p), and third, one OPV-labeled foldamer (OQ_n) and one non-labeled foldamer (Q_p). The three equilibria are assumed to take place with the equilibrium constants K_n for the dimerization of OQ_n, which was determined experimentally to equal 1.1 ($\pm$0.2)$\times 10^6$ M^{-1} for the dimerization of OPV-Q_8A in Section 2.3.4, K_p for the dimerization of Q_p, and K_c for the complexation of OQ_n and Q_p. In this analysis, K_p and K_c were assumed to take similar values ($K_p \sim K_c$) to reduce the number of unknowns. This assumption was also supported by the finding that the equilibrium constant did not change much with oligoquinoline chain length as was determined in Section 2.3.3 for longer foldamers.

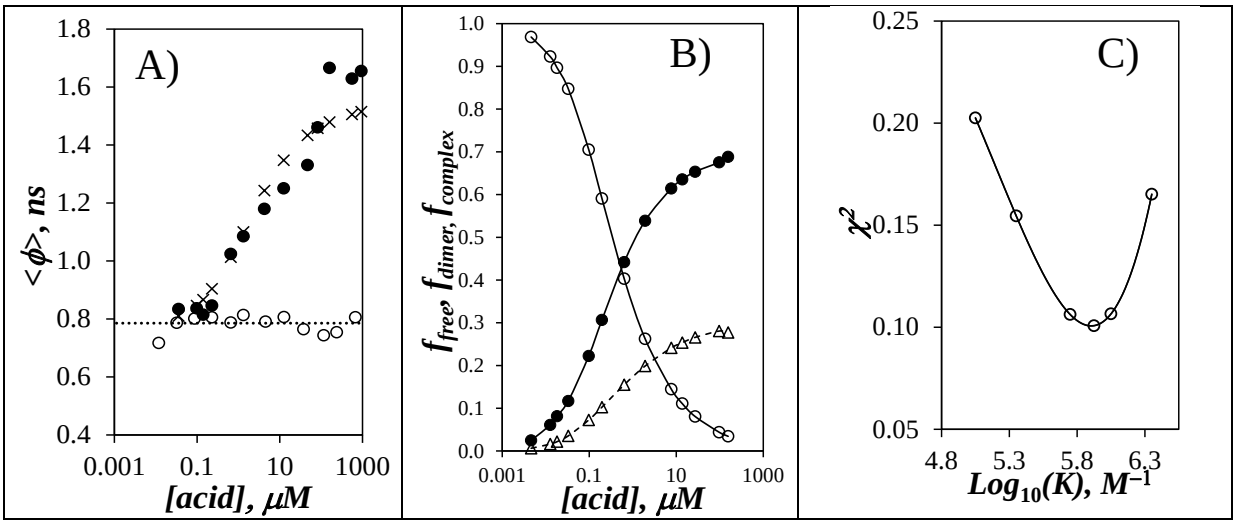

Figure 2.6. Results for the complexation of OPV-Q_8A and Q_{16}A. Plot of A) the (●) experimental and (×) calculated average rotational time for solutions with and (○) without 0.1 g of 16 M NaOH aqueous solution as a function of total acid concentration, B) the molar fractions of (○) free acids, (△) OPV-Q_8A dimers, and (●) complexes as a function of total acid concentration for the K_c value of 7.50×10^5 M^{-1}, and C) χ^2 as a function of $log_{10}(K_c)$ fitted with a fourth-order polynomial yielding a K_c value of 7.50×10^5 M^{-1} at the minimum.

$OQ_n + OQ_n \overset{K_n}{\rightleftharpoons} (OQ_n)_2$	$Q_p + Q_p \overset{K_p}{\rightleftharpoons} (Q_p)_2$	$OQ_n + Q_p \overset{K_c}{\rightleftharpoons} (OQ_nQ_p)$
(2.18a)	(2.18b)	(2.18c)

The three equilibria shown in Equations 2.18a-c resulted in the three relationships given as Equations 2.19 – 2.21.

$$K_n = \frac{[(OQ_n)_2]}{[OQ_n]^2} \tag{2.19}$$

$$K_p = \frac{[(Q_p)_2]}{[Q_p]^2} = K_c \tag{2.20}$$

$$K_c = \frac{[(OQ_nQ_p)]}{[OQ_n][Q_p]} \tag{2.21}$$

The law of mass conservation can be applied to the OQ_n and Q_p species resulting in Equations 2.22 and 2.23, where $[OQ_n]_o$ and $[Q_p]_o$ are the total concentrations of the OQ_n and Q_p species used to prepare a solution.

$$[OQ_n]_o = [OQ_n] + 2\times[(OQ_n)_2] + [(OQ_nQ_p)] \tag{2.22}$$

$$[Q_p]_o = [Q_p] + 2\times[(Q_p)_2] + [(OQ_nQ_p)] \tag{2.23}$$

Finally, Equation 2.24 represents the average rotational time $<\phi>$ retrieved from the time-resolved fluorescence anisotropy experiments as a function of the rotational times and concentrations ϕ_1 and $[OQ_n]$ for the OPV-Q_nA unimer, ϕ_2 and $[(OQ_n)_2]$ for the OPV-Q_nA dimer, and ϕ_c and $[OQ_nQ_p]$ for the complex between OPV-Q_nA and Q_pA. In Equation 2.24, ϕ_1 and ϕ_2 were taken to equal 0.8 (±0.0) and 1.4 (±0.0) ns, respectively, as determined in Figure 2.3. ϕ_c equaled 1.7 (±0.1) ns, which represented the rotational time of a hypothetical OPV-Q_{24}E foldamer, determined from the calibration curve derived earlier.[28]

$$<\phi> = \frac{[OQ_n]\times\phi_1 + 2[(OQ_n)_2]\times\phi_2 + [(OQ_nQ_p)]\times\phi_c}{[OQ_n]_o} \tag{2.24}$$

The six Equations 2.19 – 2.24 can be used to resolve the six unknowns $[OQ_n]$, $[(OQ_n)_2]$, $[(OQ_nQ_p)]$, $[Q_p]$, $[(Q_p)_2]$, and K_c (= K_p). The following procedure was implemented to find the six unknowns from these six equations. First, a K_c value was assumed and used to solve Equation 2.25 obtained by combining Equations 2.19 – 2.23 to yield $[OQ_n]$.

$$-2K_c(K_c-4K_n)[OQ_n]^4-(K_c-6K_n)[OQ_n]^3+(1+(K_c-8K_n)[OQ_n]_o-K_c[Q_p]_o)[OQ_n]^2 \\ -3[OQ_n]_o[OQ_n]+2[OQ_n]_o^2=0 \quad (2.25)$$

Knowing $[OQ_n]$ provided the concentrations $[(OQ_n)_2]$, $[Q_p]$, and $[(OQ_nQ_p)]$ as shown in Equations 2.26 – 2.28 derived from Equations 2.19 – 2.23.

$$[(OQ_n)_2]=K_n[OQ_n]^2 \quad (2.26)$$

$$[Q_p]=\frac{[OQ_n]_o-[OQ_n]-2\times[(OQ_n)_2)]}{K_c[OQ_n]} \quad (2.27)$$

$$[(OQ_nQ_p)]=K_c[OQ_n][Q_p] \quad (2.28)$$

Having determined the concentrations of all the species containing an OPV-label for a given K_c value allowed the calculation of $<\phi>$, referred to as $<\phi>_{cal}$, with Equation 2.24. Minimizing the difference between the experimentally determined $<\phi>_{exp}$ and calculated $<\phi>_{cal}$ values with Equation 2.16 provided a means to optimize K_c. The optimal K_c led to a set of $<\phi>_{cal}$ values that would satisfyingly represent the experimental $<\phi>_{exp}$ values.

Minimization of χ^2 in Equation 2.16 was accomplished by assuming different K_c values and applying the procedure described above to determine a set of $<\phi>_{cal}$ values obtained for the complexation of OPV-Q_8A and Q_{16}A, which were compared to $<\phi>_{exp}$. The χ^2 values obtained for different K_c were plotted as a function of K_c in Figure 2.6C. The plot could be fitted with a fourth order polynomial, whose minimum yielded the optimum K_c value of 7.5×10^5 M^{-1}, whose magnitude was comparable with the equilibrium constants obtained in Section 2.3.3 for the dimerization of the larger OPV-Q_nA foldamers with $n \geq 8$. The molar fractions of OPV-Q_8A involved in free foldamers (f_{free}), OPV-Q_8A dimers (f_{dimer}), and complexed foldamers ($f_{complex}$) were plotted as a function of total foldamer concentration ($[OQ_n]_o + [Q_p]_o$) in Figure 2.6B. At low foldamer concentration, the foldamers exist mainly as unimers with f_{free} being close to unity. As the foldamer concentration increases, f_{free} decreases and f_{dimer} and $f_{complex}$ increase as the foldamers generate more complexes. The quality of the optimization procedure can be visualized in Figure 2.6A, where the crosses represent the calculated $<\phi>_{cal}$, which were found to follow the experimental $<\phi>_{exp}$ values.

2.3.5 Analysis of the Intrinsic Anisotropy of the Foldamer Complexes

Analysis of the polarized fluorescence decays also yielded the intrinsic anisotropy r_o from Equation 2.10, which is a function of the angle between the absorption and emission dipole moments of a chromophore.[31] The maximum theoretical value of r_o is 0.4. This value indicates that the absorption and emission dipole moments are parallel, whereas the minimum r_o value of –0.2 would correspond to perpendicular moments.[31] The r_o for OPV bound to short oligoquinoline foldamers has been reported to equal 0.39 (±0.01),[28] close to the theoretical maximum value indicating parallel absorption and emission dipole moments, as determined in earlier studies.[35]

However, as *NU* increased for the OPV-Q_nE foldamers, r_o has been found to decrease due to a loss of initial orientation between the absorption and emission dipole moments.[28] This orientation loss was attributed to the wobbling of the OPV unit with respect to the helical foldamer, that would occur on a timescale too short to be probed by the time-resolved fluorescence experiments.

The r_o obtained in the complexation experiments of the OPV-Q_nA foldamers are shown in Figure 2.7. Generally speaking, the r_o values of the deprotonated samples were similar to those of the unassociated foldamer samples at low foldamer concentrations. A gradual decrease in r_o from ~ 0.35-0.40 to ~0.25 was observed with increasing concentration of both unimers and complexes, although the decrease was much more pronounced for the OPV-Q_4NaC dimers. The decrease in r_o was also more pronounced than that from 0.40 to 0.31, that had been found as *NU* of the OPV-Q_nE foldamers increased from 4 to 32.[28] The gentle decrease in r_o observed with increasing concentration of both the unimers and complexes might have been a consequence of residual re-absorption of the polarized fluorescence, that might have taken place at the higher foldamer concentrations despite the use of front face geometry in the TRFA experiments. This effect might have resulted in an apparent loss in orientation between the absorption and emission dipole moments of OPV, which was reflected in the reduction in r_o. The most significant reduction in r_o between dimer and unimer was observed for the OPV-Q_4NaC dimer in Figure 2.7A. It was attributed to energy transfer between the two OPV moieties since the OPV-Q_4NaC dimer generated the shortest separation distance between the two OPV moieties, which would have been more conducive of energy transfer.

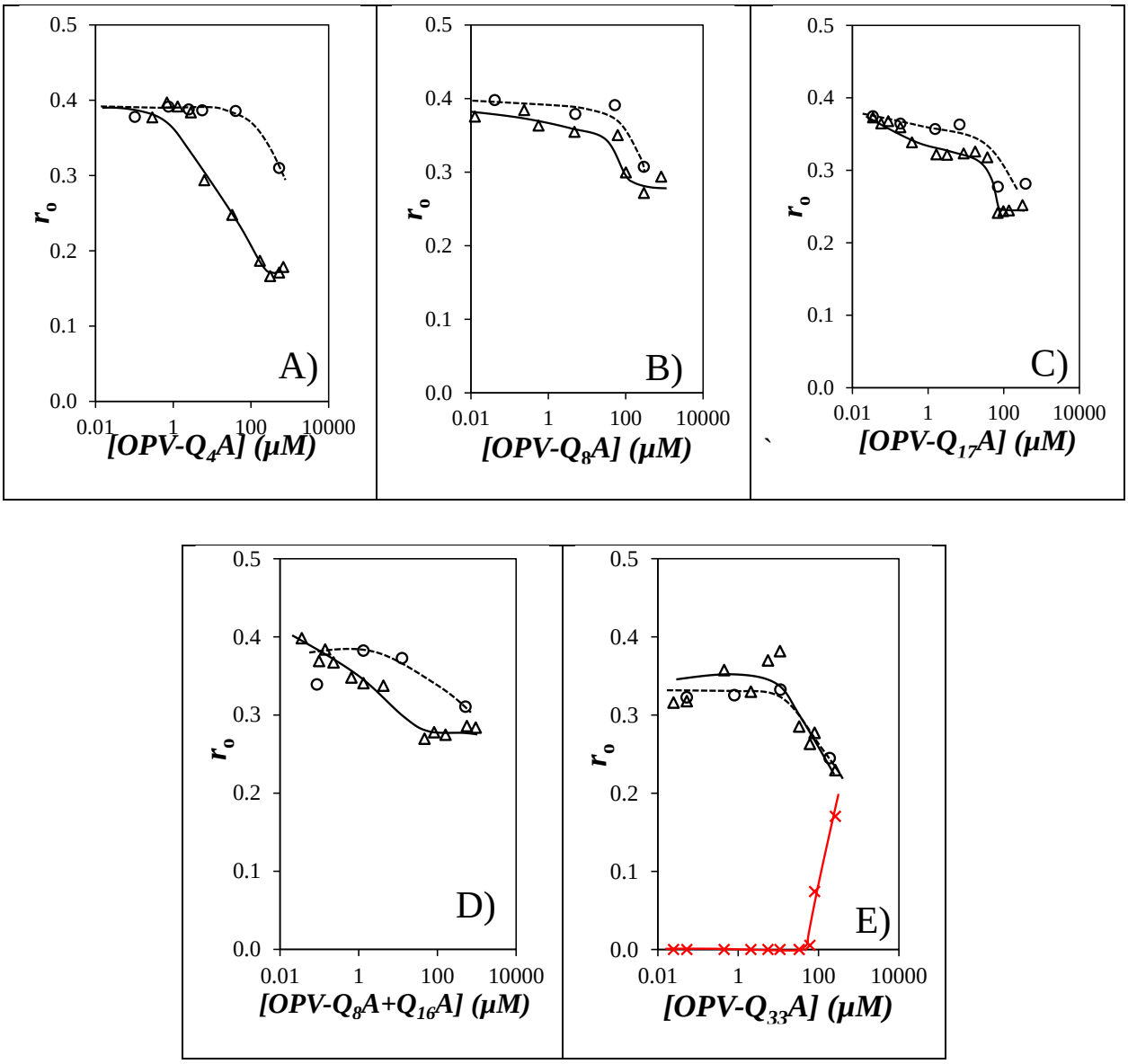

Figure 2.7. Plot of the intrinsic anisotropy (r_o) as a function of acid concentration before (○) and after (△) the addition of 0.1 g of 16 M $NaOH_{(aq)}$ for A) OPV-Q_4A, B) OPV-Q_8A, C) OPV-Q_{17}A, D) OPV-Q_8A + Q_{16}A, and E) OPV-Q_{33}A with r_∞ (×) as a function of acid concentration.

Contrary to all the other samples, the analysis of the polarized decays acquired with OPV-Q_{33}A required two rotational times (n = 2 in Equation 2.10) at intermediate to high concentrations (> 2 μM) and the inclusion of a parameter known as r_∞ at very high concentrations (> 60 μM), representing those OPV-Q_{33}NaC molecules whose rotational time was much longer than τ_o. At these high concentrations, the fit of the $I_{VM}(t)$ decay required two exponentials, whose pre-exponential factors and decay times were fixed in the global analysis of the $I_{VH}(t)$ and $I_{VV}(t)$ decays. The bi-exponential $I_{VM}(t)$ decay was probably due to OPV-Q_{33}NaC molecules, involved in large aggregates resulting from the poor solubility of OPV-Q_{33}NaC in chloroform, which yielded a non-zero r_∞ value. Residual aggregation of OPV-Q_{33}A molecules might have brought OPV moieties in close contact, that might have led to the formation of OPV dimers, which after excitation would emit with a different lifetime.[36] r_∞ was plotted as a function of OPV-Q_{33}A concentration in Figure 2.7E and was found to increase with increasing OPV-Q_{33}NaC concentration above 60 μM, as would be expected if more aggregates were generated. The need of two rotational times for $r(t)$ in Equation 2.10 was justified by considering that OPV-Q_{33}NaC dimers were long enough to yield sufficiently different rotational times, that could be resolved through the analysis of TRFA decays.[28]

2.4. DISCUSSION

The K values obtained for the dimerization of OPV-Q_4A, OPV-Q_8A, OPV-Q_{17}A, and OPV-Q_{33}A and the complexation of OPV-Q_8A and Q_{16}A were plotted in Figure 2.8 as a function of the NU for the complexes, that the different foldamer mixtures were expected to form. The equilibrium

constants determined from the analyses described in Sections 2.3.3 and 2.3.4 yielded an average value of 9.4 (±1.8)×10^5 M^{-1} for all foldamers, except for the notable exception of OPV-Q_4A, the shortest foldamer studied, which had an equilibrium constant equal to 1.1 (±0.1)×10^5 M^{-1}. Except for OPV-Q_4A, the value of these equilibrium constants reflected strong association between the foldamers, conducive of their effective self-assembly. For instance, a *K* value of 2.2×10^6 M^{-1} has been reported for the self-association of 2-ureido-4-pyrimidones,[37] which has the same magnitude as the association equilibrium constants of the longer OPV-Q_nA foldamers in Figure 2.8.

The lower equilibrium constant obtained for OPV-Q_4A could be viewed as a consequence of the Derjaguin-Landau-Verwey-Overbeek (DLVO) theory,[38] which states that the potential between two charged particles in solution results from the balance between long-range repulsive electrostatic forces and short-range attractive van der Waals (vdW) forces. At short distances, vdW forces dominate, the interaction potential passes through a deep minimum, and the charged particles are bound to each other. At intermediate distances the combination of electrostatic and vdW forces generates a maximum, which needs to be overcome by two incoming charged particles to result in aggregation. At very long distances, the potential passes through a shallow minimum and reaches zero at extremely large distances, where the charged particles no longer interact. In order to associate, two charged particles must overcome the potential energy maximum at intermediate distances. This requires that charged particles have sufficient kinetic energy, which is related to their velocity and mass. Smaller particles with a lower mass will have a lower kinetic energy and will not be as capable as larger particles to overcome the energy barrier of the interaction potential.

A similar situation is probably at play with the OPV-Q_nNaC foldamers in chloroform. The sodium carboxylate ions lead to long-range electrostatic repulsion between the foldamer ends in solution, whereas π–π stacking and hydrogen bonding between the oligoquinoline foldamer ends result in short-range attractive forces. These opposite forces generate an interaction potential similar to the DLVO one, whereby OPV-Q_nNaC foldamers must be sufficiently large to have enough kinetic energy to clear the potential maximum at intermediate distances. The smaller size, and thus mass of OPV-Q_4NaC, results in a lower kinetic energy, that does not allow this foldamer to clear the potential maximum at intermediate distances as efficiently as the larger foldamers with a larger mass and thus larger kinetic energy. The trend shown in Figure 2.8 suggests the existence of a threshold, whereby the larger oligoquinolines with 8 or more quinoline units have sufficient kinetic energy to clear the potential maximum leading to their efficient association. Those foldamers yield a large association constant of 9.4 (±1.8)×10^5 M^{-1}.

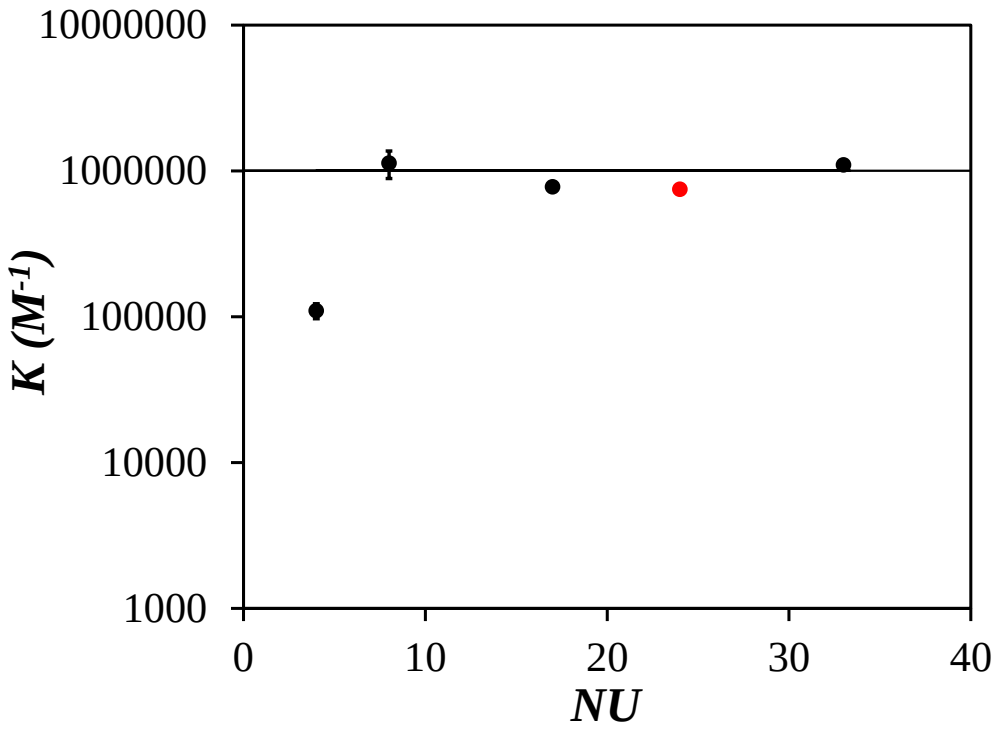

Figure 2.8. Plot of the equilibrium constants for (black) the dimerization of OPV-Q_4A, OPV-Q_8A, OPV-Q_{17}A, OPV-Q_{33}A and (red) the complexation of OPV-Q_8A with Q_{16}A.

The dimerization of the oligoquinoline foldamers described in this study also illustrates that large well-defined foldamers can be generated in solution through self-association. As demonstrated in Figure 2.2, a single large complex exists at OPV-Q_nA concentration larger than 100 μM. The dimer of an OPV-Q_{33}A construct would have been constituted of 66 quinolines, one of the largest oligoquinolines prepared to date, since the largest oligoquinoline foldamer reported in the literature was 96 units-long.[39] However, compared to the traditional multistep strategy applied to synthesize oligoquinoline constructs, the ability to generate a 66 quinoline-long

foldamer by simply mixing an OPV-Q_{33}A solution in chloroform with a drop of 16 M $NaOH_{(aq)}$ seems to offer a facile alternative for producing long oligoquinoline foldamers.

2.5 CONCLUSIONS

The association in chloroform of five different foldamer species was characterized by TRFA. These studies included the dimerization of OPV-Q_nA, where n = 4, 8, 17, and 33, and the complexation of OPV-Q_8A with a 5-fold molar excess of Q_{16}A. The concentration of the oligoquinoline foldamers in solution was confirmed by measuring the absorbance of the solutions, and TRFA was applied to obtain $<\phi>$ for foldamers in chloroform with and without exposure to 16 M $NaOH_{(aq)}$. This study used the established correlation between $<\phi>$ and foldamer size to characterize the extent of association between the foldamers generating foldamer complexes,[28] as larger $<\phi>$ determined by TRFA for solutions of OPV-Q_nNaC foldamers reflected the formation of large complexes. These complexes were found to form between deprotonated OPV-Q_nA foldamers in chloroform solution after exposure to $NaOH_{(aq)}$. The sigmoidal trends obtained by plotting $<\phi>$ as a function of foldamer concentration for all deprotonated OPV-Q_nA samples indicated that the foldamers underwent closed association resulting in the formation of well-defined products. The products obtained from the complexation of the deprotonated OPV-Q_nA samples were confirmed to be in fact dimers by noting that $\phi(\infty)$, obtained from the plateau regions of the sigmoidal curves in Figure 2.2, increased linearly with $2\times NU$ in Figure 2.3 with a slope equal to that of the straight line obtained by plotting ϕ for the oligoquinoline unimers as a function of NU in Figure 2.1. The sigmoidal trends could be analyzed further to determine the equilibrium constants of dimerization and complexation of several oligoquinoline foldamers, which took an

average value of 9.4 (±1.8)×10^5 M^{-1}, excluding the outlier value of 1.1 (±0.1)×10^5 M^{-1} for OPV-Q_4A. The negative carboxylate anions generated by the deprotonation of the OPV-Q_nA samples is believed to drive this association mechanism, that leads to the formation of polar ion pairs shielded from the apolar chloroform by the oligoquinoline backbones. Additional stabilization of the complexes is provided by π-π stacking between the terminal quinolines of the dimerized foldamers. The application of TRFA to characterize the size of the OPV-Q_nNaC products formed in apolar chloroform upon exposure of the OPV-Q_nA samples to 16 M $NaOH_{(aq)}$ illustrates how well-defined extended oligoquinoline foldamers can be generated through self-association in solution. It opens the path to the simple preparation of oligoquinoline foldamers that can be at least 66 quinoline-long, as found for the OPV-Q_{33}A dimer.

Chapter 3

Open Association Mechanism for Oligoquinoline Foldamers Characterized by Time-Resolved Fluorescence Anisotropy

3.1.0 ABSTRACT

The complexation between a quinoline octamer terminated at one end with an oligo(phenylene vinylene) and a carboxylic acid at the other end (OPV-Q_8A) and an AQ_2PQ_2A monomer made of a central pyridine flanked by two quinoline units and terminated at either end with a carboxylic acid were characterized in chloroform with the addition of a concentrated 16 M sodium hydroxide aqueous solution. Each sample was analyzed through a combination of UV-Vis absorption to determine the concentration of each species in solution and time-resolved fluorescence anisotropy (TRFA) to yield the average rotational time $<\phi>$ of the mixture of complexed foldamers across a range of foldamer concentration spanning 4 orders of magnitude. Plots of $<\phi>$ as a function of the concentration ratios of AQ_2PQ_2A to OPV-Q_8A demonstrated that $<\phi>$ increased with increasing foldamer concentration only when the foldamer solution in chloroform was vigorously mixed with the 16 M sodium hydroxide aqueous solution. For the two sets of experimental conditions studied, where a constant concentration of 1 and 10 μM of OPV-Q_8A was used, the plots demonstrated an exponential increase in $<\phi>$ at high AQ_2PQ_2A concentrations. The increase in $<\phi>$ reflected the association of foldamers into larger objects by ion pairing of the carboxylate anions generated by deprotonation of the carboxylic acids of OPV-Q_8A and AQ_2PQ_2A with NaOH, while the absence of a plateau at higher concentration indicated that these interactions occurred *via* an open association mechanism. Analysis of the trends obtained for $<\phi>$ yielded the equilibrium constants (K) describing the foldamer complexation, whose value equaled 4.25×10^5 M^{-1} for both OPV-Q_8A concentrations studied. These experiments illustrate the robust nature of TRFA as an experimental method to probe the size of self-assembled foldamers in solution.

3.1.1 INTRODUCTION

Polymers are a class of materials composed of repeating subunits generated through the reaction of monomers. Whether natural or synthetic, these macromolecules are pervasive in everyday life, from synthetic plastics composed of a variety of polymers such as poly(ethylene terephthalate),[1] polyethylene,[2] or poly(vinyl chloride)[3] to biological macromolecules such as polysaccharides,[4] polynucleotides,[5] and polypeptides,[6] which are crucial to biological functions. These polymers are formed through the successive reactions of smaller monomer molecules, which are linked together by covalent bonds, that endow the polymer with remarkable physical properties, that include high elasticity,[7] viscoelasticity,[8] and mechanical strength[9] as a result of their large molecular mass. Supramolecular polymers on the other hand, represent a genre of macromolecules that are generated by self-assembly,[10] where monomers are linked *via* weak, reversible, and highly directional non-covalent interactions[11] that include hydrogen bonding[12] and π-π stacking,[13,14] to name but a few. Self-assembly allows for the generation of complex architectures by spontaneous association under equilibrium conditions.[15] Many biological processes exist thanks to self-assembly, whose underlying physical principles have been applied to various areas of chemistry[16] and nano-engineering.[17] Self-assembled macromolecules have the disadvantage of lacking the mechanical strength and durability of their covalent counterparts, but have the advantage of being extremely tunable and adaptive materials capable of applications beyond the scope of conventional polymers in a variety of fields including drug delivery,[18] tissue engineering,[19] and molecular electronics.[20-22]

Foldamers represent a class of synthetic macromolecules, that fold into ordered secondary structures in solution, stabilized by intramolecular non-covalent interactions.[23] In the case of

oligoquinoline foldamers, they adopt a rigid helical conformation as a result of hydrogen bonding and aromatic stacking interactions.[24] With an electron-rich backbone and helical architecture conducive of electron transfer,[25] the ability of oligoquinoline foldamers to act as molecular wires has been investigated.[26] However, such applications require fairly long oligoquinoline constructs, whose stepwise synthesis is tedious and time-consuming. In contrast, the directional self-assembly of specifically designed building blocks into large and ordered foldamers could circumvent some of the challenges encountered with conventional synthetic strategies. In particular, the self-assembly of shorter oligoquinolines into larger constructs could yield large foldamers with potential applications as molecular wires of adjustable length in molecular electronics.[25] As a result of their appealing properties, oligoquinoline foldamers have been the focus of concerted research effort, which includes the characterization of their macromolecular size. Numerous analytical techniques have been applied to determine the dimensions of foldamers in particular and macromolecules in general, which include UV-Visible spectrophotometry (UV-Vis),[27] nuclear magnetic resonance spectroscopy (NMR),[28] dynamic light scattering (DLS),[29] and single crystal X-ray diffraction (SCXRD).[30] While crystallography yields the size of a foldamer in the crystalline state, crystal packing forces might lead the foldamer to adopt a different conformation than that obtained in solution, as was found for oligonucleotides,[31,32] whereas spectroscopy-based techniques provide information about the conformation of a foldamer in solution but not about its size. An ideal characterization technique would probe the size of a foldamer in solution. For the time being, time-resolved fluorescence anisotropy (TRFA) appears to be a most suitable technique capable of providing this type of information for the short length scales of helical oligomers, as illustrated in several studies with oligonucleotide duplexes and hairpins,[33] and oligoquinoline

foldamers end-labeled with an oligo(phenylene vinylene) (OPV) dye.[34] Additionally, the high sensitivity of fluorescence allows the characterization of fluorescently labeled macromolecules at concentrations, that are 2 – 3 orders of magnitudes lower compared to the NMR and SCXRD techniques discussed earlier.[30]

A typical TRFA experiment begins by irradiating a sample with vertically polarized light. While the fluorophores are randomly oriented in solution, those whose absorption dipole moment is parallel to the excitation light have the greatest likelihood of being excited, and therefore emit a photon along the direction of the emission dipole moment with a likelier orientation in a process known as photoselection.[35] If the fluorophore is rigidly attached to a macromolecule, the tumbling of the fluorophore reflects the tumbling of the macromolecule in solution, and through the measurement of the emission parallel and perpendicular to the direction of the polarized excitation light, the anisotropy can be determined.[30] As time elapses, the intensities of the vertically and horizontally polarized emissions eventually reach a same value, and the anisotropy equals zero. If the TRFA can be described by a single exponential, the resulting decay time is called the rotational time, ϕ, of the fluorophore, and therefore of the macromolecule to which it is attached. The rotational time of the macromolecule found from the analysis of the TRFA decay can then be used to calculate the hydrodynamic volume of the macromolecule as shown in Equation 3.1, where η, R, and T are the solvent viscosity, the ideal gas constant, and the absolute temperature in K, respectively.

$$\phi = \frac{\eta V_h}{RT} \tag{3.1}$$

As a result, a TRFA measurement yields the volume of a macromolecule in solution by determining its rotational time.

This feature was recently taken advantage of to establish a calibration curve between the ϕ values of a series of oligoquinoline foldamers, terminated at one end with a methyl ester and at the other end with an oligo(phenylene vinylene) (OPV-Q_nE with n = 4, 7, 9, 17, 24, and 32), as a function of their number of quinoline units (*NU*). The linear relationship obtained between ϕ and *NU* suggested that TRFA could be applied to predict the size of oligoquinoline foldamers, where the methyl ester functionality had been hydrolyzed into a carboxylic acid, which once deprotonated with a strong base, could induce their directional self-assembly into larger foldamers through the formation of ion pairs. The aim of the present study was to assess the validity of this proposal by considering the oligomerization of a pentamer composed of a central pyridine flanked by two quinoline units, terminated at both ends with a carboxylic acid (AQ_2PQ_2A) in a mixture with a quinoline octamer terminated at one end with an OPV and at the other with a carboxylic acid (OPV-Q_8A) to act as a fluorescent capping agent. The average rotational times ($<\phi>$) of mixtures prepared with a constant OPV-Q_8A concentration and increasing AQ_2PQ_2A concentration under basic conditions led to an exponential increase in $<\phi>$ with increasing AQ_2PQ_2A concentration. The exponential increase in $<\phi>$ with increasing AQ_2PQ_2A concentration reflected the oligomerization of the AQ_2PQ_2A monomers, whose extent was controlled by the equilibrium constant for this open association mechanism. Analysis of the $<\phi>$-*vs*-[AQ_2PQ_2A] profiles yielded the equilibrium constant for this association, which was found to equal 4.25×10^5 M^{-1}, a value large enough to induce the oligomerization of AQ_2PQ_2A. Consequently, this study further demonstrates that TRFA yields not only the size of a foldamer in solution as had been done before,[34] but also

the size of self-assembled foldamers and the equilibrium constant for foldamer complexation. It further establishes TRFA as a major analytical technique for characterizing foldamer size in solution.

3.2 EXPERIMENTAL

Chemicals: Chloroform (HPLC grade, Sigma-Aldrich), sodium hydroxide (NaOH, ACS grade, Sigma Aldrich), and hydrochloric acid (HCl, 12.2 M Sigma-Aldrich) were used without further purification. The foldamer samples OPV-Q_8A and AQ_2PQ_2A were supplied by the Institute of Chemistry and Biology of Membranes and Nano-objects (CBMN) at the University of Bordeaux, France.

Steady-State Fluorescence (SSF): The right-angle geometry was employed to acquire the fluorescence spectra of mixtures of either 1 or 10 μM of OPV-Q_8A with AQ_2PQ_2A concentrations ranging from 1 μM to 1 mM with a Horiba QM-400 spectrofluorometer equipped with a xenon arc lamp.

UV-Visible Spectrophotometer: A Cary 100 UV-Visible spectrophotometer was used to acquire all absorption spectra with quartz cells of path lengths equal to 0.1 mm, 1.0 mm, and 1.0 cm. The cell pathlength was selected to obtain an absorbance around unity for improved accuracy.

Preparation of the foldamer solutions: Complexation of OPV-Q_8A and AQ_2PQ_2A was induced by first, adding 0.1 g of a 16 M $NaOH_{(aq)}$ solution into 4.0 g of an OPV-Q_8A stock solution containing a known amount of AQ_2PQ_2A, and second, by vigorously stirring the solution for 2 minutes. The AQ_2PQ_2A concentrations ranged from 1 μM to 1 mM, while the OPV-Q_8A concentration was set to either 1 or 10 μM in two separate sets of experiments, to monitor chain extension from the

pentamer. After allowing the aqueous phase to separate from the organic phase over two days, the foldamer solution in chloroform was withdrawn and placed in a fluorescence cell to conduct the fluorescence measurements.

Determination of the concentration of the foldamer species in solution: With their negative carboxylate anion(s), the deprotonated foldamers and particularly the disodium carboxylate $NaCQ_2PQ_2NaC$ could remain in the aqueous phase, where they would be prevented from participating in the oligomerization with OPV-Q_8A. However, the exact foldamer concentration in the chloroform solution could be determined from careful analysis of the absorption spectra before and after addition of 0.1 g of the 16 M $NaOH_{(aq)}$ solution to the foldamer solutions in chloroform. The absorption spectra were analyzed by applying Beer-Lambert's Law based on the molar extinction coefficients ε_{OPV}(326 nm), ε_{OPV}(450 nm), and ε_{Q}(326 nm) for OPV at 326 and 450 nm and a single quinoline unit at 326 nm, which had been determined to equal 13,284, 32,400, and 5,600 $M^{-1}\cdot cm^{-1}$, respectively.[28] The molar absorbance coefficient of AQ_2PQ_2A at 326 nm was found to equal 27,700 (±400) $M^{-1}\cdot cm^{-1}$ in pure chloroform. However, after the addition of 0.1 g of 16 M $NaOH_{(aq)}$ solution, $\varepsilon_{AQ2PQ2A}$(326 nm) became concentration dependent due to hypochromicity, where π–π stacking between the two terminal quinoline units resulted in a decrease in absorbance.[36] Upon increasing the AQ_2PQ_2A concentration, $\varepsilon_{AQ2PQ2A}$(326 nm) in chloroform with base added decreased from 27,700 $M^{-1}\cdot cm^{-1}$ to 18,900 (±200) $M^{-1}\cdot cm^{-1}$, as displayed in Figure 3.1A. The effect that the hypochromicity observed in Figure 3.1A had on the absorbance can be viewed in Figure 3.1B, where the onset of hypochromicity at ~ 7 μM results in a break in the linear relationship between the absorbance and AQ_2PQ_2A concentration. Since both OPV and the quinoline units absorb at 326 nm and only the OPV absorbs at 450 nm, the Beer-

Lambert law could be applied to derive Equations 3.2 and 3.3, where L is the pathlength of the quartz cuvette used for the absorption measurements and [OPV] and [AQ_2PQ_2A] are the concentrations of OPV and AQ_2PQ_2A in the solution.

$$Abs(326\text{ nm}) = \varepsilon_{OPV}(326\text{ nm})[OPV]\times L + \varepsilon_{AQ_2PQ_2A}(326\text{ nm})[AQ_2PQ_2A]\times L \quad (3.2)$$

$$Abs(450\text{ nm}) = \varepsilon_{OPV}(450\text{ nm})[OPV]\times L \quad (3.3)$$

Equation 3.3 could be rearranged into Equation 3.4 to obtain the concentration of OPV and thus, the concentration of OPV-Q_8A foldamers.

$$[OPV] = \frac{Abs(450\text{ nm})}{\varepsilon_{OPV}(450\text{ nm})\times L} \quad (3.4)$$

Having determined the concentration of OPV, $\varepsilon_{OPV}(326\text{ nm})$, and $\varepsilon_{AQ2PQ2A}(326\text{ nm})$, the concentration of AQ_2PQ_2A species could be obtained with Equation 3.5.

$$[AQ_2PQ_2A] = \frac{Abs(326\text{ nm}) - [OPV]\times\varepsilon_{OPV}(326\text{ nm})\times L}{\varepsilon_{AQ_2PQ_2A}(326\text{ nm})\times L} \quad (3.5)$$

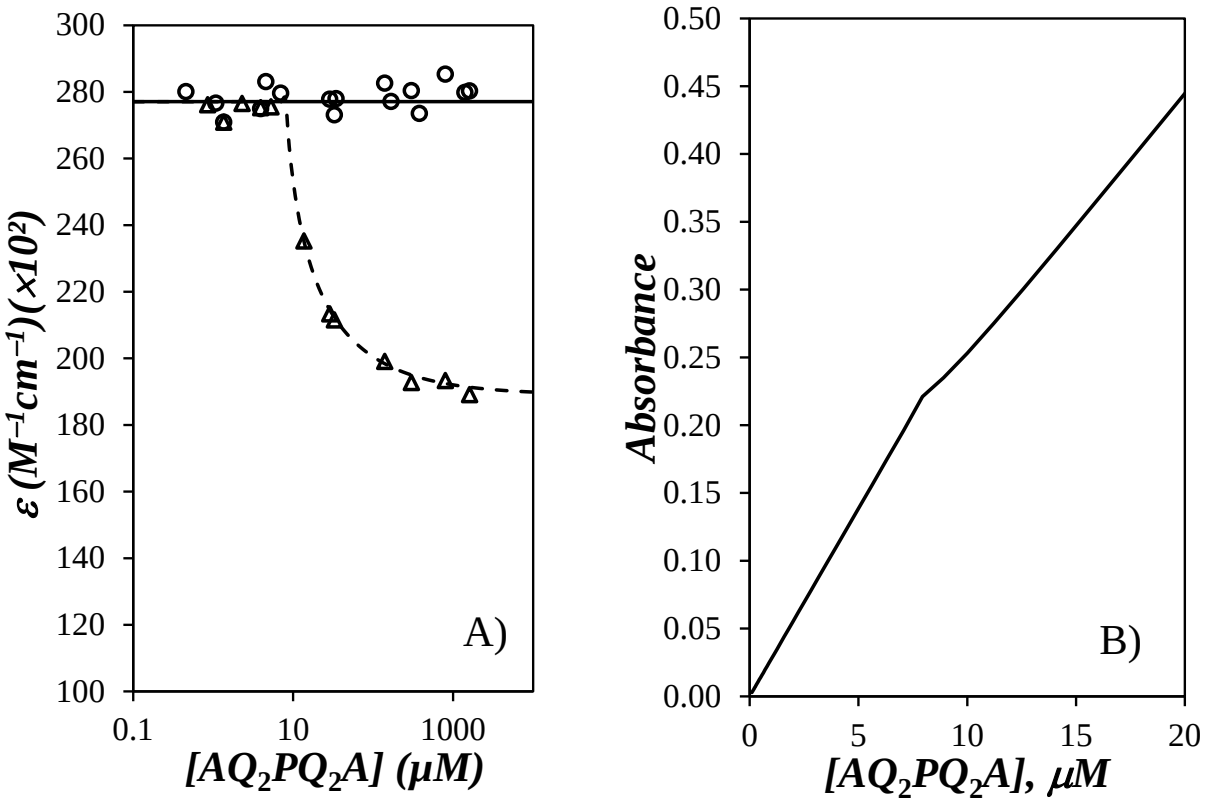

Figure 3.1. A) Plot of the molar extinction coefficient (ε) at 326 nm of AQ_2PQ_2A in chloroform (O) without NaOH and (Δ) with NaOH as a function of concentration. B) Plot of absorbance as a function of AQ_2PQ_2A concentration in chloroform with NaOH showing the breakpoint at ~ 7 μM marking the onset of hypochromicity upon AQ_2PQ_2A oligomerization.

Time-Resolved Fluorescence Anisotropy (TRFA): A HORIBA Ultima Ultrafast time-resolved fluorometer equipped with an excitation and emission polarizer using a 479 nm delta-diode laser as light source was used to acquire all fluorescence decays. A 480 nm bandpass filter and a 495 nm cut-off filter were placed on the excitation and emission sides, respectively, to minimize residual stray light from reaching the detector during decay acquisition, up to a decay peak

maximum of 20,000 counts. The same sample geometry employed for the SSF spectra was applied to acquire the TRFA decays, depending on their OPV concentration. A triangular aluminum monolith was used to acquire the instrument response function by collecting the reflected nano-LED light without the 495 nm cut-off filter and using neutral density filters to attenuate the light intensity. A time-per-channel of 1.28×10^{-2} ns/channel was used for all decay collections across 4,096 channels. Fluorescence decay acquisition was conducted with an excitation light that was vertically polarized, and with the polarization of the emission set at the magic angle (54.7 º for $I_{VM}(t)$) or the vertical ($I_{VV}(t)$) and horizontal ($I_{VH}(t)$) direction with respect to the vertical excitation light.

TRFA decay analysis: The analysis started by fitting the fluorescence decays acquired at the magic angle with a single exponential, as shown with Equation 3.6, to determine the lifetime τ_o of the OPV label covalently attached to the foldamer.

$$I_{VM}(t) = I_o \exp(-t/\tau_o) \tag{3.6}$$

In Equation 3.6, I_o is the initial fluorescence intensity and t is the time in nanoseconds. The vertically and horizontally polarized fluorescence decays were then fitted globally according to Equations 3.7 and 3.8, respectively.

$$I_{VV}(t) = \frac{I_o}{3}\exp(-t/\tau_o)\times[1+2r(t)] \tag{3.7}$$

$$I_{VH}(t) = \frac{I_o}{3G}\exp(-t/\tau_o)\times[1-r(t)] \tag{3.8}$$

The G-factor, used to account for the difference in detection efficiency between the two observation channels, was optimized during the analysis. The TRFA is represented by the function *r(t)* in Equations 3.7 and 3.8, which can be approximated by a sum of 3 exponentials for a symmetric top macromolecule as shown in Equation 3.9.[33]

$$r(t) = r_o \sum_{i=1}^{n} a_i \exp(-t/\phi_i) + r_\infty \qquad (3.9)$$

The TRFA analysis yielded the intrinsic anisotropy, or anisotropy at time *t* equal to zero, given by r_o in Equation 3.9. The pre-exponential factors a_i were normalized to unity and corresponded to the i^{th} rotational time ϕ_i. The polarized fluorescence decays $I_{VV}(t)$ and $I_{VH}(t)$ were analysed globally. The parameters of the fits were optimized according to the Marquardt-Levenberg algorithm and are listed in Tables B1-B6 in the Supporting Information (SI). For foldamer mixtures containing 10 μM of OPV-Q_8A, below an AQ_2PQ_2A/OPV-Q_8A ratio of 6, *r(t)* required only one rotational time (*n* = 1 in Equation 3.9). Analysis of the fluorescence decays with [AQ_2PQ_2A]/[OPV-Q_8A] ratios above 6 required two rotational times (*n* = 2 in Equation 3.9). For foldamer mixtures containing 1 μM of OPV-Q_8A, *r*(*t*) required two rotational times past a [AQ_2PQ_2A]/[OPV-Q_8A] ratio of 50.

3.3 RESULTS

TRFA was applied to characterize the size of the oligomerization products formed between OPV-Q_8A and AQ_2PQ_2A in chloroform, where OPV-Q_8A and AQ_2PQ_2A are terminated with a carboxylic acid at one and both ends, respectively, with or without addition of 0.1 g of 16 M $NaOH_{(aq)}$ solution. The rotational time of the foldamers was monitored across a range of AQ_2PQ_2A concentrations, that spanned four orders of magnitude, as determined by absorption measurements.

3.3.1 Oligomerization of AQ_2PQ_2A with OPV Q_8A Foldamers Characterized by TRFA

As mentioned earlier, the complexation of AQ_2PQ_2A and OPV-Q_8A in chloroform was induced by the addition of 0.1 g of 16 M $NaOH_{(aq)}$ solution. These experiments were expected to yield a mixture of free AQ_2PQ_2A and OPV-Q_8A, OPV-Q_8A dimers, and complexes of AQ_2PQ_2A, that could be labeled at either end with OPV-Q_8A, all of these species having different rotational times. Theoretically, each species containing an OPV label yields a rotational time, that is specific to that OPV-labeled species, so that the TRFA representative of this mixtures of species should be an infinite sum of exponentials, where each exponential represents a single OPV-containing species. In practice however, a sum-of-exponentials analysis conducted on a multiexponential fluorescence decay cannot resolve more than 4 exponentials, and only if the decay times are well separated. This is not expected to be the case for the mixture of OPV-containing species resulting from the oligomerization of OPV-Q_8A and AQ_2PQ_2A. As it turned out, the TRFAs were well-described by one exponential at [AQ_2PQ_2A]:[OPV-Q_8A] ratios below 50 and 6, for the experiments conducted with 1 and 10 µM OPV-Q_8A, respectively, and two exponentials at [AQ_2PQ_2A]:[OPV-Q_8A] ratios greater than 50 and 6, where little and more substantial oligomerization had occurred, respectively.

Instead of attempting to assign a given rotational time to one of the many OPV-containing species present in solution, the average rotational time, $<\phi>$, was considered, since this parameter was more representative of the mixture of species present in the solution. Plots of $<\phi>$ determined by TRFA as a function of the $[AQ_2PQ_2A]$:[OPV-Q_8A] ratio determined by UV-Visible spectrophotometry are displayed in Figure 3.2A. In these experiments, OPV-Q_8A, which was used as the fluorescent capping agent for the oligomers, was held at a constant concentration of 1 and 10 μM in two sets of experiments, while the AQ_2PQ_2A concentration was gradually increased across 4 orders of magnitude.

The protonated samples in chloroform before the addition of base yielded a constant $<\phi>$ value equal to 0.81 (±0.02), regardless of the AQ_2PQ_2A and OPV-Q_8A concentrations. This $<\phi>$ value matched that expected for unassociated OPV-Q_8A, since the protonated AQ_2PQ_2A did not interact with OPV-Q_8A and did not fluoresce at 510 nm. In contrast, $<\phi>$ was larger than the rotational time of the unimers upon addition of $NaOH_{(aq)}$ at $[AQ_2PQ_2A]$/[OPV-Q_8A] ratios smaller than unity, and approached the $<\phi>$ value expected for a mixture of OPV-Q_8A mixtures at the corresponding OPV-Q_8A concentration studied. For the 1 and 10 μM experiments, the rotational times at $[AQ_2PQ_2A]$/[OPV-Q_8A] ratios smaller than unity equaled 1.09 (±0.03) and 1.16 (±0.04) ns, respectively, which agreed with the $<\phi>$ values of 1.04 (±0.02) and 1.24 (±0.01) ns determined for the association curves of OPV-Q_8A at those concentrations, as seen is Figure 3.2B. As the $[AQ_2PQ_2A]$/[OPV-Q_8A] ratio was gradually increased above unity, $<\phi>$ showed a continuous increase with increasing $[AQ_2PQ_2A]$/[OPV-Q_8A] ratio, as observed in Figure 3.2A. This trend reflects the oligomerization of AQ_2PQ_2A into larger objects complexed with OPV-Q_8A, where higher AQ_2PQ_2A concentrations result in larger $<\phi>$ values. A remarkable feature of the $<\phi>$-*vs*-

[AQ_2PQ_2A]/[OPV-Q_8A] plot in Figure 3.2A was the absence of a plateau at higher ratios when compared to the <ϕ>-*vs*-[OPV-Q_8A] sigmoidal curves shown in Figure 3.2B, that was obtained for the dimerization of OPV-Q_8A and which is indicative of a closed association mechanism. Sigmoidal curves like that shown in Figure 3.2B were observed in Chapter 2 for the complexation of four OPV-Q_nA constructs with n = 4, 8, 17, and 33, which led to the conclusion, that these samples dimerized through complexation of their carboxylated ends. The absence of a plateau in the trends shown in Figure 3.2A indicates that solutions of AQ_2PQ_2A and OPV-Q_8A in chloroform exposed to 0.1 g of 16 M $NaOH_{(aq)}$ led to the formation of a thermodynamically stable mixture of species as a result of the deprotonation of the carboxylic acid terminals of AQ_2PQ_2A and OPV-Q_8A.

The most apparent difference between the experiments conducted with 1 and 10 μM of OPV-Q_8A was the [AQ_2PQ_2A]/[OPV-Q_8A] ratio at which a significant increase in <ϕ> occurred. For experiments with a constant concentration of 10 μM of OPV-Q_8A, the increase in <ϕ> began at an [AQ_2PQ_2A]/[OPV-Q_8A] ratio, that was one order in magnitude larger than with a 1 μM OPV-Q_8A concentration. As these associations are reminiscent of condensation polymerization, a higher concentration of capping moieties could have been expected to result in shorter oligomers and smaller <ϕ> values. The opposite was observed in Figure 3.2A due to the fact that a 10-fold larger OPV-Q_8A concentration required a 10-fold larger AQ_2PQ_2A concentration to bring the [AQ_2PQ_2A]/[OPV-Q_8A] ratio above unity, and that this much larger overall concentration of foldamers pushed the association equilibrium towards increased complexation and the formation of larger complexes. These considerations are further supported by the mathematical derivation

used to extract the equilibrium constant of this association mechanism conducted in the following section.

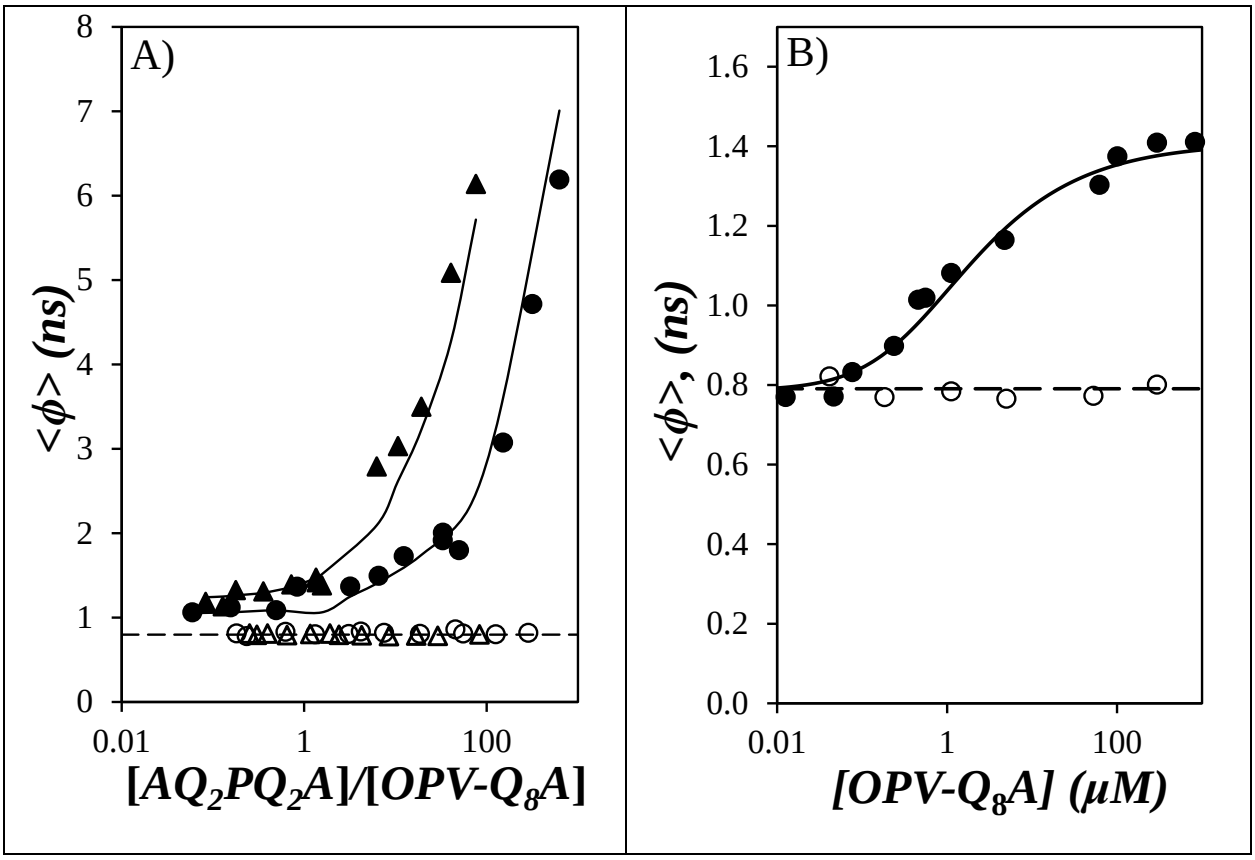

Figure 3.2. A) Plot of <ϕ> as a function of the [AQ_2PQ_2A]/[OPV-Q_8A] ratio for sample mixtures in chloroform (empty) before and (filled) after addition of 0.1 g of 16 M $NaOH_{(aq)}$ with (circle) 1 μM and (triangle) 10 μM of OPV-Q_8A. B) Plot of <ϕ> as a function of [OPV-Q_8A] in chloroform with (●) and without (O) the addition of 0.1 g of 16 M NaOH aqueous solution.

The oligomerization of AQ_2PQ_2A demonstrated by the continuously increasing <ϕ>-*vs*-[AQ_2PQ_2A]/[OPV-Q_8A] profiles shown in Figure 3.2A is a result of the deprotonation of the carboxylic acids by NaOH, that generates two sodium carboxylates (NaC), whose exposure to

apolar chloroform is minimized through their association in solution. This mechanism results in the formation of large OPV-Q_nNaC/NaCQ_2PQ_2NaC aggregates held together by the associated ion pairs and stabilized in chloroform by the oligoquinoline moieties. This conclusion agrees with the mechanism proposed in Chapter 2 for the dimerization of the OPV-Q_nA samples.

3.3.2 Model and Results for Oligomerization between AQ_2PQ_2A and OPV-Q_8A

The oligomerization of AQ_2PQ_2A with OPV-Q_8A serving as a fluorescent capping agent was assumed to involve three equilibria between the AQ_2PQ_2A monomer (M) and the OPV-Q_8A end-group (E) as shown in Equations 3.10a-c, where the species M_i, EM_i, and EM_iE represent an oligomer made of *i* AQ_2PQ_2A monomers, that is uncapped, capped with one end-group, and capped with two end-groups, respectively. Since the equilibria represented in Equations 3.10a-c describe the association between similar oligoquinolines terminated with a sodium carboxylate group, the same constant *K* was assumed for the three equilibria.

$M + M_{i-1} \overset{K}{\rightleftharpoons} M_i$	$M_i + E \overset{K}{\rightleftharpoons} EM_i$	$EM_i + E \overset{K}{\rightleftharpoons} EM_iE$
(3.10a)	(3.10b)	(3.10c)

Taking into account the fact that the M_i, EM_i, and EM_iE species involve two, one, and no associating groups, Equations 3.11a-c could be derived to represent their concentration as a function of the concentration of unassociated unimers ($[M_1]$) and end groups ([E]) at equilibrium.

$$[M_i] = (2K)^{i-1}[M_1]^i \qquad (3.11a)$$

$$[EM_i] = (2K[M_1])^i[E] \tag{3.11b}$$

$$[EM_iE] = 2^i K^{i+1}[M_1]^i[E]^2 \tag{3.11c}$$

The total concentration of monomers $[M]_o$ can be written as a function of K and the concentration of unassociated M_1 and E as described in Equation 3.12.

$$[M]_o = \sum_{i=1}^{\infty} i[M_i] + \sum_{i=1}^{\infty} i[EM_i] + \sum_{i=1}^{\infty} i[EM_iE] = [M]_1 \frac{1 + 2K[E] + 2K^2[E]^2}{(1 - 2K[M_1])^2} \tag{3.12}$$

Multiplying both sides of Equation 3.12 by the equilibrium constant K yields Equation 3.13a, which can be parametrized by replacing the products $K\times[E]$ and $K\times[M_1]$ by x and y, respectively, to yield Equation 3.13b.

$$K[M]_o = K[M_1]\frac{1 + 2K[E] + 2K^2[E]^2}{(1 - 2K[M_1])^2} \tag{3.13a}$$

$$K[M]_o = y\frac{1 + 2x + 2x^2}{(1 - 2y)^2} \tag{3.13b}$$

A similar procedure can be applied for the total concentration of end groups, $[E]_o$, shown in Equation 3.14a, whih can be parametrized with the variables x and y to yield Equation 3.14b.

$$[E]_o = \sum_{i=0}^{\infty} [EM_i] + 2\sum_{i=0}^{\infty} [EM_iE] = \frac{[E] + 2K[E]^2}{1 - 2K[M_1]} \tag{3.14a}$$

$$K[E]_o = \frac{x + 2x^2}{1 - 2y} \tag{3.14b}$$

To determine the concentrations [M_1] and [E], or x and y, respectively, Equation 3.14b is rearranged into Equation 3.15 to isolate for y. Substitution of Equation 3.15 into 3.13b yields Equation 3.16.

$$y = \frac{1}{2}\left[1 - \frac{1}{K[E]_o}(x + 2x^2)\right] \tag{3.15}$$

$$\frac{2K[M]_o}{K[E]_o}(x + 2x^2)^2 = (K[E]_o - x - 2x^2)(1 + 2x + 2x^2) \tag{3.16}$$

This expression can be rearranged into a polynomial by introducing the parameters a (= $[M]_o/[E]_o$) and b (= $K[E]_o$) into Equation 3.16 to yield Equation 3.17.

$$4x^4(2a+1) + 2x^3(4a+3) + 2x^2(a-b-2) + x(1-2b) - b = 0 \tag{3.17}$$

Since the total concentrations of monomers ($[M]_o$) and end-groups ($[E]_o$) were known for each mixture of AQ_2PQ_2A and OPV-Q_8A, the quantity a was known experimentally. Different K values were assumed and for a given K value, a value for b was obtained for each $[E]_o$ concentration, which was used to solve Equation 3.17 and obtain x. In turn, x could be introduced into Equation 3.15 to yield y. Dividing the variables x and y by K yielded the concentrations [M_1] and [E] of unassociated monomers and end-groups, respectively, which could be used to calculate the concentration of all the species M_i, EM_i, and EM_iE from Equations 3.11a-c.

Since only the species EM_i and EM_iE, representing the oligomers capped with OPV-Q_8A, could be probed in the TRFA experiments, their rotational times were estimated with Equations 3.18 and 3.19, respectively. In these equations, ϕ_E and ϕ_{E2} are the rotational times of the OPV-Q_8A unimers and dimers, determined to equal 0.79 and 1.4 ns, respectively.[24] m refers to the

contribution of one quinoline unit to the rotational time of an oligoquinoline foldamer, determined to equal 0.057 (±0.001) ns.[28] $n(M_1)$ refers to the number of quinoline units constituting an AQ_2PQ_2A unit, which was taken as 4 in the calculations.

$$\phi_{EM_i} = \phi_E + m \times n(M_1) \times i \tag{3.18}$$

$$\phi_{EM_iE} = \phi_{E_2} + m \times n(M_1) \times i \tag{3.19}$$

Since the variables x and y had been determined for each mixture of AQ_2PQ_2A and OPV-Q_8A, the theoretical average rotational times ($<\phi>_{cal}$) could be calculated with Equation 3.20.

$$<\phi>_{cal} = \frac{\sum_{i=0}^{\infty}[EM_i] \times \phi_{EM_i} + 2\sum_{i=0}^{\infty}[EM_iE] \times \phi_{EM_iE}}{\sum_{i=0}^{\infty}[EM_i] + 2\sum_{i=0}^{\infty}[EM_iE]} = \frac{x(1-2y)(\phi_E + 2x\phi_{E_2}) + 2xymn(M_1)(1+2x)}{(x+2x^2)(1-2y)} \tag{3.20}$$

For an assumed K value, $<\phi>_{cal}$ could be calculated for each AQ_2PQ_2A and OPV-Q_8A composition and was compared to the experimental rotational time $<\phi>_{exp}$ with the function χ^2 defined in Equation 3.21, where N represents the number of experiments having been conducted.

$$\chi^2 = \frac{1}{N}\sum_i (<\phi>_{cal} - <\phi>_{exp})^2 \tag{3.21}$$

Minimization of χ^2 in Equation 3.21 was accomplished by assuming different K values and applying the procedure described above to determine a set of $<\phi>_{cal}$ values obtained for the complexation of AQ_2PQ_2A and OPV-Q_8A, which were compared to the experimental $<\phi>$ values

shown in Figure 3.2A. The χ^2 values obtained for different K were plotted as a function of K in Figure B3 in Supporting Information. The plot could be fitted with a fourth order polynomial, whose minimum yielded the optimum K value of 4.25×10^5 M^{-1}.

3.3.3 Analysis of the Intrinsic Anisotropy of the AQ_2PQ_2A Oligomers

As described in Equation 3.5, the TRFA experiments also yielded the intrinsic anisotropy, r_o, which is related to the angle between the absorption and emission dipole moments of a chromophore.[30] An r_o value of 0.39 (±0.01) has been reported for OPV[37] and the short OPV-Q_nE foldamers studied earlier were also found to have an r_o value, that approached 0.40.[34] The longer OPV-Q_nE foldamers yielded lower r_o values, and this decrease in r_o was attributed to a loss of initial orientation between the absorption and emission dipole moments, probably due to wobbling of the small OPV unit with respect to the much larger helical foldamers.[34]

The r_o values obtained for the complexation experiments between AQ_2PQ_2A and OPV-Q_8A are presented in Figure 3.5. For mixtures of AQ_2PQ_2A and OPV-Q_8A in chloroform without NaOH, r_o remained constant and equal to 0.38 (± 0.00), close to 0.4. For the dimerization studies described in Chapter 2, r_o was found to decrease from a value around 0.35-0.40, depending on the length of the OPV-Q_nA foldamer, to ~0.25 with increasing concentration. The gradual decrease in r_o observed with increasing OPV-Q_nA concentration might have been a consequence of residual re-absorption of the polarized fluorescence, that might have taken place at the higher foldamer concentrations. In the present complexation studies, r_o showed a near consistent decrease across the entire range of AQ_2PQ_2A concentration studied when 16 M $NaOH_{(aq)}$ was added to the solutions, taking an average value of 0.34 (±0.02) and 0.34 (±0.01) for the 1 and 10 μM OPV-Q_8A solutions, respectively. The fact that no decrease in r_o was observed with increasing AQ_2PQ_2A

concentration is reasonable, since the absorption of AQ_2PQ_2A does not overlap the fluorescence of OPV-Q_8A (see Figure B4 in the Supporting Information (SI)) and a constant concentration of dye was utilised.

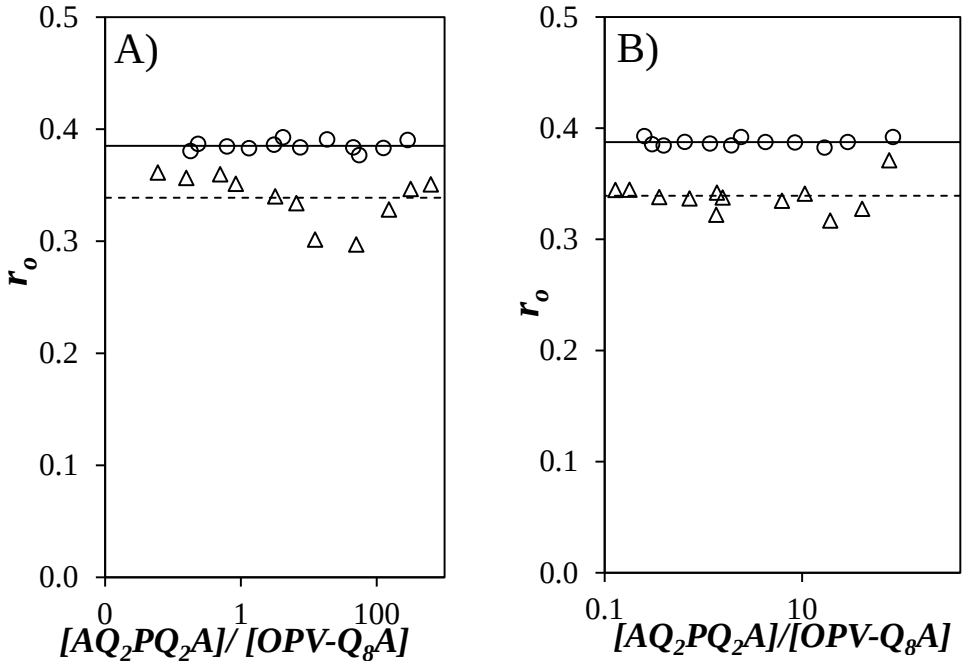

Figure 3.3. Plot of the intrinsic anisotropy (r_o) as a function of the [AQ_2PQ_2A]/[OPV-Q_8A] ratio before (O) and after (Δ) the addition of 0.1 g of 16 M $NaOH_{(aq)}$ for the complexation of AQ_2PQ_2A with A) 1 μM and B) 10 μM of OPV-Q_8A.

Such a decrease in r_o from 0.38 to 0.34 observed in both sets of data is typically attributed to a loss in the initial orientation between the absorption and emission dipole moments, that would occur on a much faster time scale than that probed in the TRFA measurements.[28] Such an instantaneous loss in orientation could be due to increased wobbling of the OPV unit with respect to the helical foldamer, when the OPV-Q_8A moiety is interacting with an AQ_2PQ_2A oligomer via ion-pairing and π–π forces. This ionic bond is expected to be weaker than the amide bonds linking

two quinolines in a foldamer. Contrary to the dimerization experiments, where an increase in *NU* resulted in more significant reductions in r_o, the complexation between AQ_2PQ_2A and OPV-Q_8A led to a slightly reduced but constant r_o value, regardless of the length of the AQ_2PQ_2A oligomer produced.

3.3.4 DISCUSSION

The increase in rotational time with increasing AQ_2PQ_2A concentration observed in Figure 3.2A with the TRFA measurements suggested aggregation of the foldamers. However, one key question to answer was whether the association of AQ_2PQ_2A occurred in a directional manner, through the negatively charged carboxylate end groups, leading to the formation of extended complexes, or randomly, leading to the formation of isotropic aggregates. That AQ_2PQ_2A association into long extended oligoquinoline constructs occurred through its carboxylate end groups could be inferred from the hypochromism discussed in the experimental section to determine the exact concentration of the foldamers in chloroform after phase separation of the aqueous and organic phases. As shown in Figure 3.1, hypochromism is observed for an AQ_2PQ_2A concentration between about 10 μM and 1 mM. The 10 μM AQ_2PQ_2A concentration matches the onset of AQ_2PQ_2A association in Figure 3.2A. The hypochromism identified in Figure 3.1 can only be the result of increased π–π stacking between the quinoline units, that are located at the ends of the AQ_2PQ_2A constructs. Consequently, the self-assembly of AQ_2PQ_2A requires π–π stacking of the terminal quinolines, which demonstrates that it leads to the formation of extended polyquinoline chains, that must adopt the helical conformation expected of oligoquinoline foldamers. The rigidity expected from these helical constructs is also supported by the fairly large r_o value of 0.34 (±0.02) obtained from the

TRFA experiments, indicating that little delocalisation is taking place between the absorption and emission dipole moments of the OPV labels bound to the self-assembled AQ_2PQ_2A oligomers.

The *K* value obtained for the complexation between AQ_2PQ_2A and OPV-Q_8A was determined to equal 4.25×10^5 M^{-1} from the analysis described in Section 3.3.2, which was performed by combining the results obtained with the experiments conducted with an OPV-Q_8A concentration of 1 and 10 μM. This *K* value can now be compared to the *K* values obtained earlier for the dimerization of the OPV-Q_nA foldamers. The effect, that the oligoquinoline length has on *K* for the dimerization of the OPV-Q_nA foldamers, was investigated in Chapter 2. It was found that *K* equaled 1.0 (±0.2)$\times10^6$ M^{-1} for the OPV-Q_nA foldamers with n = 8, 17, and 33 but 1.1 (±0.1)$\times10^5$ M^{-1} for the OPV-Q_4A sample. The 10-fold reduction in *K* found for the shorter construct was attributed to its lower mass, which did not endow OPV-Q_4A with sufficient kinetic energy to overcome the potential energy barrier generated by the electrostatic repulsion induced by the negatively charged carboxylate anions located at the end of the oligoquinoline constructs. It is thus interesting that the *K* value of 4.25×10^5 M^{-1} obtained for the oligomerization of AQ_2PQ_2A, whose size was similar to that of the tetraquinoline OPV-Q_4A, is about half that found for the dimerization of the OPV-Q_nA foldamers with n = 8, 17, and 33. The smaller size of AQ_2PQ_2A should make it difficult for this construct to overcome the energy barrier generated by the intermolecular electrostatic repulsion between the negatively charged end groups. Yet the equilibrium constant for the oligomerization of AQ_2PQ_2A is about 4-fold larger than the *K* value found for the dimerization of OPV-Q_4A, despite the fact that both constructs share a similar size. The 4-fold larger *K* value found for the oligomerization of AQ_2PQ_2A is attributed to its two carboxylate anions compared to OPV-Q_4A, which only bears a single carboxylate anion. Since the carboxylate anions

promote the associations between the foldamers in chloroform, they promote the associations of the doubly charged $NaCQ_2PQ_2NaC$ species resulting in the larger K value found for its oligomerization.

A single equilibrium constant K was assumed for the derivation of Equations 3.11 – 3.21, that were applied to determine the equilibrium constant for the oligomerization of AQ_2PQ_2A. While the use of a single equilibrium constant for the oligomerization of AQ_2PQ_2A might be view as an oversimplification, the model represented the experimental trends fairly well. First, the $\langle\phi\rangle_{cal}$ values retrieved with an equilibrium constant of 4.25×10^5 M^{-1} showed a similar exponential increase in rotational time with increasing $[AQ_2PQ_2A]/[OPV\text{-}Q_8A]$ ratio as that observed for the experimental $\langle\phi\rangle$ shown in Figure 3.2A. Furthermore, the model also reproduced the shift by one order of magnitude of the onset $[AQ_2PQ_2A]/[OPV\text{-}Q_8A]$ ratio observed in Figure 3.2A for the increase in the experimental $\langle\phi\rangle$, when the oligomerization experiments were conducted with an $OPV\text{-}Q_8A$ concentration of 1 and 10 μM. Together, these observations suggest that the approximations made for the modelling of the oligomerization of AQ_2PQ_2A with a single equilibrium constant were reasonable.

The oligomerization experiments yielded $\langle\phi\rangle$ values that were as large as 6.2 ns in Figure 3.2A for $OPV\text{-}Q_8A$ and AQ_2PQ_2A concentrations equal to 9.5×10^{-6} and 7.2×10^{-4} M, respectively. Using the derivation described in Equations 3.11 – 3.21, the concentration profiles of the AQ_2PQ_2A oligomers that were non-capped (M_i), capped with one $OPV\text{-}Q_8A$ (EM_i), and capped with two $OPV\text{-}Q_8A$ (EM_iE), could be determined and were plotted as a function of their number of quinoline units (NU) in Figure 3.4. Under these conditions, the dominant species appeared to be the non capped AQ_2PQ_2A oligomers, followed by the oligomers capped with one $OPV\text{-}Q_8A$,

with the doubly capped oligomers being the sparsest species. The number- (NU_n) and weight- (NU_w) average *NU* could be determined based on the concentration profiles shown in Figure 3.4 and were found to equal 88 and 158, respectively, displayed as the vertical red and green lines, respectively. Since the largest oligoquinoline foldamer synthesized to date had an *NU* of 96 quinolines, NU_n and NU_w indicate that the self-assembled oligoquinoline species in this solution would represent the largest, by far, oligoquinoline foldamers produced up to now. In fact, since these species are the product of an association mechanism similar to condensation polymerization, the oligoquinoline species had a broad *NU* distribution, implying that much larger species were present in the solution. The polydispersity index (NU_w/NU_n) of this distribution approaches the value of 2 expected for condensation polymerization at high conversion and equals 1.8 under the present conditions.

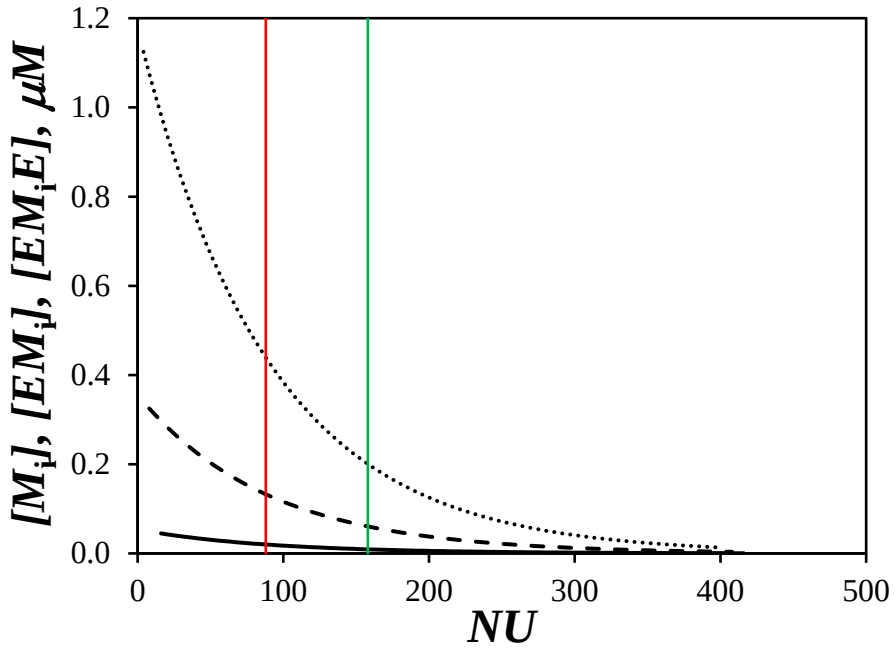

Figure 3.4. Plot of the concentrations of (·····) M_i, (– – –) EM_i, and (———) EM_iE species in the solution prepared with [OPV-Q_8A] = 9.5×10^{-6} M and [AQ_2PQ_2A] = 7.2×10^{-4} M.

The significance of the size of the oligoquinoline species generated in this experiment cannot be understated. For comparison, the longest oligoquinoline foldamer prepared to date was 96 units long through time-consuming stepwise synthesis, with very low yields by the end of the process.[20] The self-assembly of smaller, monomeric foldamer units such as AQ_2PQ_2A into longer insertion products offers oligoquinoline products of much larger length, in large numbers, and in much shorter times, although the products of this self-assembly are no longer monodisperse.

3.4 CONCLUSIONS

The associations between AQ_2PQ_2A and OPV-Q_8A in chloroform were investigated using TRFA. These experiments were conducted at constant concentrations of OPV-Q_8A equal to 1 and 10 μM, with varying amounts of AQ_2PQ_2A. The concentration of each species in solution was determined by measuring the absorbance of the solutions and TRFA was applied to obtain the average rotational time $<\phi>$ for these mixtures before and after the addition of 0.1 g of 16 M NaOH aqueous solution. From the relationship between $<\phi>$ and foldamer size established in a previous publication,[28] the extent of self-association between oligoquinoline foldamers could be characterized from the long insertion products generated by self-assembly in chloroform after addition of 16 M $NaOH_{(aq)}$. The exponential increase obtained in Figure 3.2A by plotting $<\phi>$ as a function of the $[AQ_2PQ_2A]/[OPV\text{-}Q_8A]$ concentration ratio after the addition of base indicated that the foldamers underwent an open association mechanism, resulting in the formation of a mixture of products. These trends were then further analyzed to determine the equilibrium constant controlling the formation of these complexes. It was found to equal 4.25×10^5 M^{-1} for both sets of

data obtained with a constant OPV-Q_8A concentration of 1 or 10 μM. The negative carboxylate anions generated by the deprotonation of the foldamer samples was driving this association, that led to the formation of polar sodium carboxylate ion pairs shielded from apolar chloroform by the oligoquinoline backbone. Additional stabilization of the complexes was provided by π-π stacking between the terminal quinolines of the oligomerized foldamers. This was further illustrated by the difference between the two $<\phi>$ profiles obtained for the 1 and 10 μM OPV-Q_8A concentrations, where the $<\phi>$ of the 10 μM concentration began its exponential increase an order of magnitude earlier in terms of the [AQ_2PQ_2P]/[OPV-Q_8A] ratio than that of the 1 μM concentration. The increase in carboxylate anions increased the tendency for the foldamers to self-associate by shielding the charges from apolar chloroform. The mathematical derivation conducted to determine the equilibrium constant for the oligomerization of AQ_2PQ_2A provided the concentration distribution of the different oligomers generated through self-association as a function of their *NU*. Considering the solution prepared with the largest concentrations of AQ_2PQ_2A and OPV-Q_8A, analysis of the concentration profiles provided in Figure 3.4 yielded an NU_n and NU_w equal to 88 and 158, respectively. These values indicated that much larger foldamers must have been generated in solution than the longest foldamer of 96 units prepared synthetically to date.[20] Consequently, this study opens the path for the preparation of much longer oligoquinoline constructs through self-assembly.

Chapter 4

Conclusions and Future Work

4.1 Summary of Thesis

Foldamers represent a class of artificial molecules designed to fold into a conformationally ordered state,[1] dictated by non-covalent interactions when in solution.[2] The typical forces in such systems include hydrogen bonding[3], hydrophobic,[4] and π-π stacking interactions,[5] which are often involved in the process of self-assembly. Present in many biological phenomena,[6] self-assembly allows for the generation of complex structures by spontaneous association under equilibrium conditions.[7] Through combination of hydrogen bonding and aromatic stacking interactions, oligoquinoline-based foldamers assume a rigid, helical conformation in solution.[8] Combined with their electron-rich backbone,[9] these molecules make excellent candidates for molecular wires.[10] However, elongation of these molecules by synthetic means becomes progressively more laborious with increasing chain length.[9] If non-covalent forces could be harnessed to drive the self-assembly of building blocks into larger foldamers, it would provide alternative, non-synthetic strategies to conventional synthetic problems encountered for longer foldamers.

The first goal of this thesis was to demonstrate that OPV-labeled, carboxylic acid terminated oligoquinoline foldamers of various lengths, referred to as OPV-Q_nA with *n* equal to 4, 8, 17, and 33, could self-assemble into well-defined complexes after deprotonation of their terminal carboxylic acid in apolar choloroform. Since this complexation was a result of an equilibrium between the carboxylate anions, experiments were conducted to determine the equilibrium constant, *K*, that dictates the extent of complexation between the OPV-Q_nA constructs. Complexation in a solution of most OPV-Q_nA foldamers led to the formation of dimers, while mixed complexes were generated from mixtures of OPV-Q_8A with a 5-fold excess of unlabeled Q_{16}A. The two important parameters, that needed to be determined experimentally to characterize

these equilibria, were the concentration of the foldamers in solution and the size of the complexes created in solution. UV-Visible spectroscopy was used to determine the concentrations of the foldamer species in solution. Time-resolved fluorescence anisotropy (TRFA) was applied to characterize the size of the complexes by determination of their rotational times, ϕ, a parameter proportional to the hydrodynamic volume of the macromolecule, V_h. In turn, ϕ could be related to the size of the complexes by taking advantage of a calibration curve established in earlier studies between ϕ and the number of quinoline units (*NU*) that composed a series of OPV end-labeled, methyl ester-terminated foldamers (OPV-Q_nE).[11] Comparison of the ϕ values obtained for OPV-Q_nA and OPV-Q_nE foldamers showed that the acids exhibited the same hydrodynamic behaviour and helical conformation as their methyl ester counterparts. Measurements were then conducted on foldamer samples before and after the addition of 0.1 g of 16 M NaOH aqueous solution by TRFA. The protonated foldamers in chloroform yielded constant ϕ values across 5 orders of magnitude in concentration, confirming the absence of association even at the highest foldamer concentrations of about 1 mM. The ϕ values obtained for protonated foldamers equaled 0.58 (±0.01), 0.80 (±0.02), 1.30 (±0.02), and 2.2 (±0.1) ns for OPV-Q_4A, OPV-Q_8A, OPV-Q_{17}A, and OPV-Q_{33}A, respectively. Addition of 16 M NaOH solution led to an increase in ϕ with increasing concentration. In these experiments ϕ was taken as an average rotational time, $<\phi>$, representing the mixture of species expected in solution, that included the unassociated and complexed foldamers. At concentrations below 0.1 µM, the $<\phi>$ values obtained for the OPV-Q_nA solutions were those expected for the protonated and unassociated foldamers, confirming the absence of association at this low foldamer concentration, due to the concentration-driven equilibrium. For all the OPV-Q_nA samples studied, $<\phi>$ increased with increasing foldamer concentration until a

plateau was reached at concentrations greater than 80 μM, where a single rotational time was obtained, reflecting the generation of larger and well-defined objects in solution, as would be expected from a closed association mechanism. The values obtained for $<\phi>$ in these plateau regions were 0.98 (±0.01), 1.40 (±0.02), 2.50 (±0.03), and 4.40 (±0.04) ns for OPV-Q_4A, OPV-Q_8A, OPV-Q_{17}A, and OPV-Q_{33}A, respectively. The formation of a thermodynamically stable species was induced by deprotonation of the carboxylic acid termini into sodium carboxylate anions, which associated into ion pairs. The formation of ion pairs reduced the exposure of the sodium carboxylate end groups to apolar chloroform, while the oligoquinoline foldamers allowed their stabilization.

Plotting the $<\phi>$ values in the plateau region of the sigmoidal curves obtained after exposure of the OPV-Q_nA samples to the 16 M NaOH aqueous solution, and referred to as $\phi(\infty)$, yielded straight lines as a function of *NU* and 2×*NU*, whose slopes were, respectively, double and the same as the slope of the straight line obtained by plotting ϕ for the OPV-Q_nA and OPV-Q_nE samples in chloroform as a function of *NU*. This result indicated that the size of the OPV-Q_nA aggregates formed by this closed association mechanism increased with increasing *NU* in the same manner as the protonated OPV-Q_nA. This observation was taken as strong evidence that these OPV-Q_nA aggregates were in fact dimers. The only difference between the lines obtained for the unassociated OPV-Q_nA and OPV-Q_nE samples and the OPV-Q_nA complexes was the visible and constant offset, attributed to the additional V_h provided by the second OPV unit in the OPV-Q_nA dimers. Mixtures between OPV-Q_8A with a 5-fold excess of Q_{16}A were also characterized by TRFA and yielded the same sigmoidal trace as observed with the dimerization experiments. In the high concentration regime after the addition of 0.1 g of 16 M NaOH aqueous solution, the expected

species in solution would consist of OPV-Q_8A dimers, complexes between OPV-Q_8A and Q_{16}A, and Q_{16}A dimers, the latter species being unobservable by fluorescence. The TRFA data could be analyzed by assuming a ϕ_c of 1.7 (±0.1) ns of the complex formed between OPV-Q_8A and Q_{16}A, which represented the rotational time of a hypothetical OPV-Q_{24}E foldamer.

Another parameter obtained by TRFA is the intrinsic anisotropy, r_o, which is a function of the angle between the absorption and emission dipole moments of a chromophore.[4] For OPV, r_o has been reported as 0.39 (±0.01),[12] which is close to the theoretical maximum of 0.4, demonstrating parallel dipole moments. In an earlier study, it was found that r_o decreased from a value close to 0.4 with increasing length of OPV-Q_nE foldamers, which indicated an initial orientation loss between the dipole moments,[11] probably due to wobbling of the OPV moiety with respect to the perpendicular axis of the foldamer helix. A similar effect was also observed for the protonated foldamers and deprotonated foldamer complexes at the high concentrations, where longer foldamers were generated, with r_o values decreasing from ~ 0.35-0.40 to ~0.25. Since this decrease in r_o was significantly larger than that observed with increasing length of the OPV-Q_nE foldamers, it was attributed to re-absorption of the polarized fluorescence. The most significant decrease in r_o occurred for the shortest construct studied, OPV-Q_4A, for which r_o reached its lowest value of 0.18. This was taken as an indication that the shorter distance between the two OPV units on the dimerized OPV-Q_4A foldamer resulted in energy transfer between them, especially at higher concentrations, where the dimer was generated.

The sigmoidal $<\phi>$-*vs*[OPV-Q_nA] profiles obtained in Chapter 2 for the dimerization of the OPV-Q_nA samples as well as the complexation between OPV-Q_8A and Q_{16}A were analyzed by conducting a least squares optimization to retrieve the *K* values for these equilibria. The

equilibrium constants were determined to equal 1.1 (±0.1)×10^5, 1.1 (±0.2)×10^6, 7.8 (±0.4)×10^5, 1.10 (±0.03)×10^6, and 7.5 ×10^5 M^{-1} for the dimerization of OPV-Q_4A, OPV-Q_8A, OPV-Q_{17}A, OPV-Q_{33}A, and the complexation of OPV-Q_8A and Q_{16}A, respectively. For the longer constructs studied, *K* took an average value of 9.4 (±0.2)×10^5 M^{-1}, a value suggesting that foldamer concentrations of about 1 mM are required to form the complexes. For comparison, the association constant for compounds prepared from ureido-pyrimidinone, a well-known self-assembling moiety capable of strong hydrogen bonding[13] and frequently used in supramolecular polymerizations, ranges from 10^5 to 10^7 M^{-1} depending on the nature of their chemical composition.[14, 15] If the ureido-pyrimidinone-based compounds are capable of self-association, so are the oligoquinoline foldamers as observed experimentally, since their *K* values are of a similar magnitude. This self-association mechanism suggests that molecular wires of well-defined length could be prepared by self-assembly of oligoquinolines, whereby the last, and usually most synthetically demanding step consisting in clicking two long oligoquinolines together, could be dramatically simplified.

Having demonstrated that the deprotonation of OPV-Q_nA constructs led to their dimerization in chloroform, this interesting self-association mechanism was exploited to examine the oligomerization between monomeric units of AQ_2PQ_2A and OPV-Q_8A, which would act as a fluorescent capping agent. Again, UV-Visible spectroscopy was used to determine the concentrations of the foldamer species in solution, but was complicated by hypochromicity affecting the AQ_2PQ_2A species at high concentrations.[16] At AQ_2PQ_2A concentrations larger than 10 μM, a decrease in absorbance was observed for AQ_2PQ_2A after the addition of 0.1 g of 16 M NaOH, which was attributed to interactions between the terminal quinolines induced by aromatic

stacking. For AQ_2PQ_2A, ε(326 nm) was found to equal 27,700 (±400) $M^{-1}\cdot cm^{-1}$ in pure chloroform solution without NaOH but decreased gradually to 18,900 (±200) $M^{-1}\cdot cm^{-1}$ at concentrations larger than 1 mM in the presence of NaOH. Accounting for this effect enabled the determination of the concentration of deprotonated AQ_2PQ_2A in chloroform. This effect was also used to confirm that the AQ_2PQ_2A monomers must have been associating via their end quinolines resulting in the formation of elongated complexes.

TRFA was also applied to characterize the extent of oligomerization, by monitoring the average rotational time as a function of the ratio between AQ_2PQ_2A and OPV-Q_8A concentrations. Two sets of experiments were conducted with constant concentrations of OPV-Q_8A equal to 1 and 10 μM, and with varying concentrations of AQ_2PQ_2A that spanned 4 orders of magnitude. The species expected to form in solution through complexation between AQ_2PQ_2A and OPV-Q_8A included free AQ_2PQ_2A and OPV-Q_8A, OPV-Q_8A dimers, and elongated AQ_2PQ_2A complexes of various lengths, that would be terminated by no, one, or two OPV-Q_8A moieties, with each OPV-Q_8A terminated complex having its own rotational time. For [AQ_2PQ_2A]:[OPV-Q_8A] ratios smaller than 50 and 6, TRFA decays were well fitted with a single rotational time, whereas ratios greater than 50 and 6 required two rotational times for the experiments conducted with OPV-Q_8A concentrations of 1 and 10 μM, respectively. For these analyses, the average rotational time, $<\phi>$, was used to represent the numerous labeled species present in the mixture. Without 16 M $NaOH_{(aq)}$, $<\phi>$ remained constant and equal to 0.81 (±0.02) ns, matching the values of unassociated OPV-Q_8A foldamers. Upon addition of 16 M $NaOH_{(aq)}$, the rotational times obtained for AQ_2PQ_2A and OPV-Q_8A equaled 1.09 (±0.03) and 1.16 (±0.04) ns at low [AQ_2PQ_2]/[OPV-Q_8A] ratios for the 1 and 10 μM conditions, respectively. This discrepancy between the rotational times obtained at

different OPV-Q_8A concentrations agreed with the values of 1.04 (±0.02) and 1.24 (±0.01) ns determined from the association curves of OPV-Q_8A at concentrations of 1 and 10 μM. An exponential increase in rotational time was obtained after the addition of 16 M NaOH, demonstrating the formation of larger objects in solution *via* an open association mechanism in both sets of experiments as a result of the deprotonation of the carboxylic acids of AQ_2PQ_2A and OPV-Q_8A. Similarly to the OPV-Q_nA complexation studied in Chapter 2, deprotonation of the terminal carboxylic acids by NaOH yields sodium carboxylate (NaC) ions, that minimize their exposure to apolar chloroform through pairing, which leads to the formation of longer insertion products, held together by the associated ion pairs and stabilized in chloroform by the oligoquinoline moieties. The consistency of this effect was demonstrated by conducting these experiments with two OPV-Q_8A concentrations, where the increase in $<\phi>$ began at a [AQ_2PQ_2A]/[OPV-Q_8A] ratio that was one order in magnitude larger for the 1 μM than with the 10 μM OPV-Q_8A concentration.

The trends obtained for these complexation experiments were analyzed by a least squares optimization to yield the optimal *K* value for that system, following the same procedure as that applied for the dimerization and complexation studies in Chapter 2. The equilibrium constant was determined to equal 4.25×10^5 M^{-1} by combination of both sets of experiments. From Chapter 2, the *K* values determined for the OPV-Q_nA constructs with n = 8, 17, and 33 were found to equal 1.0 (±0.2)$\times10^6$ M^{-1} on average, but *K* took a much lower value of 1.1 (±0.1)$\times10^5$ M^{-1} for the shorter OPV-Q_4A construct. The decrease of *K* by one order in magnitude for OPV-Q_4A was attributed to its inability to overcome the repulsion between two negatively charged sodium carboxylates of the oligoquinoline foldamers. A same effect should also apply to the AQ_2PQ_2A

monomers, which are composed of four quinolines each, yet, *K* obtained for the complexation of AQ_2PQ_2A and OPV-Q_8A mixtures was roughly 4 times greater than that for the dimerization of OPV-Q_4A. This increase in *K* for the oligomerization of AQ_2PQ_2A was most certainly a result of its double acid functionalization, which must have increased its drive to shield its ionic ends from apolar chloroform.

The self-association of shorter AQ_2PQ_2A monomeric units into longer oligoquinoline complexes provides an avenue for the production of quinoline-based molecular wires in solution. During the oligomerization experiments, $<\phi>$ values as large as 6.2 ns were obtained for OPV-Q_8A and AQ_2PQ_2A concentrations equal to 9.5×10^{-6} and 7.2×10^{-4} M, respectively. At these concentrations, the three main species present in solution were the AQ_2PQ_2A complexes with no (M_i), one (EM_i), and two (EM_iE) OPV-Q_8A moieties. The concentration profiles of these three species plotted as a function of *NU* revealed that the prevalent species in solution was that of the unlabeled complexes, followed by the singly capped products, and finally, the doubly capped complexes. Based on these concentration profiles, the number- (NU_n) and weight- (NU_w) averages of *NU* were determined, and found to equal 88 and 158 units, respectively. Considering that the largest oligoquinoline segment synthesized to date is 96 units long,[9] these experiments demonstrated that the self-association of oligoquinoline foldamers can produce complexes whose size is competitive with that of oligoquinolines prepared via conventional synthetic methods, if not larger if the broad *NU* distribution is taken into consideration.

Lastly, the intrinsic anisotropy, r_o, was determined by TRFA for the AQ_2PQ_2A and OPV-Q_8A mixtures. For those samples studied before the addition of 0.1 g of 16 M NaOH aqueous solution, r_o remained constant and equal to 0.38 (±0.00) for the 1 and 10 μM OPV-Q_8A

concentrations, and at all concentrations of AQ_2PQ_2A. After addition of base, r_o displayed a nearly constant decrease relatively to those samples in pure chloroform, with values of 0.34 (±0.02) and 0.34 (±0.01) for the 1 and 10 μM OPV-Q_8A solutions, respectively. For the dimerization studies, the decrease in r_o from ~0.35-0.40 to ~0.25 at higher OPV-Q_nA concentrations had been attributed to re-absorption of the polarized emissions from one chromophore to another. No decrease in r_o upon increasing the AQ_2PQ_2A concentration was found, as would be expected since a constant concentration of OPV-Q_8A was employed in these experiments. Consequently, the decrease in r_o observed for mixtures of AQ_2PQ_2A and 1 or 10 μM OPV-Q_8A was a result of orientation loss between the absorption and emission dipole moments, probably due to the wobbling of OPV with respect to the main axis of the foldamer helix when OPV-Q_8A associates with AQ_2PQ_2A.[11] From this perspective, the formation of oligoquinoline complexes combining a fairly extended length and a satisfactory rigidity at high AQ_2PQ_2A concentrations suggests that the self-association of AQ_2PQ_2A monomers provides a convenient, non-synthetic route towards the preparation of long oligoquinoline constructs, with potential use as molecular wires.

4.2 Future Work

Throughout this investigation, the dimerization, complexation, and oligomerization of carboxylic acid terminated oligoquinoline foldamers was induced by the deprotonation of the carboxylate end groups upon exposure to 16 M NaOH aqueous solution. The equilibrium studies demonstrated that shorter oligoquinoline foldamers had significantly lower *K* values, when compared to those constructs prepared from oligoquinolines more than 8 units-long. This effect was attributed to the inability of the shorter foldamers to overcome the potential energy barrier generated by the

negatively charged carboxylate anions. In this context, it would be interesting to investigate the effect of ionic strength on *K* by adding some salts soluble in chloroform such as sodium tetraphenyl borate. The presence of salt would be expected to screen the electrostatic repulsion experienced by the negatively charged sodium carboxylate, thus reducing the height of the potential energy barrier, which would lead to an increase in *K* for AQ_2PQ_2A.[17,18] Association of the shorter foldamers could be enhanced by addition of concentrated solutions of sodium tetraphenylborate, with continued exposure to sodium hydroxide to achieve the deprotonation of the carboxylic acids of AQ_2PQ_2A in chloroform. The methodology based on TRFA presented in this thesis should enable the determination of *K* as a function of ionic strength, which would confirm whether adding salt to the solution would result in an increase in *K*.

Another follow-up study based on the results obtained in this thesis would be to use atomic force microscopy (AFM) to confirm that the oligoquinoline complexes composed of AQ_2PQ_2A do indeed form long elongated wires. The association of AQ_2PQ_2A into longer complexes was suggested in Chapter 3, where the hypochromism, or reduction in absorbance by aromatic stacking interactions, served as proof that complexation occurred through the quinolines located at the ends of AQ_2PQ_2A and led to the formation of linear polyquinolines, as opposed to random, undefined AQ_2PQ_2A aggregates. Using AFM to image the AQ_2PQ_2A complexes would confirm the formation of a distribution of ordered structures as expected for these oligoquinoline foldamers. One potential barrier in the application of this technique is the macromolecular sizes that can be detected by AFM. In one example, a poly(oligo(ethylene glycol) methyl ether methacrylate) ($PEG_{19}MA$) with number- (M_n) and weight- (M_w) average molecular weights of 134,000 and 193,000 $g \cdot mol^{-1}$, respectively, was imaged by AFM.[19] The polymer length ranged from 20 to 90

nm with a 10-20 nm diameter and a 0.5-1.0 nm height, in agreement with the dimensions expected from pyrene excimer fluorescence experiments.[19] For the polyquinolines, the number, NU_n and weight, NU_w averages of *NU* determined in Chapter 3 were found to equal 88 and 158 units, respectively. Considering that the helical diameter is 2.0 nm with rise of 0.136 nm per quinoline, NU_n and NU_w correspond to 12 and 21 nm, respectively.[11] These dimensions suggest that AQ_2PQ_2A could be imaged by AFM. In terms of sample preparation, the solvent would need to be evaporated to conduct the AFM measurements, thereby increasing the AQ_2PQ_2A concentration and, consequently, the length of the complexes as well. These conditions may not be representative of what occurs in solution but may illustrate the fact that linear rods are being formed rather than random aggregates.

References

Chapter 1

(1) Gellman, S. H. Foldamers: A Manifesto. *Acc. Chem. Res*. **1998**, *31*, 173-180.

(2) Clayden, J.; Le Bailly, B. A. F. Dynamic Foldamer Chemistry. *Chem. Commun.* **2016**, *52*, 4852-4863.

(3) Tomasini, C.; Huc, I.; Aitken, D. J.; Fulop, F. Foldamers. *Eur. J. Org. Chem*. **2013**, *17*, 3408-3409.

(4) Guichard, G.; Huc, I. Synthetic Foldamers. *Chem. Commun.* **2011**, *47*, 5933–5941.

(5) Liu, C.-Z.; Yan, M.; Wang, H.; Zhang, D.-W.; Li, Z.-T. Making Molecular and Macromolecular Helical Tubes: Covalent and Noncovalent Approaches. *ACS Omega* **2018**, *3*, 5165-5176.

(6) Whitesides, G. M.; Boncheva, M. Beyond Molecules: Self-Assembly of Mesoscopic and Macroscopic Components. *Proc. Natl. Acad. Sci. U S A.* **2002**, *99*, 4769–4774.

(7) Whitesides, G.; Mathias, J.; Seto, C. Molecular Self-Assembly and Nanochemistry: A Chemistry Strategy for the Synthesis of Nanostructures. (Engineering a Small World: From Atomic Manipulation to Microfabrication). *Science* **1991**, *254*, 1312–1319.

(8) Douglas, P.; Stoddart, J. F. Self-Assembly in Natural and Unnatural Systems. *Angew. Chem. Int. Ed. Engl*. **1996**, *35*, 1154-1196.

(9) Tominaga, M.; Kawahata, M.; Itoh, T.; Yamaguchi, K. Self-Assembly Behavior Shifting to Crystal Formation of Chiral Macrocyclic Tetraimines. *Cryst. Growth Des*. **2019**, *19*, 1118-1124.

(10) Jones, M. N.; Chapman, D. Micelles, Monolayers and Biomembranes. *Cell Biochem. Funct.* **1996**, *14*, 75-75.

(11) Edwin, T. L. The ABCs of Self-Assembly. *Science* **1999**, *286*, 1307-1307.

(12) Whitley, K. D.; Comstock, M. J.; Chemla, Y. R. Elasticity of the Transition State for Oligonucleotide Hybridization. *Nucleic Acids Res*. **2017**, *45*, 547-555.

(13) Wychowaniec, J. K.; Patel, R.; Leach, J.; Mathomes, R.; Chhabria, V.; Patil-Sen, Y.; Hidalgo‐Bastilda, A.; Forbes, R. T.; Hayes, J. M.; Elsawy, M. A. Aromatic Stacking Facilitated Self-Assembly of Ultrashort Ionic Complementary Peptide Sequence: β-Sheet Nanofibers with Remarkable Gelation and Interfacial Properties. *Biomacromolecules* **2020**, *21*, 2670-2680.

(14) Nisanci, B.; Dastan, A.; Bozedemir, O. A. Aromatic Stacking of a Perylenetetracarboxylic Tetraester: Self-Assembly in both Water and Chloroform. *Tetrahedron Lett.* **2018**, *59*, 3558-3562.

(15) Sathaye, S.; Zhang, H.; Sonmez, C.; Schneider, J. P.; MacDermaid, C. M.; Von Bargen, C. D.; Saven, J. G.; Pochan, D. J. Engineering Complementary Hydrophobic Interactions to

Control β-Hairpin Peptide Self-Assembly, Network Branching, and Hydrogel Properties. *Biomacromolecules*. **2014**, *15*, 3891-3900.

(16) Lehn, J.-M. Toward Self-Organization and Complex Matter. *Science* **2002**, *295*, 2400–2403.

(17) Zhang, D-W.; Wang, W.-K.; Li, Z.-T. Hydrogen-Bonding-Driven Aromatic Foldamers: Their Structural and Functional Evolution. *Chem. Rec.* **2015**. *15*, 233-251.

(18) Wang, X.; Cao, K.; Liu, Y.; Tsang, B.; Liew, S. Migration Insertion Polymerization (MIP) of Cyclopentadienyldicarbonyldiphenylphosphinopropyliron (FpP): A New Concept for Main Chain Metal-Containing Polymers (MCPs). *J. Am. Chem. Soc.* **2013**, *135*, 3399-3402.

(19) Foucher, D. A.; Tang, B. Z.; Manners, I. Ring-Opening Polymerization of Strained, Ring-Tilted Ferrocenophanes: A Route to High-Molecular-Weight Poly(ferrocenylsilanes). *J. Am. Chem. Soc.* **1992**, *114*, 6246-6248.

(20) Engel, J. Thermodynamics and Kinetics of Self-Assembly. In *Biophysics*; Eds. Hoppe, W.; Lohmann, W.; Markl, H.; Ziegler, H. Springer-Verlag: Berlin, Heidelberg, New York, Tokyo **1983**, Chapter 11, pp 408-412.

(21) Hecht, S.; Huc, I. Foldamers: Structure, Properties, and Applications. Wiley-VCH, 2007.

(22) Li, X.; Markandeya, N.; Jonusauskas, G.; McClenaghan, N. D.; Maurizot, V.; Denisov, S. A.; Huc, I. Photoinduced Electron Transfer and Hole Migration in Nanosized Helical Aromatic Oligoamide Foldamers. *J. Am. Chem. Soc.* **2016**, *138*, 13568–13578.

(23) Lefler, K. M.; Co, D. T.; Wasielewski, M. R. Self-Assembly-Induced Ultrafast Photodriven Charge Separation in Perylene-3,4-dicarboximide-Based Hydrogen-Bonded Foldamers. *J. Phys. Chem. Lett.* **2012**¸*3*, 3798-3805.

(24) Zhuo, M.-P.; Wu, J.-J.; Wang, X.-D.; Tao, Y.-C.; Yuan, Y.; Liao, L.-S. Hierarchical Self-Assembly of Organic Heterostructure Nanowires. *Nat. Commun*. **2019**, *10*, 3839-3839.

(25) Wang, J.; Little, H.; Duhamel, J.; Li, X.; Markandeya, N.; Maurizot, V.; Huc, I. Application of Time-Resolved Fluorescence Anisotropy to Probe Quinoline-Based Foldamers Labeled with Oligo(phenylene vinylene). *Macromolecules* **2019**, *52*, 5829-5837.

(26) Riaz, R.; Ali, M.; Answer, H.; Ko, M.-J.; Jeong, S.-H. Highly Porous Self-assembly of Nitrogen-doped Graphene Quantum Dots over Reduced Graphene Sheets for Photo-electrocatalytical Electrodes. *J. Colloid Interface Sci*. **2019**, *557*, 174-184.

(27) Neniskis, A.; Ulcinas, A.; Valiokas, R.; Brown, S. P.; Warnmark, K.; Orentas, E. A Tautoleptic Approach to Chiral Hydrogen-Bonded Supramolecular Tubular Polymers with Large Cavity. *Chem. Eur. J*. **2018**, *24*, 14028-14033.

(28) Jiang, H.; Léger, J.-M.; Huc, I. Aromatic *δ*-Peptides. *J. Am. Chem. Soc*. **2003**, *125*, 3448-3449.

(29) Li, X.; Qi, T.; Srinivas, K.; Massip, S.; Maurizot, V.; Huc, I. Synthesis and Multibromination of Nanosized Helical Aromatic Amide Foldamers via Segment-Doubling Condensation. *Org. Lett.* **2016**, *18*, 1044–1047.

(30) Qi, T.; Deschrijver, T.; Huc, I. Large-Scale and Chromatography-Free Synthesis of an Octameric Quinoline-Based Aromatic Amide Helical Foldamer. *Nature Protoc.* **2013**, *8*, 693–708.

(31) Hjelmgaard, T.; Plesner, M.; Dissing, M. M.; Andersen, J. M.; Frydenvang, K.; Nielsen, J. Advances towards Aromatic Oligoamide Foldamers: Synthesis and X-ray Structures of Dimeric Arylpeptoids with Conformation – Directing Side Chains. *Eur. J. Org. Chem*. **2014**, *2014 (19)*, 3971-3975.

(32) Bonnel, C.; Legrand, B.; Bantignies, J.-L.; Petitjean, H.; Martinez, J.; Masurier, N.; Maillard, L. T. FT-IR and NMR structural markers for thiazole-based γ-peptide foldamers. *Org. Biomol. Chem*. **2016**, *14*, 8664-8669.

(33) Luo, Z.; Zhu, N.; Zhao, D. Helical Folding Competing with Unfolded Aggregation in Phenylene Ethynylene Foldamers. *Chem. Eur. J*. **2016**, *22*, 11028-11034.

(34) Zhang, D.-W.; Zhao, X.; Hou, J.-L.; Li, Z.-T. Aromatic Amide Foldamers: Structures, Properties, and Functions. *Chem. Rev.* **2012**, *112*, 5271–5316.

(35) Cheong, C.; Varani, G.; Tinoco, I. Solution Structure of an Unusually Stable RNA Hairpin, 5’GGAC(UUCG)GUCC. *Nature* **1990**, *346*, 680-682.

(36) Holbrook, S. R.; Cheong, C.; Varani, G.; Tinoco, I.; Kim, S.-H. Crystal Structure of an RNA Double Helix Incorporating a Track of non-Watson-Crick Base Pairs. *Nature* **1991**, *353*, 579-581.

(37) Kanyo, J. E.; Duhamel, J.; Lu, P. Secondary Structure of the r(CUUCGG) Tetraloop. *Nucleic Acids Res.* **1996**, *24*, 4015–4022.

(38) Soptokova-de Olivera Santos, J.; Voisin-Chiret, A. S.; Burzicki, G.; Sebaoun, L.; Sebban, M.; Lohier, J.-F.; Legay, R.; Oulyadi, H.; Bureau, R.; Rault, S. Structural Characterizations of Oligopyridyl Foldamers, α-Helix Mimetics. *J. Chem. Inf. Model.* **2012**, *52*, 429-439.

(39) Carini, M.; Ruiz, M. P.; Usabiaga, I.; Fernández, J. A.; Cocinero, E. J.; Melle-Franco, M.; Diez-Perez, I.; Mateo-Alonso, A. High Conductance Values in π-Folded Molecular Junctions. *Nat. Commun.* **2017**, *8*, 15195.

(40) Bornhof, A.-B.; Bauzá, A.; Aster, A.; Pupier, M.; Frontera, A.; Vauthey, E.; Sakai, N.; Matile, S. Synergistic Anion–(π)*n* –π Catalysis on π-Stacked Foldamers. *J. Am. Chem. Soc.* **2018**, *140*, 4884–4892.

(41) Berne, B. J.; Pecora, R. Dynamic Light Scattering with Applications to Chemistry, Biology, and Physics. Dover Publications, Toronto, 2000.

(42) Chuang, T. J.; Eisenthal, K. B. Theory of Fluorescence Depolarization by Anisotropic Rotational Diffusion. *J. Chem. Phys.* **1972**, *57*, 5094-5097.

(43) Duhamel, J.; Kanyo, J.; Dinter-Gottlieb, G.; Lu, P.; Fluorescence Emission of Ethidium Bromide Intercalated in Defined DNA Duplexes: Evaluation of Hydrodynamics Components. *Biochemistry* **1996**, *35*, 16687-16697.

(44) Lakowicz, J. R. Principles of Fluorescence Spectroscopy 2nd Ed., Kluwer Acad. New York, 1999.

(45) Little, H.; Wang, J.; Duhamel, J.; Li, X.; Markandeya, N.; Maurizot, V.; Huc, I. Simplification in the Acquisition and Analysis of Fluorescence Decays Acquired with Polarized Emission for Time-Resolved Fluorescence Anisotropy Measurements. *Anal. Chem*. **2020**, *92*, 668-673.

(46) Jiskoot, W.; Hoogerhout, P.; Beuvery, E. C.; Herron, J. N.; Crommelin, D. J. A. Preparation and Application of a Fluorescein-Labeled Peptide for Determining the Affinity Constant of a Monoclonal Antibody-Hapten Complex by Fluorescence Polarization. *Anal. Biochem*. **1991**, *196*, 421-426.

(47) Murakami, A.; Nakaura, M.; Nakatsuji,Y.; Nagahara,S.; Tran-Cong, Q.; Makino, K. Fluorescent-Labeled Oligonucleotide Probes: Detection of Hybrid Formation in Solution by Fluorescence Polarization Spectroscopy. *Nucleic Acids Res*. **1991**, *19*, 4097–4102.

(48) Cook, J.; Holtom, G.; Lu, P. Detection of Protein-DNA Complex Formation by Time-Resolved Fluorescence Depolarization of Bound Ethidium Bromide. *Anal. Biochem*. **1990**, *190*, 331-339.

(49) Weber, G. Polarization of the Fluorescence of Macromolecules. I. Theory and Experimental Method. *Biochem J.* **1952**, *51*, 145-155.

(50) Jameson, D. M.; Ross, J. A. Fluorescence Polarization/Anisotropy in Diagnostics and Imaging. *Chem. Rev.* **2010**, *110*, 2685-2708.

(51) Kasprzak, A. A.; Villafranca, J. J. Interactive Binding between the Substrate and Allosteric Sites of Carbamoyl-Phosphate Synthetase. *Biochemistry* **1988**, *27*, 8050-8056.

Chapter 2

(1) Gellman, S. H. Foldamers: A Manifesto. *Acc. Chem. Res*. **1998**, *31*, 173-180.

(2) Clayden, J.; Le Bailly, B. A. F. Dynamic Foldamer Chemistry. *Chem. Commun.* **2016**, *52*, 4852-4863.

(3) Tomasini, C.; Huc, I.; Aitken, D. J.; Fulop, F. Foldamers. *Eur. J. Org. Chem*. **2013**, *17*, 3408-3409.

(4) Gratzer, K.; Diemer, V.; Clayden, J. Signal transduction in oligoamide foldamers by selective non-covalent binding of chiral phosphates at a urea binding site. *Org. Biomol. Chem.* **2017**, *15*, 3585-3589.

(5) De Greef, T. F. A.; Smulders, M. M. J.; Wolffs, M.; Schennings, A. P. H. J.; Sijbesma, R. P.; Meijer, E. W. Supramolecular Polymerization. *Chem. Rev*. **2009**, *109*, 5687 – 5754.

(6) Whitesides, G. M.; Boncheva, M. Beyond Molecules: Self-Assembly of Mesoscopic and Macroscopic Components. *Proc. Natl. Acad. Sci. U S A*. **2002**, *99*, 4769–4774.

(7) Douglas, P.; Stoddart, J. F. Self-Assembly in Natural and Unnatural Systems. *Angew. Chem. Int. Ed.* **1996**, *35*, 1154-1196.

(8) Zwillinger, M.; Reddy, P. S.; Wicher, B.; Mandal, P. K.; Csekei, M.; Fischer, L.; Kotschy, A.; Huc, I. Aromatic Foldamer Helices as α-Helix Extended Surface Mimetics. *Chem. Eur. J.* **2020**, *26*, 17366-17370.

(9) Kwon, S.; Jin, B. J.; Lim, H.-K.; Kang, K.; Yoo, S. H.; Gong, J.; Yoon, E.; Lee, J.; Choi, I. S.; Kim, H.; Lee, H.-S. Magnetotactic Molecular Architectures from Self-assembly of b-Peptide Foldamers. *Nat. Commun*. **2015**, *6*, 8747-8756.

(10) Comes, R.; Liu, H.; Khokhlov, M.; Kasica, R.; Lu, J.; Wolf, S.A. Directed Self-Assembly of Epitaxial $CoFe_2O_4$–$BiFeO_3$ Multiferroic Nanocomposites. *Nano. Lett*. **2012**, *12*, 2367-2373.

(11) Riaz, R.; Ali, M.; Answer, H.; Ko, M.-J.; Jeong, S.-H. Highly Porous Self-assembly of Nitrogen-doped Graphene Quantum Dots over Reduced Graphene Sheets for Photo-electrocatalytical Electrodes. *J. Colloid Interface Sci*. **2019**, *557*, 174-184.

(12) Neniskis, A.; Ulcinas, A.; Valiokas, R.; Brown, S. P.; Warnmark, K.; Orentas, E. A Tautoleptic Approach to Chiral Hydrogen-Bonded Supramolecular Tubular Polymers with Large Cavity. *Chem. Eur. J*. **2018**, *24*, 14028-14033.

(13) Lehn, J.-M. Toward Self-Organization and Complex Matter. *Science* **2002**, *295*, 2400–2403.

(14) Zhang, D.-W.; Wang, W.-K.; Li, Z.-T. Hydrogen-Bonding-Driven Aromatic Foldamers: Their Structural and Functional Evolution. *Chem. Rec.* **2015**. *15*, 233-251.

(15) Sathaye, S.; Zhang, H.; Sonmez, C.; Schneider, J. P.; MacDermaid, C. M.; Von Bargen, C. D.; Saven, J. G.; Pochan, D. J. Engineering Complementary Hydrophobic Interactions to Control β-Hairpin Peptide Self-Assembly, Network Branching, and Hydrogel Properties. *Biomacromolecules*. **2014**, *15*, 3891-3900.

(16) Wychowaniec, J. K.; Patel, R.; Leach, J.; Mathomes, R.; Chhabria, V.; Patil-Sen, Y.; Hidalgo‐Bastilda, A.; Forbes, R. T.; Hayes, J. M.; Elsawy, M. A. Aromatic Stacking Facilitated Self-Assembly of Ultrashort Ionic Complementary Peptide Sequence: β-Sheet Nanofibers with Remarkable Gelation and Interfacial Properties. *Biomacromolecules* **2020**, *21*, 2670-2680.

(17) Nisanci, B.; Dastan, A.; Bozedemir, O. A. Aromatic Stacking of a Perylenetetracarboxylic Tetraester: Self-Assembly in both Water and Chloroform. *Tetrahedron Lett.* **2018**, *59*, 3558-3562.

(18) Li, X.; Markandeya, N.; Jonusauskas, G.; McClenaghan, N. D.; Maurizot, V.; Denisov, S. A.; Huc, I. Photoinduced Electron Transfer and Hole Migration in Nanosized Helical Aromatic Oligoamide Foldamers. *J. Am. Chem. Soc.* **2016**, *138*, 13568–13578.

(19) Lefler, K. M.; Co, D. T.; Wasielewski, M. R. Self-Assembly-Induced Ultrafast Photodriven Charge Separation in Perylene-3,4-Dicarboximide-Based Hydrogen-Bonded Foldamers. *J. Phys. Chem. Lett.* **2012**¸*3*, 3798-3805.

(20) Zhuo, M.-P.; Wu, J.-J.; Wang, X.-D.; Tao, Y.-C.; Yuan, Y.; Liao, L.-S. Hierarchical Self-Assembly of Organic Heterostructure Nanowires. *Nat. Commun*. **2019**, *10*, 3839-3839.

(21) Jiang, H.; Léger, J.-M.; Huc, I. Aromatic δ-Peptides. *J. Am. Chem. Soc.* **2003**, *125*, 3448-3449.

(22) Wolffs, M.; Delsuc, N.; Veldman, D.; Anh, N. V.; Williams, R. M.; Meskers, S. C. J.; Janssen, R. A. J.; Huc, I.; Schenning, A. P. H. J. Helical Aromatic Oligoamide Foldamers as Organizational Scaffolds for Photoinduced Charge Transfer. *J. Am. Chem. Soc.* **2009**, *131*, 4819-4829.

(23) Luo, Z.; Zhu, N.; Zhao, D. Helical Folding Competing with Unfolded Aggregation in Phenylene Ethynylene Foldamers. *Chem. Eur. J*. **2016**, *22*, 11028-11034.

(24) Bonnel, C.; Legrand, B.; Bantignies, J.-L.; Petitjean, H.; Martinez, J.; Masurier, N.; Maillard, L. T. FT-IR and NMR Structural Markers for Thiazole-based γ-Peptide Foldamers. *Org. Biomol. Chem*. **2016**, *14*, 8664-8669.

(25) Soptokova-de Olivera Santos, J.; Voisin-Chiret, A. S.; Burzicki, G.; Sebaoun, L.; Sebban, M.; Lohier, J.-F.; Legay, R.; Oulyadi, H.; Bureau, R.; Rault, S. Structural Characterization of Oligopyridyl Foldamers, α-Helix Mimetics. *J. Chem. Inf. Model.***2012**, *52*, 429-439.

(26) Hartley, C. S. Folding of *ortho*-Phenylenes. *Acc. Chem. Res.* **2016**, *49*, 646-654.

(27) Hjelmgaard, T.; Plesner, M.; Dissing, M. M.; Andersen, J. M.; Frydenvang, K.; Nielsen, J. Advances towards Aromatic Oligoamide Foldamers: Synthesis and X-ray Structures of Dimeric Arylpeptoids with Conformation – Directing Side Chains. *Eur. J. Org. Chem*. **2014**, *19*, 3971-3975.

(28) Wang, J.; Little, H.; Duhamel, J.; Li, X.; Markandeya, N.; Maurizot, V.; Huc, I. Application of Time-Resolved Fluorescence Anisotropy to Probe Quinoline-Based Foldamers Labeled with Oligo(phenylene vinylene). *Macromolecules* **2019**, *52*, 5829-5837.

(29) Duhamel, J.; Kanyo, J.; Dinter-Gottlieb, G.; Lu, P. Fluorescence Emission of Ethidium Bromide Intercalated in Defined DNA Duplexes: Evaluation of Hydrodynamics Components. *Biochemistry* **1996**, *35*, 16687-16697.

(30) Yuan, W.; Casier, R.; Duhamel, J. Unfolding of Helical Poly(L-Glutamic Acid) in *N*,*N* – Dimethylformamide Probed by Pyrene Excimer Fluorescence. *Polymers* **2021**, *13*, 1690.

(31) Lakowicz, J. R. Principles of Fluorescence Spectroscopy 2nd Ed., Kluwer Acad. New York, **1999**.

(32) Odian, G. Principles of Polymerization, 3rd Ed. Wiley, NY, 1991, pp 422-424.

(33) Little, H.; Wang, J.; Duhamel, J.; Li, X.; Nagula, M.; Maurizot, V.; Huc, I. Simplification in the Acquisition and Analysis of Fluorescence Decays Acquired with Polarized Emission for Time-Resolved Fluorescence Anisotropy Measurements. *Anal. Chem.* **2020**, *92*, 668-673.

(34) Chuang, T. J.; Eisenthal, K. B. Theory of Fluorescence Depolarization by Anisotropic Rotational Diffusion. *J. Chem. Phys.* **1972**, *57*, 5094−5097.

(35) Gierschner, J.; Egelhaaf, H.-J.; Oelkrug, D.; Mullen, K. Electronic Deactivation and Energy Transfer in Doped Oligophenylenevinylene Nanoparticles. *J. Fluoresc*. **1998**, *8(1)*, 37-44.

(36) Sagara, Y.; Kubo, K.; Nakamura, T.; Tamaoki, N.; Weder, C. Temperature-Dependent Mechanochromic Behavior of Mechanoresponsive Luminescent Compounds. *Chem. Mater.* **2017**, *29*, 1273-1278.

(37) Sijbesma, R. P.; Beijer, F. H.; Brunsveld, L.; Folmer, B. J. B.; Hirschberg, J. H. K. K.; Lange, R. F. M.; Lowe, J. K. L.; Meijer, E. W. Reversible Polymers Formed from Self Complementary Monomers Using Quadruple Hydrogen Bonding. *Science* **1997**, *278*, 1601-1604.

(38) Schafer, B.; Hecht, M.; Harting, J.; Nirschl, H. Agglomeration and Filtration of Colloidal Suspensions with DVLO Interactions in Simulation and Experiment. *J. Colloid Interface Sci*. **2010**, *349*, 186-195.

(39) Li, X.; Qi, T.; Srinivas, K.; Massip, S.; Maurizot, V.; Huc, I. Synthesis and Multibromination of Nanosized Helical Aromatic Amide Foldamers via Segment-Doubling Condensation. *Org. Lett*. **2016**, *18*, 1044–1047.

Chapter 3

(1) Piergiovanni, L.; Limbo, S. Plastic Packaging Materials. In *Food Packaging Materials*, 1st ed.; SpringerBriefs in Molecular Science, Vol. 1; Springer International Publishing, 2016; pp 33-49.

(2) Thomas, J.; Minu, E. T.; Thomas, S. Crosslinked Polyethylene: State-of-the-Art and New Challenges. In *Crosslinkable Polyethylene Manufacture, Properties, Recycling and Applications*, 1st ed.; Material Horizons: From Nature to Nanomaterials, Vol. 1; Springer Nature Singapore Pte Ltd, 2021; pp 1-15.

(3) Moulay, S. Chemical Modification of poly(vinyl chloride) – Still on the Run. *Prog. Polym. Sci*. **2010**, *35*, 303-331.

(4) Qingbin, G.; Lianzhong, A.; Cui, S. W. Strategies for Structural Characterization of Polysaccharides. In *Methodology for Structural Analysis of Polysaccharides*, 1st ed.; SpringerBriefs in Molecular Science, Vol. 1; Springer International Publishing, 2018; pp 1-7.

(5) Cleaves II, H.J. Nucleobases on the Primitive Earth: Their Sources and Stabilites. In *Prebiotic Chemistry and Chemical Evolution of Nucleic Acids*, 1st ed. Nucleic Acids and Molecular Biology, Vol. 35; Springer International Publishing, 2018; pp 1-19.

(6) Kurochkina, N. Proteins and Protein Structure. In *Protein Structure and Modeling*, 1st ed. Springer Singapore Pte Ltd, 2019; pp 1-42.

(7) Yang, C.; Tian, X.; Li, D.; Cao, Y.; Zhao, F.; Shi, C. Influence of Thermal Processing Conditions in 3D Printing on the Crystallinity and Mechanical Properties of PEEK Material. *J. Mater. Process. Technol*. **2017**, *248*, 1-7.

(8) Gell, C. B.; Graessly, W. W.; Fetters, L. J. Viscoelasticity and Self-Diffusion in Melts of Entangled Linear Polymers. *J. Polym. Sci*. **1997**, *35*, 1935-1942.

(9) Sharma, U.; Concagh, D.; Core, L.; Kuang, Y.; You, C.; Pham, Q.; Zugates, G.; Busold, R.; Webber, S.; Merlo, J.; Langer, R.; Whitesides, G.M.; Palasis, M. The Development of Bioresorbable Composite Polymeric Materials with High Mechanical Strength. *Nat. Mater*. **2017**, *17*, 96-103.

(10) Fouquey, C.; Lehn, J.-M.; Levelut, A. M. Molecular Recognition Directed Self-Assembly of Supramolecular Liquid Crystalline Polymers from Complementary Chiral Components. *Adv. Mater*. **1990**, *2*, 254–257.

(11) Lehn, J.-M. Toward Self-Organization and Complex Matter. *Science* **2002**, *295*, 2400–2403.

(12) Zhang, D.-W.; Wang, W.-K.; Li, Z-T. Hydrogen-Bonding-Driven Aromatic Foldamers: Their Structural and Functional Evolution. *Chem. Rec.* **2015**, *15*, 233-251.

(13) Wychowaniec, J. K.; Patel, R.; Leach, J.; Mathomes, R.; Chhabria, V.; Patil-Sen, Y.; Hidalgo-Bastilda, A.; Forbes, R. T.; Hayes, J. M.; Elsawy, M. A. Aromatic Stacking Facilitated Self-Assembly of Ultrashort Ionic Complementary Peptide Sequence: β-Sheet

Nanofibers with Remarkable Gelation and Interfacial Properties. *Biomacromolecules* **2020**, *21*, 2670-2680.

(14) Nisanci, B.; Dastan, A.; Bozedemir, O. A. Aromatic Stacking of a Perylenetetracarboxylic Tetraester: Self-Assembly in both Water and Chloroform. *Tetrahedron. Lett.* **2018**, *59*, 3558-3562.

(15) Whitesides, G. M.; Boncheva, M. Beyond Molecules: Self-Assembly of Mesoscopic and Macroscopic Components. *Proc. Natl. Acad. Sci. U S A.* **2002**, *99*, 4769–4774.

(16) Douglas, P.; Stoddart, J. F. Self-Assembly in Natural and Unnatural Systems. *Angew. Chem. Int. Ed. Engl*. **1996**, *35*, 1154-1196.

(17) Riaz, R.; Ali, M.; Answer, H.; Ko, M.-J.; Jeong, S.-H. Highly Porous Self-Assembly of Nitrogen-Doped Graphene Quantum Dots over Reduced Graphene Sheets for Photo-Electrocatalytical Electrodes. *J. Colloid Interface Sci*. **2019**, *557*, 174-184.

(18) Mielanczyk, A.; Odrobinska, J.; Grzadka, S.; Mielanczyk, L.; Neugebauer, D. Miktoarm Star Copolymers from D-(-)-Salicin Core Aggregated Intodandelion-like Structures as Anticancer Drug Delivery Systems: Synthesis, Self-Assembly and Drug Release. *Int. J. Pharm*. **2016**, *515*, 515-526.

(19) Alvarez, Z.; Kolberg-Edelbrock, A. N.; Sasseli, I. R.; Ortega, J. A.; Qiu, R.; Syrgiannis, Z.; Chen, F.; Chin, S. M.; Weigand, S.; Kiskinis, E.; Stupp, S. I. Bioactive Scaffolds with

Enhanced Supramolecular Motion Promote Recovery from Spinal Cord Injury. *Science* **2021**, *374*, 848-856.

(20) Li, X.; Qi, T.; Srinivas, K.; Massip, S.; Maurizot, V.; Huc, I. Synthesis and Multibromination of Nanosized Helical Aromatic Amide Foldamers via Segment-Doubling Condensation. *Org. Lett*. **2016**, *18*, 1044–1047.

(21) Lefler, K. M.; Co, D.T.; Wasielewski, M. R. Self-Assembly-Induced Ultrafast Photodriven Charge Separation in Perylene-3,4-dicarboximide-Based Hydrogen-Bonded Foldamers. *J. Phys. Chem. Lett.* **2012**, *3*, 3798-3805.

(22) Zhuo, M.-P.; Wu, J.-J.; Wang, X.-D.; Tao, Y.-C.; Yuan, Y.; Liao, L.-S. Hierarchical Self-Assembly of Organic Heterostructure Nanowires. *Nat. Commun*. **2019**, *10*, 3839-3839.

(23) Gellman, S. H. Foldamers: A Manifesto. *Acc. Chem. Res*. **1998**, *31*, 173-180.

(24) Jiang, H.; Léger, J.-M.; Huc, I. Aromatic δ-Peptides. *J. Am. Chem. Soc.* **2003**, *125*, 3448-3449.

(25) Li, X.; Markandeya, N.; Jonusauskas, G.; McClenaghan, N. D.; Maurizot, V.; Denisov, S. A.; Huc, I. Photoinduced Electron Transfer and Hole Migration in Nanosized Helical Aromatic Oligoamide Foldamers. *J. Am. Chem. Soc.* **2016**, *138*, 13568–13578.

(26) Wolffs, M.; Delsuc, N.; Veldman, D.; Van Anh, N.; Williams, R.M.; Meskers, S.C.J.; Janssen, R.A.; Huc, I. Schenning, A.P.H.J. Helical Aromatic Oligoamide Foldamers as

Organizational Scaffolds for Photoinduced Charge Transfer. *J. Am. Chem. Soc*. **2009**, *131*, 4819-4829.

(27) Luo, Z.; Zhu, N.; Zhao, D. Helical Folding Competing with Unfolded Aggregation in Phenylene Ethynylene Foldamers. *Chem. Eur. J*. **2016**, *22*, 11028-11034.

(28) Bonnel, C.; Legrand, B.; Bantignies, J.-L.; Petitjean, H.; Martinez, J.; Masurier, N.; Maillard, L. T. FT-IR and NMR Structural Markers for Thiazole-Based γ-Peptide Foldamers. *Org. Biomol. Chem*. **2016**, *14*, 8664-8669.

(29) Berne, B. J.; Pecora, R. Dynamic Light Scattering with Applications to Chemistry, Biology, and Physics; Dover Publications: Mineola, NY, 2000.

(30) Wang, X.; Wicher, B.; Ferrand, Y.; Huc, I. Orchestrating Directional Molecular Motions: Kinetically Controlled Supramolecular Pathways of a Helical Host on Rodlike Guests. *J. Am. Chem. Soc*. **2017**, *139*, 9350−9358.

(31) Holbrook, S. R.; Cheong, C.; Tinoco, I. Jr.; Kim, S-H. Crystal Structure of an RNA Double Helix Incorporating a Track of non-Watson-Crick Base Pairs. *Nature* **1991**, *353(6344)*, 579-581.

(32) Cheong, C.; Varani, G.; Tinoco, I. Solution Structure of an Unusually Stable RNA Hairpin, 5'GGAC(UUCG)GUCC. *Nature*. **1990**, *346*, 680−682.

(33) Duhamel, J.; Kanyo, J.; Dinter-Gottlieb, G.; Lu, P.; Fluorescence Emission of Ethidium Bromide Intercalated in Defined DNA Duplexes: Evaluation of Hydrodynamics Components. *Biochemistry* **1996**, *35*, 16687-16697.

(34) Wang, J.; Little, H.; Duhamel, J.; Li, X.; Markandeya, N.; Maurizot, V.; Huc, I. Application of Time-Resolved Fluorescence Anisotropy to Probe Quinoline-Based Foldamers Labeled with Oligo(phenylene vinylene). *Macromolecules* **2019**, *52*, 5829-5837.

(35) Lakowicz, J. R. Principles of Fluorescence Spectroscopy 2nd Ed., Kluwer Acad. New York, **1999**.

(36) Nwokeoji, A. O.; Kilby, P. M.; Portwood, D. E.; Dickman, M. J. Accurate Quantification of Nucleic Acids Using Hypochromicity Measurements in Conjunction with UV Spectrophotometry. *Anal. Chem*. **2017**, *89*, 13567-13574.

(37) Egelhaaf, H.-J.; Lüer, L.; Tompert, A.; Bauerle, P.; Müllen, K.; Oelkrug, D. Fluorescence Anisotropy and Rotational Diffusion of Polyene-like Molecules in Solution. *Synth. Met.* **2000**, *115*, 63−68.

Chapter 4

(1) Clayden, J.; Le Bailly, B. A. F. Dynamic Foldamer Chemistry. *Chem. Commun.* **2016**, *52*, 4852-4863.

(2) Gratzer, K.; Diemer, V.; Clayden, J. Signal Transduction in Oligoamide Foldamers by Selective Non-Covalent Binding of Chiral Phosphates at a Urea Binding Site. *Org. Biomol. Chem.* **2017**, *15*, 3585-3589.

(3) Lehn, J.-M. Toward Self-Organization and Complex Matter. *Science* **2002**, *295*, 2400–2403.

(4) Sathaye, S.; Zhang, H.; Sonmez, C.; Schneider, J. P.; MacDermaid, C. M.; Von Bargen, C. D.; Saven, J. G.; Pochan, D. J. Engineering Complementary Hydrophobic Interactions to Control β-Hairpin Peptide Self-Assembly, Network Branching, and Hydrogel Properties. *Biomacromolecules*. **2014**, *15*, 3891-3900.

(5) Wychowaniec, J. K.; Patel, R.; Leach, J.; Mathomes, R.; Chhabria, V.; Patil-Sen, Y.; Hidalgo‐Bastilda, A.; Forbes, R. T.; Hayes, J. M.; Elsawy, M. A. Aromatic Stacking Facilitated Self-Assembly of Ultrashort Ionic Complementary Peptide Sequence: β-Sheet Nanofibers with Remarkable Gelation and Interfacial Properties. *Biomacromolecules* **2020**, *21*, 2670-2680.

(6) Zwillinger, M.; Reddy, P. S.; Wicher, B.; Mandal, P. K.; Csekei, M.; Fischer, L.; Kotschy, A.; Huc, I. Aromatic Foldamer Helices as α-Helix Extended Surface Mimetics. *Chem. Eur. J.* **2020**, *26*, 17366-17370.

(7) Whitesides, G. M.; Boncheva, M. Beyond Molecules: Self-Assembly of Mesoscopic and Macroscopic Components. *Proc. Natl. Acad. Sci. U S A.* **2002**, *99*, 4769–4774.

(8) Jiang, H.; Léger, J.-M.; Huc, I. Aromatic δ-Peptides. *J. Am. Chem. Soc.* **2003**, *125*, 3448-3449.

(9) Li, X.; Qi, T.; Srinivas, K.; Massip, S.; Maurizot, V.; Huc, I. Synthesis and Multibromination of Nanosized Helical Aromatic Amide Foldamers via Segment-Doubling Condensation. *Org. Lett.* **2016**, *18*, 1044–1047.

(10) Li, X.; Markandeya, N.; Jonusauskas, G.; McClenaghan, N. D.; Maurizot, V.; Denisov, S. A.; Huc, I. Photoinduced Electron Transfer and Hole Migration in Nanosized Helical Aromatic Oligoamide Foldamers. *J. Am. Chem. Soc.* **2016**, *138*, 13568–13578.

(11) Wang, J.; Little, H.; Duhamel, J.; Li, X.; Markandeya, N.; Maurizot, V.; Huc, I. Application of Time-Resolved Fluorescence Anisotropy to Probe Quinoline-Based Foldamers Labeled with Oligo(phenylene vinylene). *Macromolecules* **2019**, *52*, 5829-5837.

(12) Egelhaaf, H.-J.; Lüer, L.; Tompert, A.; Bauerle, P.; Müllen, K.; Oelkrug, D. Fluorescence Anisotropy and Rotational Diffusion of Polyene-like Molecules in Solution. *Synth. Met.* **2000**, *115*, 63−68.

(13) Besenius, P. Controlling Supramolecular Polymerization Through Multicomponent Self-Assembly. *J. Polym. Sci. A Polym. Chem.* **2017**, *55*, 34-78.

(14) Sijbesma, R. P.; Meijer, E. W. Quadruple Hydrogen Bonding Systems. *Chem. Commun*. **2003**, 5–16.

(15) Nieuwenhuizen, M. M. L.; de Greef, T. F. A.; van der Bruggen, R. L. J.; Paulusse, J. M. J.; Appel, W. P. J.; Smulders, M. M. J.; Sijbesma, R. P.; Meijer, E. W. Self-Assembly of Ureido-Pyrimidinone Dimers into One-Dimensional Stacks by Lateral Hydrogen Bonding. *Chem. Eur. J.* **2010**, *16*, 1601-1602.

(16) Nwokeoji, A. O.; Kilby, P. M.; Portwood, D. E.; Dickman, M. J. Accurate Quantification of Nucleic Acids Using Hypochromicity Measurements in Conjunction with UV Spectrophotometry. *Anal. Chem*. **2017**, *89*, 13567-13574.

(17) Mahoney, J. M.; Davis, J. P.; Smith, B. D. Ditopic Salt-Binding Receptors for Anion Separation Processes. In *Fundamentals and Applications of Anionic Separations*. *Proceedings of the American Chemical Society (ACS) Symposium*, Chicago, IL. August 26-31, 2001; Moyer, B. A., Singh, R. P., Eds.; Kluwer Academic Publishers: New York, New York, 2004; Vol. 1, pp 116-117.

(18) Montalvo, G. L.; Zhang, Y.; Young, T. M.; Costanzo, M. J.; Freeman, K. B.; Wang, J.; Clements, D. J. Magavern, E.; Kavash, R. W. Scott, R. W.; Liu, D.; DeGrado, W. F. De Novo Design of Self-Assembling Foldamers That Inhibit Heparin− Protein Interactions. *ACS Chem. Biol*. **2014**, *9*, 967-975.

(19) Thoma, J. L. Characterizing Polymers with Complex Architecture using Pyrene Excimer Fluorescence. Ph. D Dissertation, University of Waterloo, Waterloo, ON, 2021.

Appendices

Appendix A – Supporting Information for Chapter 2

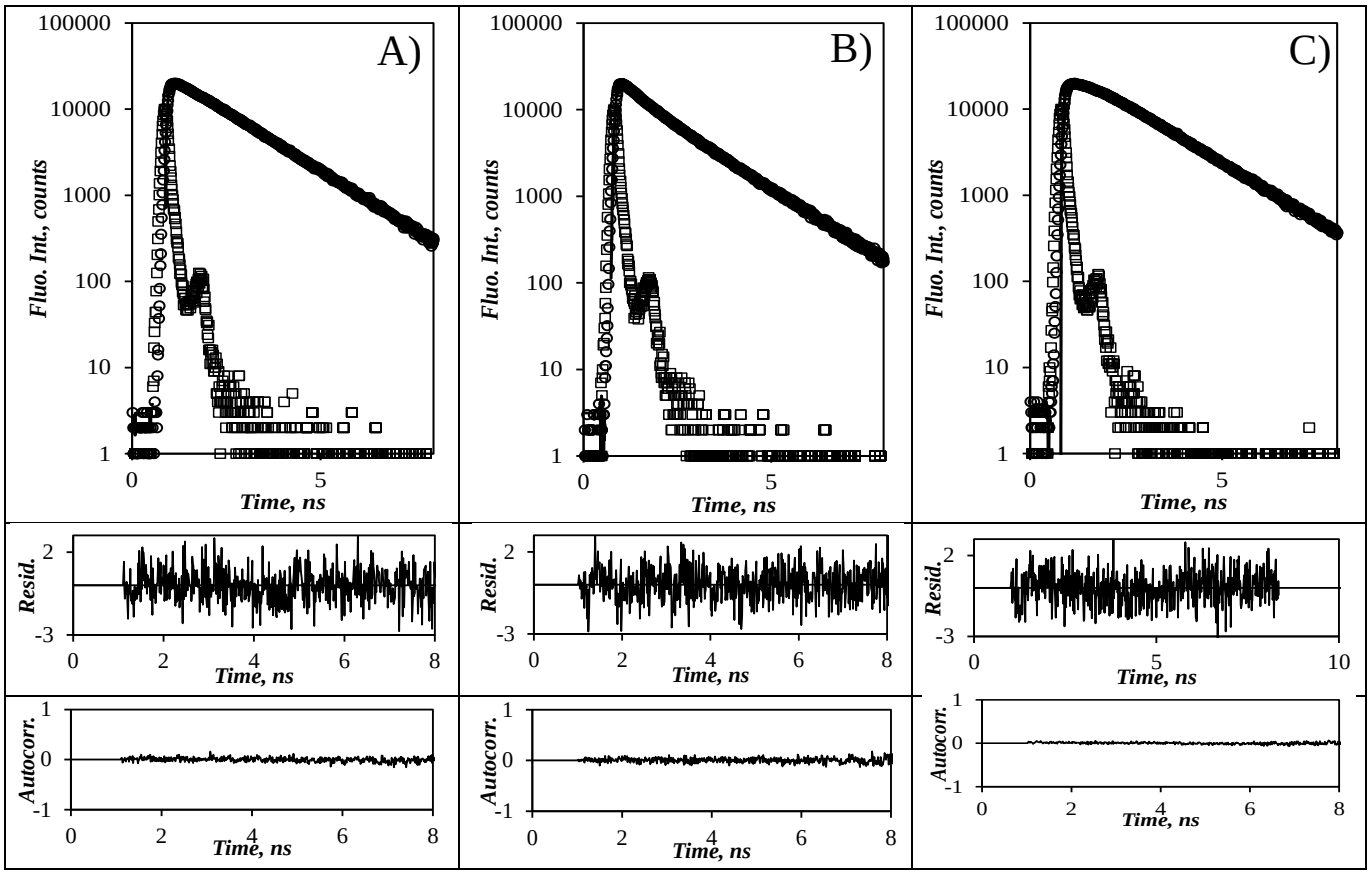

Figure A1. Fluorescence decays for OPV-labeled octamer in chloroform (with residuals and autocorrelation of the residuals) acquired with vertically polarized light at 479 nm and with the emission at 510 nm obtained with the emission polarizer placed A) at the magic angle ($I_{VM}(t)$), B) vertically ($I_{VV}(t)$), and C) horizontally ($I_{VH}(t)$).

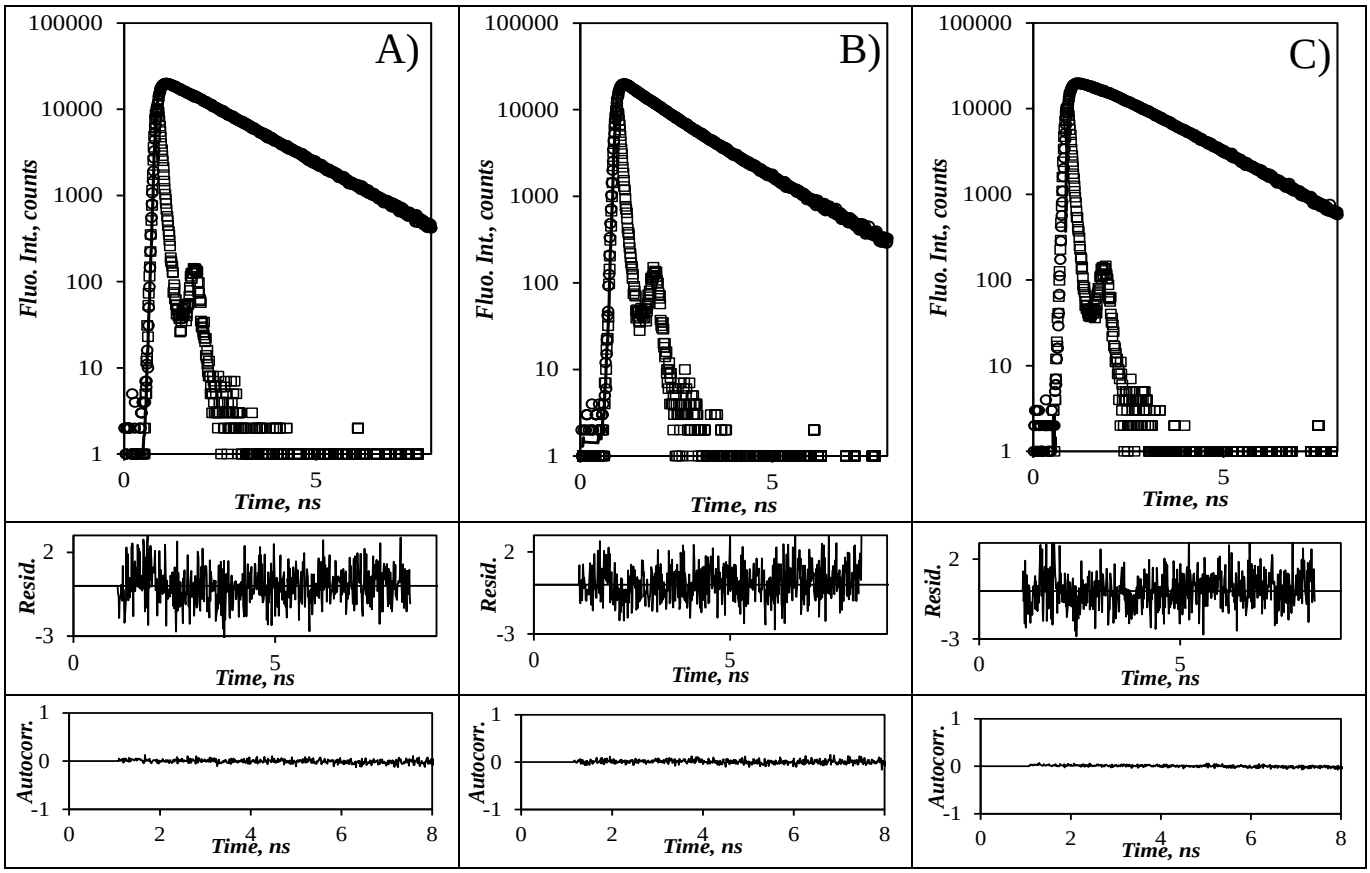

Figure A2. Fluorescence decays for OPV-labeled octamer in chloroform after the addition of 0.1 g of 16 M NaOH aqueous solution (with residuals and autocorrelation of the residuals) acquired with vertically polarized light at 479 nm and with the emission at 510 nm obtained with the emission polarizer placed A) at the magic angle ($I_{VM}(t)$), B) vertically ($I_{VV}(t)$), and C) horizontally ($I_{VH}(t)$).

Figure A3. Plot of χ^2 as a function of $log_{10}(K)$ for A) OPV-Q_4A, B) OPV-Q_{17}A, and C) OPV-Q_{33}A fitted with third order polynomials yielding K values of 1.1 (±0.1)×10^5 M^{-1}, 7.8 (±0.4)×10^5 M^{-1} , and 1.10 (±0.03)×10^6 M^{-1} at their minimum, respectively.

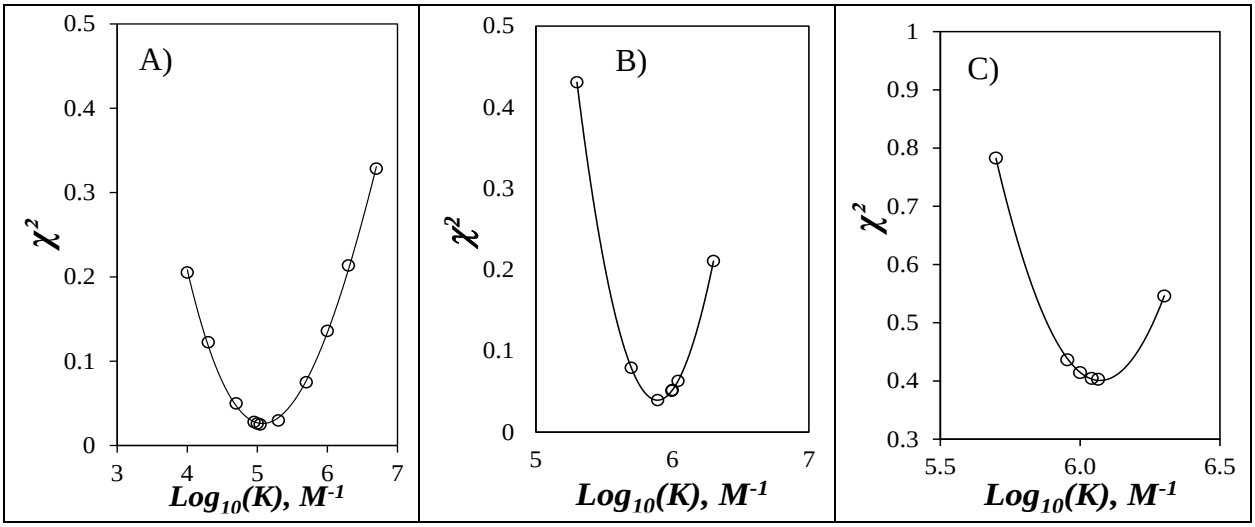

Table A1. Parameters obtained from the global analysis of $I_{VV}(t)$ and $I_{VH}(t)$ for the OPV-Q_4A samples in chloroform.

	mexpscatbg		aniso01d-extension					
Concentration (μM)	τ_o (ns)	χ^2	τ_o (ns)	r_o	ϕ (ns)	χ^2	G-factor	extension
6.3	1.70	1.13	1.70	0.294	0.73	1.15	0.51	7k
33	1.72	1.02	1.72	0.248	0.86	1.05	0.55	7k
170	1.77	1.09	1.78	0.187	0.94	0.99	0.63	4k
313	1.81	1.09	1.83	0.166	0.99	1.10	0.66	4k
532	1.83	0.99	1.85	0.171	0.97	1.10	0.65	4k
681	1.84	1.06	1.85	0.179	0.98	1.01	0.64	4k

Table A2. Parameters obtained from the global analysis of $I_{VV}(t)$ and $I_{VH}(t)$ for the OPV-Q_4A samples in chloroform after addition of 0.1 g of 16 M NaOH aqueous solution.

	mexpscatbg		aniso01d-extension					
Concentration (μM)	τ_o (ns)	χ^2	τ_o (ns)	r_o	ϕ (ns)	χ^2	G-factor	extension
0.3	1.71	1.08	1.72	0.377	0.57	1.01	0.47	4k
0.7	1.72	1.11	1.72	0.397	0.58	1.01	0.47	4k
1.3	1.72	1.09	1.72	0.392	0.58	0.99	0.47	4k
2.8	1.72	1.03	1.72	0.384	0.60	1.00	0.47	4k
6.3	1.70	1.13	1.70	0.294	0.73	1.15	0.51	7k
33	1.72	1.02	1.72	0.248	0.86	1.05	0.55	7k
170	1.77	1.09	1.78	0.187	0.94	0.99	0.63	4k
313	1.81	1.09	1.83	0.166	0.99	1.10	0.66	4k
532	1.83	0.99	1.85	0.171	0.97	1.10	0.65	4k
681	1.84	1.06	1.85	0.179	0.98	1.01	0.64	4k

Table A3. Parameters obtained from the global analysis of $I_{VV}(t)$ and $I_{VH}(t)$ for the OPV-Q_8A samples in chloroform.

	mexpscatbg		aniso01d-extension					
Concentration (μM)	τ_o (ns)	χ^2	τ_o (ns)	r_o	ϕ (ns)	χ^2	G-factor	extension
0.013	1.61	1.14	1.61	0.376	0.77	1.16	0.42	7k
0.046	1.60	1.07	1.60	0.328	0.77	1.12	0.49	7k
0.077	1.60	1.06	1.60	0.315	0.83	1.20	0.49	7k
0.458	1.59	1.19	1.59	0.327	1.01	1.21	0.43	7k
1.12	1.59	1.15	1.59	0.292	1.08	1.26	0.50	7k
62.3	1.61	1.04	1.61	0.350	1.30	1.09	0.42	4k

Table A4. Parameters obtained from the global analysis of $I_{VV}(t)$ and $I_{VH}(t)$ for the OPV-Q_8A samples in chloroform after addition of 0.1 g of 16 M NaOH aqueous solution.

	mexpscatbg		aniso01d-extension					
Concentration (μM)	τ_o (ns)	χ^2	τ_o (ns)	r_o	ϕ (ns)	χ^2	G-factor	extension
0.013	1.61	1.14	1.61	0.376	0.77	1.16	0.42	7k
0.046	1.60	1.07	1.60	0.328	0.77	1.12	0.49	7k
0.077	1.60	1.06	1.60	0.315	0.83	1.20	0.49	7k
0.2378	1.59	1.05	1.59	0.384	0.90	1.07	0.42	7k
0.458	1.59	1.19	1.59	0.327	1.01	1.21	0.43	7k
0.558	1.60	1.06	1.60	0.363	1.02	1.03	0.43	7k
1.12	1.59	1.15	1.59	0.292	1.08	1.26	0.50	7k
4.74	1.58	1.08	1.58	0.355	1.16	1.08	0.42	7k
62.3	1.61	1.04	1.61	0.350	1.30	1.09	0.42	4k
101	1.63	1.12	1.63	0.300	1.37	1.18	0.47	7k

Table A5. Parameters obtained from the global analysis of $I_{VV}(t)$ and $I_{VH}(t)$ for the OPV-Q_{17}A samples in chloroform.

	mexpscatbg		aniso01d-extension					
Concentration (μM)	τ_o (ns)	χ^2	τ_o (ns)	r_o	ϕ (ns)	χ^2	G-factor	extension
17.5	1.59	1.15	1.59	0.326	2.20	1.08	0.42	7k
36.9	1.60	0.99	1.60	0.318	2.30	1.07	0.41	7k
69.2	1.59	1.06	1.63	0.241	2.41	1.03	0.52	4k
97.4	1.60	1.10	1.65	0.244	2.51	1.07	0.53	4k
137	1.63	1.07	1.67	0.245	2.51	1.16	0.51	4k
314	1.66	1.00	1.69	0.252	2.45	1.08	0.51	4k

Table A6. Parameters obtained from the global analysis of $I_{VV}(t)$ and $I_{VH}(t)$ for the OPV-Q_{17}A samples in chloroform after addition of 0.1 g of 16 M NaOH aqueous solution.

	mexpscatbg		aniso01d-extension					
Concentration (μM)	τ_o (ns)	χ^2	τ_o (ns)	r_o	ϕ (ns)	χ^2	G-factor	extension
0.035	1.59	1.08	1.59	0.373	1.26	1.02	0.41	4k
0.057	1.60	1.05	1.59	0.365	1.28	0.99	0.42	4k
0.088	1.58	1.07	1.58	0.368	1.31	1.05	0.43	7k
0.185	1.58	1.02	1.58	0.359	1.38	1.05	0.38	7k
0.373	1.58	1.06	1.58	0.339	1.51	1.06	0.41	7k
1.65	1.58	1.05	1.58	0.322	1.77	1.05	0.44	7k
3.19	1.57	1.10	1.57	0.321	1.95	1.10	0.44	7k
8.70	1.58	0.96	1.58	0.323	2.09	1.10	0.42	7k
17.5	1.59	1.15	1.59	0.326	2.20	1.08	0.42	7k
36.9	1.60	0.99	1.60	0.318	2.30	1.07	0.41	7k
69.2	1.59	1.06	1.63	0.241	2.41	1.03	0.52	4k
97.4	1.60	1.10	1.65	0.244	2.51	1.07	0.53	4k
137	1.63	1.07	1.67	0.245	2.51	1.16	0.51	4k
314	1.66	1.00	1.69	0.252	2.45	1.08	0.51	4k

Table A7. Parameters obtained from the global analysis of $I_{VV}(t)$ and $I_{VH}(t)$ for the OPV-Q_{33}A samples in chloroform.

	mexpscatbg		aniso01d-extension					
Concentration (μM)	τ_o (ns)	χ^2	τ_o (ns)	r_o	ϕ (ns)	χ^2	G-factor	extension
0.050	1.59	0.98	1.59	0.323	2.33	1.03	0.43	7k
0.810	1.59	1.05	1.59	0.325	2.08	1.09	0.43	7k
11.3	1.58	1.05	1.58	0.332	2.27	1.09	0.43	7k
190	1.61	1.05	1.64	0.245	2.10	1.10	0.52	7k

Table A8. Parameters obtained from the global analysis of $I_{VV}(t)$ and $I_{VH}(t)$ without r_∞ for the OPV-Q_{33}A samples in chloroform after addition of 0.1 g of 16 M NaOH aqueous solution.

	mexpscatbg		aniso0X-ext								
Conc. (μM)	τ_o (ns)	χ^2	τ_o (ns)	r_{o1}	ϕ_1 (ns)	r_{o2}	ϕ_2 (ns)	$<\phi>$ (ns)	G-factor	χ^2	X-ext.
0.025	1.59	0.96	1.59	0.316	2.26	0.000	0.00	2.26	0.42	0.99	1d-7k
0.053	1.61	1.00	1.61	0.318	2.31	0.000	0.00	2.31	0.43	1.02	1d-7k
0.446	1.61	1.09	1.61	0.287	3.18	0.070	0.79	2.71	0.42	1.06	2d-3k
2.07	1.61	0.99	1.61	0.265	3.77	0.065	0.50	3.12	0.42	1.03	2d-3k
5.49	1.59	1.00	1.59	0.283	4.31	0.087	0.81	3.49	0.38	1.12	2d-3k
11.0	1.59	1.12	1.59	0.27	5.51	0.112	0.74	4.12	0.34	1.10	2d-3k
33.0	1.61	0.97	1.61	0.216	5.15	0.069	0.65	4.06	0.46	1.01	2d-3k

Table A9. Parameters obtained from the global analysis of $I_{VV}(t)$ and $I_{VH}(t)$ with r_∞ for the OPV-Q_{33}A samples in chloroform after addition of 0.1 g of 16 M NaOH aqueous solution.

	in2xpscbgk					aniso02d-4k									
Concentration (µM)	t_{o1}(ns)	a_1	t_{o2} (ns)	a_2	χ^2	t_o (ns)	ϕ_1 (ns)	χ^2	r_1	ϕ_2 (ns)	r_2	r_∞	ϕ_{total} (ns)	r_o	*G factor*
61.08	1.47	0.58	1.76	0.42	1.04	1.60	5.77	1.08	0.192	0.72	0.071	0.005	4.40	0.27	0.49
79.55	1.65	0.85	1.16	0.15	0.941	1.61	5.80	1.05	0.207	0.61	0.070	0.074	4.49	0.35	0.39
261.70	1.80	0.23	1.63	0.77	1.01	1.67	5.06	1.13	0.197	0.87	0.033	0.170	4.46	0.40	0.33

Table A10. Parameters obtained from $I_{VM}(t)$ with in1xpscbgk and the global analysis of $I_{VV}(t)$ and $I_{VH}(t)$ with inaniso01d7k for OPV-Q_8A and Q_{16}A sample mixtures in chloroform.

Concentrations (μM)			mexpscatbg		aniso01d-extension					
[acid] (μM)	[OQ_8A] (μM)	[Q_{16}A] (μM)	τ_o (ns)	χ^2	τ_o (ns)	r_o	ϕ (ns)	χ^2	G-factor	ext.
0.087	0.012	0.075	1.59	1.16	1.59	0.339	0.77	1.19	0.50	7k
1.32	0.196	1.12	1.59	1.00	1.59	0.382	0.78	1.04	0.44	7k
12.6	1.90	10.7	1.59	0.93	1.59	0.373	0.80	0.98	0.43	7k
516	434	82.2	1.61	1.13	1.63	0.311	0.82	1.05	0.49	4k

Table A11. Parameters obtained from the global analysis of $I_{VV}(t)$ and $I_{VH}(t)$ for the OPV-Q_8A and Q_{16}A samples in chloroform after addition of 0.1 g of 16 M NaOH aqueous solution.

Concentrations (μM)			mexpscatbg		aniso01d-extension					
[acid] (μM)	[OQ_8A] (μM)	[Q_{16}A] (μM)	τ_o (ns)	χ^2	τ_o (ns)	r_o	ϕ (ns)	χ^2	G-factor	ext.
0.040	0.0046	0.0311	1.62	1.13	1.62	0.398	0.83	1.11	0.42	7k
0.100	0.0127	0.0855	1.62	1.06	1.62	0.369	0.84	1.13	0.44	7k
0.140	0.0182	0.122	1.61	1.09	1.61	0.384	0.81	1.08	0.44	7k
0.230	0.0330	0.195	1.60	1.07	1.60	0.367	0.85	1.21	0.43	4k
0.650	0.0975	0.554	1.60	1.03	1.60	0.348	1.02	1.02	0.44	7k
1.32	0.196	1.12	1.61	1.17	1.61	0.341	1.09	1.19	0.44	7k
4.24	0.636	3.60	1.60	1.15	1.60	0.338	1.18	1.18	0.43	7k
46.9	7.70	39.2	1.60	1.09	1.62	0.270	1.33	1.07	0.47	4k
82.5	13.7	68.8	1.59	1.22	1.62	0.278	1.46	0.97	0.49	4k
160	27.2	133	1.58	1.10	1.62	0.275	1.67	1.05	0.43	4k
558	96.9	461	1.62	1.04	1.64	0.286	1.63	1.10	0.48	4k
937	156	781	1.67	1.10	1.69	0.284	1.66	1.04	0.50	4k

Appendix B – Supporting Information for Chapter 3

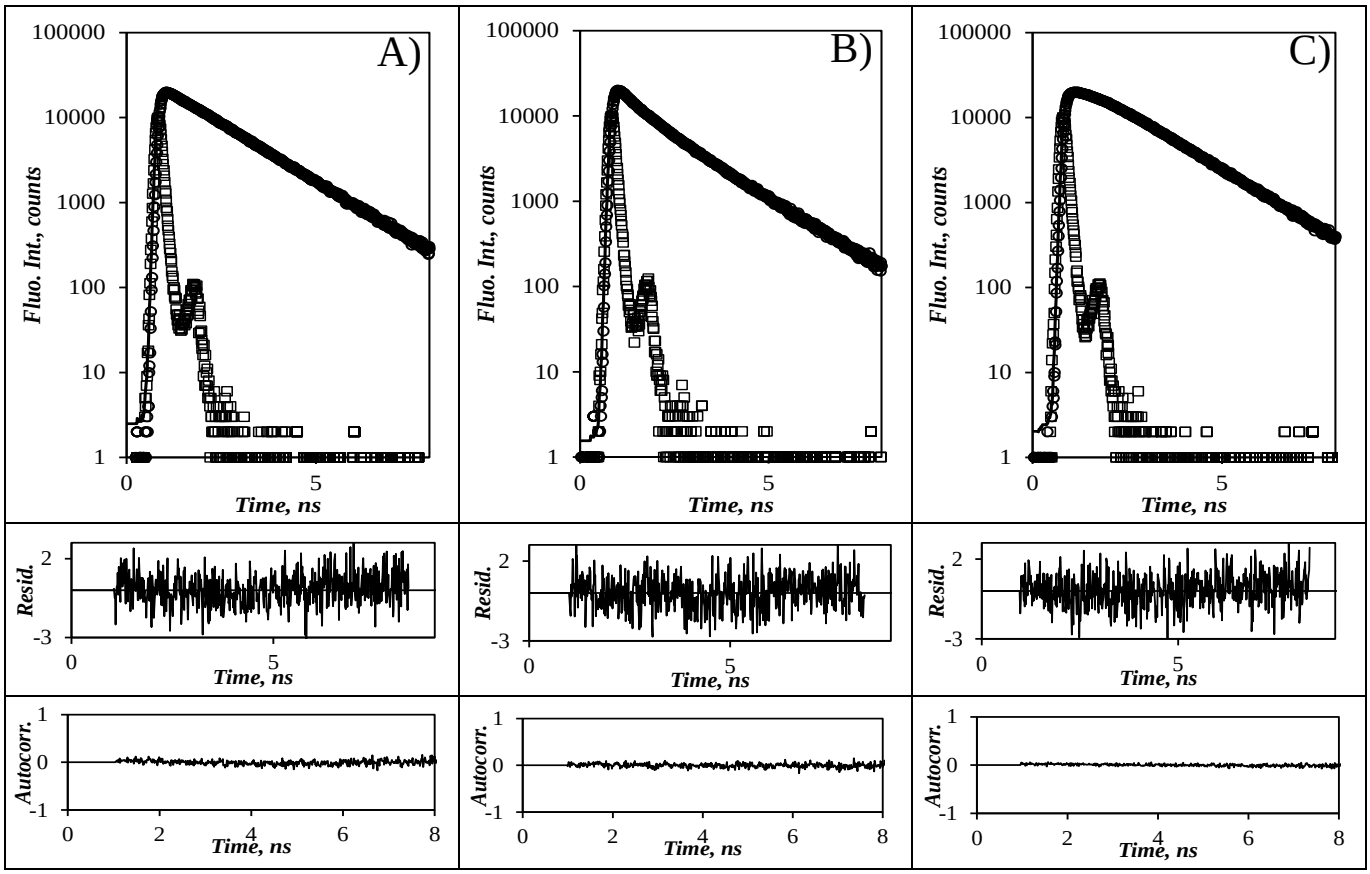

Figure B1. Fluorescence decays for a mixture of 261 µM AQ_2PQ_2A with 10 µM of OPV-labeled octamer in chloroform without 16 M $NaOH_{(aq)}$ (with residuals and autocorrelation of the residuals) acquired with vertically polarized light at 479 nm and with the emission at 510 nm obtained with the emission polarizer placed A) at the magic angle ($I_{VM}(t)$), B) vertically ($I_{VV}(t)$), and C) horizontally ($I_{VH}(t)$).

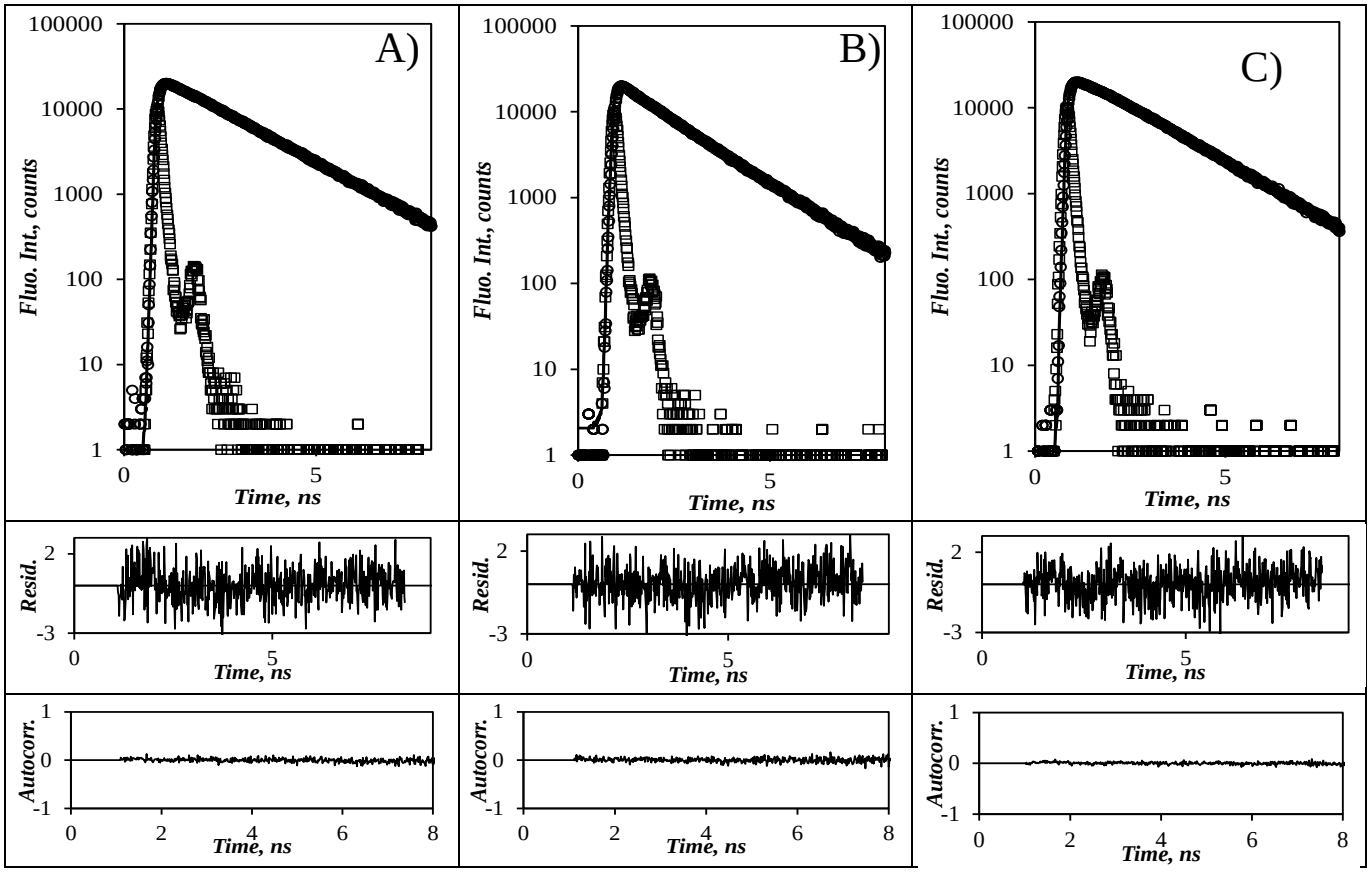

Figure B2. Fluorescence decays for a mixture of 384 μM AQ_2PQ_2A with 10 μM of OPV-labeled octamer in chloroform after the addition of 0.1 g of 16 M NaOH aqueous solution (with residuals and autocorrelation of the residuals) acquired with vertically polarized light at 479 nm and with the emission at 510 nm obtained with the emission polarizer placed A) at the magic angle ($I_{VM}(t)$), B) vertically ($I_{VV}(t)$), and C) horizontally ($I_{VH}(t)$).

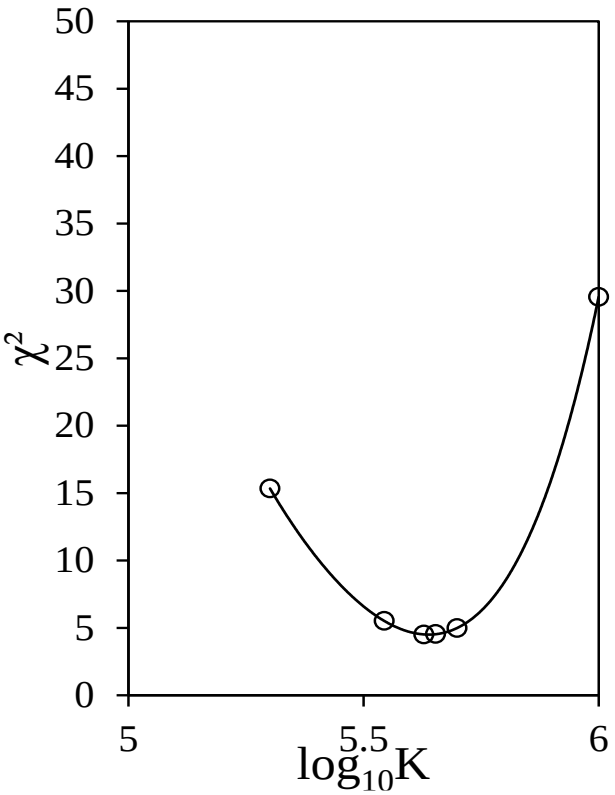

Figure B3. Plot of χ^2 as a function of $log_{10}(K)$ for mixtures of AQ_2PQ_2A and OPV-Q_8A fitted with a fourth order polynomial yielding a K value of 4.25×10^5 M^{-1}

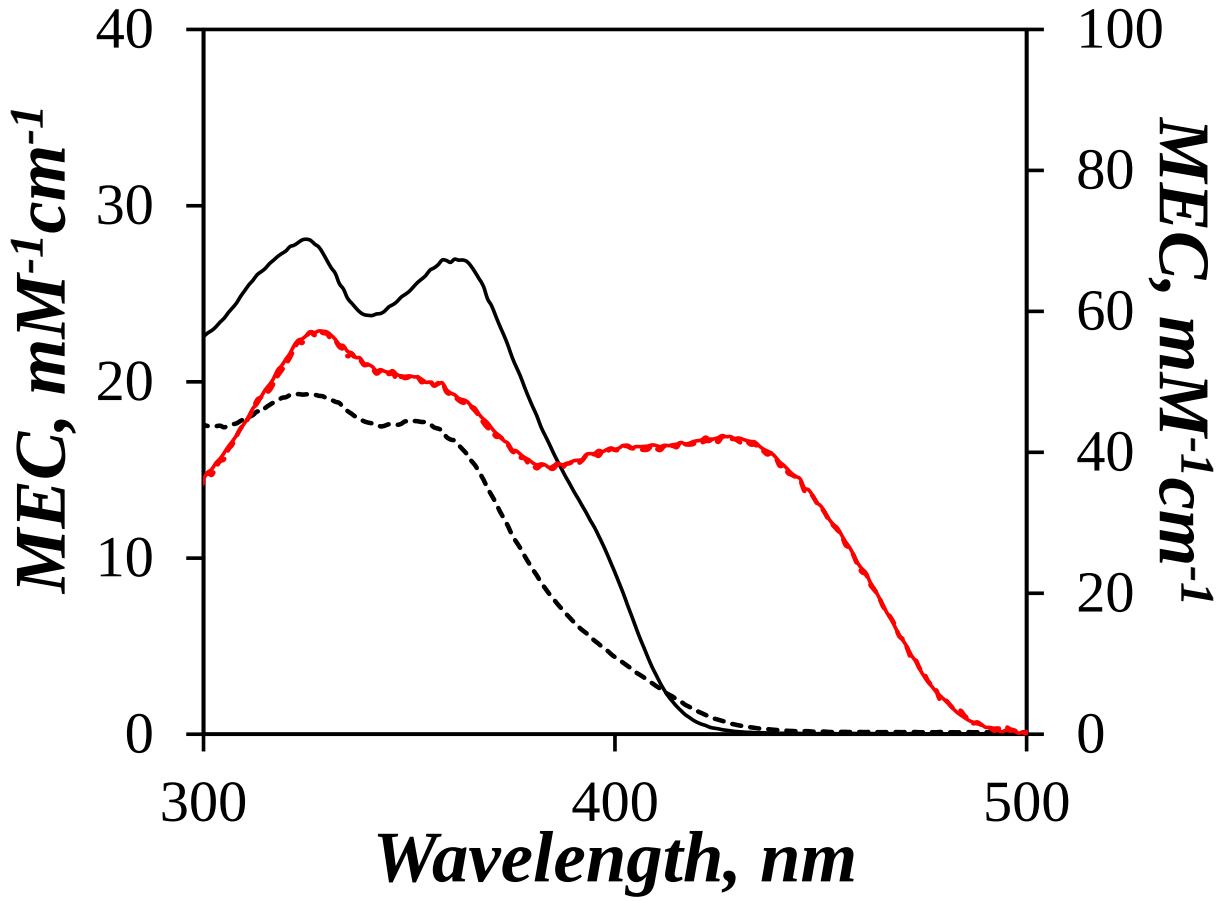

Figure B4. Plot of the molar extinction coefficient of OPV-Q_8A (red) and AQ_2PQ_2A (black) in chloroform (solid) without and (dashed) with the addition of 0.1 g of 16 M NaOH aqueous solution.

Table B1. Parameters obtained from the global analysis of $I_{VV}(t)$ and $I_{VH}(t)$ for mixtures of AQ_2PQ_2A and 1 µM OPV-Q_8A samples in chloroform without 16 M $NaOH_{(aq)}$.

			mexpscatbg		aniso01d-7k				
$[AQ_2PQ_2A]/[O_8A]$	$[O_8A]$ (µM)	$[AQ_2PQ_2A]$ (µM)	τ_o (ns)	χ^2	τ_o (ns)	r_o	ϕ (ns)	χ^2	G-factor
0.182	1.50	0.273	1.59	1.07	1.59	0.39	0.81	0.99	0.43
0.235	1.51	0.355	1.58	1.08	1.58	0.39	0.78	1.00	0.45
0.625	1.52	0.950	1.59	1.04	1.59	0.38	0.83	1.01	0.44
1.32	0.815	1.07	1.59	1.01	1.59	0.38	0.80	1.03	0.44
3.09	1.52	4.69	1.59	1.05	1.59	0.39	0.80	1.11	0.44
4.18	1.54	6.43	1.59	1.12	1.59	0.38	0.83	0.98	0.43
7.52	1.60	12.1	1.59	0.92	1.59	0.39	0.82	1.02	0.44
18.6	1.32	24.6	1.59	0.98	1.59	0.39	0.81	1.04	0.43
45.5	1.93	87.8	1.59	1.09	1.59	0.38	0.86	1.00	0.43
55.4	0.952	52.7	1.59	0.96	1.59	0.38	0.81	1.02	0.44
126	1.32	166	1.59	1.13	1.59	0.38	0.80	1.09	0.43
286	0.803	230	1.58	1.04	1.58	0.39	0.82	1.02	0.43

Table B2. Parameters obtained from the global analysis of $I_{VV}(t)$ and $I_{VH}(t)$ for mixtures of AQ_2PQ_2A and 10 µM OPV-Q_8A samples in chloroform without 16 M $NaOH_{(aq)}$.

			mexpscatbg		aniso01d-7k				
$[AQ_2PQ_2A]/[O_8A]$	$[O_8A]$ (µM)	$[AQ_2PQ_2A]$ (µM)	τ_o (ns)	χ^2	τ_o (ns)	r_o	ϕ (ns)	χ^2	G-factor
0.252	9.55	2.41	1.58	1.00	1.58	0.39	0.81	1.11	0.43
0.303	9.57	2.90	1.58	1.04	1.58	0.39	0.80	1.09	0.43
0.397	9.56	3.79	1.58	1.12	1.58	0.38	0.81	1.08	0.43
0.649	9.57	6.21	1.58	1.04	1.58	0.39	0.79	1.03	0.44
1.17	9.62	11.2	1.57	1.03	1.57	0.39	0.81	1.07	0.43
1.92	10.9	20.9	1.58	1.07	1.58	0.38	0.81	1.06	0.43
2.41	8.53	20.6	1.58	1.04	1.58	0.39	0.80	1.05	0.43
4.26	10.9	46.6	1.57	1.09	1.57	0.39	0.79	1.15	0.43
8.47	11.0	93.2	1.57	1.06	1.57	0.39	0.78	1.06	0.44
16.9	11.0	187	1.58	1.09	1.58	0.38	0.79	1.09	0.43
29.0	9.00	261	1.59	1.12	1.59	0.39	0.78	1.05	0.44
83.4	10.9	911	1.58	1.11	1.58	0.39	0.80	1.11	0.44

Table B3. Parameters obtained from the global analysis of $I_{VV}(t)$ and $I_{VH}(t)$ using one rotational time for the mixtures of AQ_2PQ_2A and 1 μM OPV-Q_8A samples in chloroform with 0.1 g of 16 M NaOH aqueous solution.

			mexpscatbg		aniso01d-7k				
$[AQ_2PQ_2A]/[O_8A]$	$[O_8A]$ (μM)	$[AQ_2PQ_2A]$ (μM)	τ_o (ns)	χ^2	τ_o (ns)	r_o	$\langle\phi\rangle$ (ns)	χ^2	G-factor
0.060	1.51	0.090	1.59	0.99	1.59	0.36	1.06	1.02	0.44
0.157	1.54	0.241	1.59	1.11	1.59	0.36	1.12	1.08	0.43
0.495	1.50	0.743	1.59	1.07	1.59	0.35	1.09	1.16	0.43
0.84	1.713	1.44	1.59	1.02	1.59	0.35	1.36	1.03	0.42
3.20	1.71	5.48	1.59	1.06	1.59	0.34	1.37	1.04	0.43
6.57	1.60	10.53	1.60	0.98	1.60	0.32	1.49	1.01	0.44
12.36	1.71	21.2	1.60	0.96	1.60	0.30	1.73	1.08	0.46
49.9	1.71	85.5	1.60	0.93	1.60	0.30	1.80	1.13	0.45

Table B4. Parameters obtained from the global analysis of $I_{VV}(t)$ and $I_{VH}(t)$ using two rotational time for the mixtures of AQ_2PQ_2A and 1 μM OPV-Q_8A samples in chloroform with 0.1 g of 16 M NaOH aqueous solution.

			mexpscatbg		aniso02d-3k								
$[AQ_2PQ_2A]/[O_8A]$	$[O_8A]$ (μM)	$[AQ_2PQ_2A]$ (μM)	τ_o (ns)	χ^2	τ_o (ns)	r_{o1}	ϕ_1 (ns)	r_{o2}	ϕ_2 (ns)	χ^2	$\langle\phi\rangle$ (ns)	$r_{o(Total)}$	G-factor
152	1.71	260	1.60	1.03	1.60	0.12	0.82	0.21	4.40	1.02	3.07	0.33	0.43
317	1.71	543	1.61	1.04	1.61	0.14	0.97	0.21	7.19	1.04	4.71	0.35	0.41
627	1.50	940	1.60	1.12	1.60	0.12	0.94	0.23	8.75	1.03	6.19	0.35	0.40

Table B5. Parameters obtained from the global analysis of $I_{VV}(t)$ and $I_{VH}(t)$ using one rotational time for the mixtures of AQ_2PQ_2A and 10 μM OPV-Q_8A samples in chloroform with 0.1 g of 16 M NaOH aqueous solution.

			mexpscatbg		aniso01d-7k				
$[AQ_2PQ_2A]/[O_8A]$	$[O_8A]$ (μM)	$[AQ_2PQ_2A]$ (μM)	τ_o (ns)	χ^2	τ_o (ns)	r_o	$\langle\phi\rangle$ (ns)	χ^2	G-factor
0.083	9.95	0.828	1.59	1.10	1.59	0.35	1.19	1.05	0.43
0.128	9.89	1.27	1.60	1.03	1.60	0.34	1.13	0.94	0.43
0.178	10.3	1.83	1.60	1.02	1.60	0.34	1.33	1.01	0.42
0.357	9.98	3.56	1.60	1.04	1.60	0.34	1.31	1.11	0.43
0.724	10.1	7.32	1.60	1.03	1.60	0.34	1.39	1.08	0.44
1.35	10.2	13.7	1.60	1.09	1.60	0.32	1.47	1.07	0.42
1.37	10.8	14.8	1.59	0.96	1.59	0.34	1.42	1.07	0.43
1.57	10.8	16.9	1.60	0.94	1.60	0.34	1.38	1.04	0.44

Table B6. Parameters obtained from the global analysis of $I_{VV}(t)$ and $I_{VH}(t)$ using two rotational time for the mixtures of AQ_2PQ_2A and 10 µM OPV-Q_8A samples in chloroform with 0.1 g of 16 M NaOH aqueous solution.

			mexpscatbg		aniso2d-3k								
$[AQ_2PQ_2A]$ /$[O_8A]$	$[O_8A]$ (µM)	$[AQ_2PQ_2A]$ (µM)	τ_o (ns)	χ^2	τ_o (ns)	r_{o1}	ϕ_1 (ns)	r_{o2}	ϕ_2(ns)	χ^2	$<\phi>$ (ns)	$r_{o(Total)}$	G-factor
6.24	10.3	64.4	1.60	1.09	1.60	0.15	1.06	0.19	4.15	1.05	2.79	0.33	0.42
10.6	12.1	129	1.60	0.92	1.60	0.14	0.86	0.20	4.56	1.03	3.03	0.34	0.42
19.2	10.9	210	1.60	0.97	1.60	0.12	0.94	0.19	5.11	1.07	3.50	0.32	0.44
40.6	9.47	385	1.60	1.01	1.60	0.13	0.98	0.20	7.63	1.06	5.09	0.33	0.43
76.2	9.47	721	1.60	1.11	1.60	0.12	0.83	0.25	8.79	1.05	6.14	0.37	0.39